Technical Report
TR-16-01
April 2016

Copper in ultrapure water

Mikael Ottosson
Mats Boman
Pedro Berastegui
Yvonne Andersson
Maria Hahlin
Marcus Korvela
Rolf Berger

SVENSK KÄRNBRÄNSLEHANTERING AB

SWEDISH NUCLEAR FUEL
AND WASTE MANAGEMENT CO

Box 250, SE-101 24 Stockholm
Phone +46 8 459 84 00
skb.se

SVENSK KÄRNBRÄNSLEHANTERING

ISSN 1404-0344
SKB TR-16-01
ID 1523018

April 2016

Copper in ultrapure water

Mikael Ottosson, Mats Boman, Pedro Berastegui,
Yvonne Andersson, Maria Hahlin, Marcus Korvela,
Rolf Berger

Uppsala University, Department of Chemistry
– Ångström Laboratory

Summary

This SKB report is a supplement to the previous R-14-07 (“Corrosion of copper in ultrapure water”) that in itself is a translation from R-13-31 written in Swedish. These two reports entail investigations of ultrapure copper immersed in ultrapure water, free from oxygen gas. The chemical system was contained in stainless steel containers that allowed evolved hydrogen to escape through a foil of palladium metal. In some setups the gas pressure was continuously monitored, and in other setups the copper and its immediate surrounding were analysed at discrete intervals, with the direct aim to find and characterize oxidation products from copper corrosion. The R-14-07 report contained a thorough description of the equipment, the choice and handling of the materials, the measurement strategies, the attained results and their critical evaluation, all from an experiment period of six months. It included continuous pressure monitoring and detailed chemical analyses. It was then concluded – and this conclusion is further strengthened in this supplement – that the corrosion rate of copper in ultrapure water must be very small, mainly based on the fact that no oxidation products were found by the very sensitive electron spectroscopy techniques of XPS and AES, backed up by measurements by other techniques. As a consequence, the corresponding hydrogen production from the reduction of water has to be very low and therefore difficult to measure. The level of the measured pressure indicated that the background dominated. As for the copper content of the water phase, evaluation from a glass blank was essential for judging whether dissolution of copper from the glass had to be taken into consideration, and it was found to be of no importance.

The equipment used in the previous report exhibited experimental difficulties, partly accidental loss of gas to the environment and partly overshadowing hydrogen out-gassing from the steel. Two major steps were taken to arrive at reliable values of the background: One concerned the palladium membrane, and one dealt with the properties of the stainless steel. Through a redesign of the equipment the leakage problem of the palladium membrane was solved, at the expense of lowering the flow rates of hydrogen through the membrane. The small extent of copper corrosion indicated would contribute very little to the total hydrogen pressure. Hence, the conventional baking-out methods were inappropriate for attaining an acceptable background. By reduction of the container wall thickness together with heat treatments (up to 450°C), the outgassing by the steel was reduced by one order of magnitude. The pressure gauges were replaced with the same objective. These measures rendered a final value for the outgassing at 10^{-12} Torr·L·s^{-1}·cm^{-2}.

Copper itself as a source of hydrogen was investigated: The previous analyses by ERDA were found less trustworthy for the low contents, favouring dedicated fusion analyses instead. The hydrogen gas treatment and heating after the initial electropolishing as steps in the copper purification process were found to lower the content rather than to introduce any hydrogen. Neither was there any change in hydrogen content after keeping copper in water. Hence, any allegation that the procedure creates an extra source of hydrogen from the copper is refuted.

Two more free-standing setups were dismantled for measuring on the copper, water and glassware. Thereby the time span from the previous study (1, 3 and 6 months) was expanded to include data from 15 and 29 months. The analysis methods used were the same as described in the previous report. Especially noteworthy is the outcome of AES. The copper Auger spectra still show only the phase features of metallic copper and no oxidation product. No obvious signs of contamination were recorded by XPS. The oxygen O *1s* contributions that were found correspond only to species most likely attributable to adsorbed OH and H_2O. Accompanying peaks belonging to Sb *3d*, although growing to some extent by time, still carry very low intensities. From comparison between oxygen and antimony contributions the amount of antimony was found to be considerably less than that of oxygen (from species residing in a monolayer). XRF corroborated that the glassware is one source of antimony that by glass corrosion enters the water phase (to the order of ppb) and is transported into the spectrometer by adhesion to the copper. The amount, concentrated in the remaining water film, is so low that it hardly would affect the corrosion properties. Still, if antimony were to be active, it would promote the corrosion of copper rather than inhibit it: No obvious signs of corrosion have been noted at all.

Two refurnished setups were used, with lower hydrogen background and new membrane fittings. The pressure evolution by time was followed in each setup with separate measurements of the background before loading with copper specimens in water, and again after measurement. Only purified copper was used, but the surface morphology (and microstructure) was for some samples deliberately changed by scratching, either by SiC or diamond as polishing materials. The idea behind was to establish whether the roughening of the smooth surface influenced the reactivity significantly. SEM was here introduced for the study of the surface on a microscale. As a complementary technique, GI-XRD (grazing incidence geometry) was used for a corresponding phase analysis, indubitably showing that foreign matter was caught in the soft metal surface, namely SiC particles not being removable by washing. Their presence might contribute to the observed enhanced hydrogen evolution from scratching by SiC, in sharp contrast to the outcome from diamond scratching where no hydrogen pressure above that of the background was measured although the surface had been mechanically affected to an even larger extent. It was found that scratching by either material creates minute copper particles that corrupt the ICP-MS analysis of the corresponding water phase.

One of the three original setups for monitoring the pressure has been kept the whole time, disassembled only after more than 3 years. The pressure readings cannot be compared with refurnished equipment. However, the contents (copper, glass, water) were still analysed, showing that neither the copper nor the antimony contents had increased linearly by time. Some parallel studies have also been made with a setup without copper and water, to follow the gas exchange properties between the compartments. In this context, indications were found that also the presence of traces of oxygen will affect the pressure, since palladium may act as a catalyst for the reaction that yields water.

With the rebuilt equipment no hydrogen pressure was observed to a significant degree above the improved lower background, not even after scratching the copper surface by diamond. However, the scratching by SiC seems to be a method that contaminates the copper surface. As a consequence, pressure measurements from material treated in that manner cannot be used as trustworthy indications of copper corrosion. On the other hand, the copper used in this study, as reported here and in SKB R-14-07, does not get contaminated during the surface purification process used in our study or by the performed experiments, but remains pure and surface clean. It shows neither any significant hydrogen pressure rise above the background on exposure to water nor any sign of copper-containing corrosion products from analyses by surface sensitive methods. Hence, the title chosen for this very report is only “Copper in ultrapure water”.

Sammanfattning

Denna SKB-rapport utgör ett supplement till den tidigare R-13-31, i engelsk översättning R-14-07 (”Corrosion of copper in ultrapure water”). Båda rapporterna omfattar undersökningar av ultraren koppar nedsänkt i ultrarent syrgasfritt vatten. Det kemiska systemet var inneslutet i behållare av rostfritt stål som tillät bildad vätgas att passera ut genom en metallfolie av palladium. I somliga uppställningar mättes trycket kontinuerligt, och i andra analyserades kopparen och dess närmaste omgivning efter olika tider för att ge upplysning om oxidationsprodukter från kopparkorrosion. Den förra rapporten innehöll en fullödig beskrivning av utrustning, val och behandling av ingående material, mätstrategier, uppnådda resultat och deras kritiska utvärdering, alltsammans från en sexmånadersperiod. Den inkluderade kontinuerliga mätningar och registreringar av tryck samt detaljerade kemiska analyser. Den slutsats som då kunde dras – och som endast har stärkts i detta supplement – var att korrosionshastigheten för koppar i ultrarent vatten måste vara mycket låg, huvudsakligen baserad på det faktum att inga oxidationsprodukter kunde upptäckas med mycket känsliga elektronspektroskopitekniker såsom XPS och AES, resultat stödda av mätningar med andra metodiker. Som en följd måste tillhörande vätgasproduktion från vattnets reduktion vara mycket låg och därför vansklig att få ett mätvärde på. Nivån på uppmätt tryck tydde på att bakgrunden dominerade. Vad gäller kopparhalten i vattenfasen kom utvärderingen av en glasblank att vara avgörande för en bedömning huruvida utlösning av koppar från glaset måste beaktas, och det befanns att denna var av föga betydelse.

Utrustningen som användes i förra rapporten uppvisade experimentella svårigheter, dels oavsiktlig gasförlust till omgivningen och dels dominerande urgasning av väte från stålet. Två steg var avgörande för att möjliggöra bestämning av tillförlitliga bakgrundsvärden: Det ena berörde membranet av palladium och det andra egenskaperna hos det rostfria stålet. Genom en omkonstruktion av utrustningen kunde problemet med membranet lösas, till kostnad av lägre väteflöden genom membranet. Bidraget från koppars korrosion, som befunnits marginell, måste utgöra en mycket liten av det totala vätgastrycket, varför sedvanliga urbakningsmetoder bedömdes otillräckliga för att en acceptabel bakgrund skulle nås. Genom en minskning av behållarens godstjocklek och påföljande värmebehandlingar (upp till 450°C) reducerades stålets urgasning med en tiopotens. Tryckmätarna byttes ut i samma avsikt. Dessa åtgärder utmynnade i ett slutligt värde på urgasningen vid 10^{-12} Torr·L·s^{-1}·cm^{-2}.

Huruvida koppar själv skulle kunna vara en vätgaskälla undersöktes noga: Tidigare analyser med ERDA befanns vara mindre trovärdiga för dessa små halter vilket medförde val av smältanalys i stället som metod. Vätgasbehandling och upphettning efter den initiala elektrolytpoleringen såsom steg i reningsprocessen av koppar visade sig sänka vätehalten snarare än att väte infördes. Inte heller ändrade sig vätehalten i kopparn efter det att koppar fått ligga i vatten. Av detta följer att framkastade påståenden att reningsproceduren skapar en extra vätekälla i form av kopparmetallen tillbakavisas.

Ytterligare två fristående uppställningar för mätningar på koppar, vatten och glas öppnades. Därmed utökades tidsutdräkten från den tidigare studien (1, 3 och 6 månader) till att omfatta data från 15 och 29 månader. De använda analysmetoderna var desamma som i den förra rapporten varvid speciellt resultaten från AES är betydelsefulla. Fortfarande visade Augerspektra förekomst endast av ren koppar och ingen oxidationsprodukt. Ingen uppenbar kontamination kunde noteras från XPS. Syrebidragen från O *1s* tillerkändes adsorbat från vattenmiljön, OH_{ads} och H_2O_{ads}, som följer med kopparprov in i spektrometern. Detsamma gäller låga halter av antimon (som toppar av Sb *3d*), betydligt mindre än de ovan angivna adsorberade syrespecies. Antimonkällan är glaset, bestyrkt av XRF, som löses ut i vattenfasen (av storleksordningen ppb) vilken transporteras in i spektrometern genom adhesion till kopparn. Antimonhalten koncentreras genom att vattenfilmens tjocklek minskar till att omfatta endast ett monolager, men den är ändå så låg att den knappast kan påverka korrosionsegenskaperna. Om mot all förmodan så ändå skulle vara fallet skulle antimon snarast påskynda än inhibera korrosionen av koppar. Inga tecken på korrosion har dock noterats.

Två ombyggda uppställningar kom i användning, med lägre vätgasbakgrund och förändrade palladiummembranskopplingar. Tryckökningen följdes i vardera uppställningen med separata mätningar av bakgrundsnivåerna. Endast renad koppar användes, men ytmorfologi (och mikrostruktur) ändrades medvetet för några prover genom repning, antingen genom SiC eller diamant som polermedel. Idén bakom var att fastställa huruvida uppruggning av en slät yta påverkade

reaktiviteten i märkbar mån. SEM infördes här för studien av ytan på mikronivå. Som en kompletterende teknik tillämpades XRD med strykande infall (GI-XRD) för en motsvarande fasanalys. Denna visade otvivelaktigt att främmande material fastnade i det mjuka ytskiktet, partiklar av SiC som inte kunde avlägsnas genom sköljning. Deras närvaro skulle kunna vara orsak till ett annat observerat tryckbeteende från SiC-repning i kontrast till effekten av diamantrepning, där inget tryck kunde mätas utöver bakgrundstrycket trots att ytan i det fallet säkert påverkats mekaniskt i än högre grad. Det befanns att repning i båda fallen skapar små partiklar som fullständigt förstör utfallet av kopparanalys med ICP-MS på motsvarande vattenfas.

En uppställning från tidigare bibehölls för mätning av trycket och togs isär först efter drygt 3 år. Tryckvärdena därifrån kan inte jämföras med den ombyggda utrustningen. Innehållet av koppar, glas och vatten analyserades ändå och visade att varken koppar- eller antimonhalter hade ökat linjärt med tiden. En uppställning utan vare sig koppar eller vatten användes parallellt för studier av gasutbytet mellan de två kamrarna. I det sammanhanget noterades att närvaro av spår av syre påverkar trycket, eftersom palladium kan utgöra en katalysator för den reaktion som ger vatten.

Med den ombyggda utrustningen kunde inget vätgastryck mätas över den genom förbättringar uppnådda lägre bakgrundsnivån, inte ens efter skrapning av kopparytan med diamantpulver. Emellertid tycks behandling med SiC vara en metod som kontaminerar metallytan. Som en följd därav kan inte mätningar utförda på material som behandlats på det sättet utgöra tillförlitliga indikationer på koppars korrosion. Å andra sidan kontamineras inte den koppar som använts i denna studie – såsom rapporterat här och i SKB R-14-07 – vare sig genom använda ytreningsprocesser eller utförda korrosionsexperiment utan den bibehålls ren både på djupet och på ytan. Den visar varken signifikant förhöjt vätgastryck ovanför bakgrundsnivån under exponering för vatten eller några tecken på kopparinnehållande korrosionsprodukter utifrån känsliga kemiska analysmetoder. Utifrån dessa fakta har titeln på denna uppföljande rapport reducerats till att lyda ”Koppar i ultrarent vatten”.

Contents

1 Introduction

1.1 Background

In a previous report (Boman et al. 2014), results were reported from long-term experiments (up to 6 months) concerning the possible corrosion of copper in ultrapure water, free from molecular oxygen. Claims that copper is not inert towards water but corrodes rather heavily, as indicated by the evolution of hydrogen gas, formed the background for the investigations (Hultquist 1986, Szakálos et al. 2007, Hultquist et al. 2009, 2011). In the current study, the pressure evolution of hydrogen gas was recorded in equipment similar to that used by previous researchers (further references in Boman et al. 2014), but the main focus was put elsewhere, namely on identifying oxidation products containing copper as a more conclusive indicator of copper corrosion. The search for such species entailed copper itself and its near environment within the closed system of the experiment. Thus, the copper, the water and the glass in contact with copper and glass were all thoroughly characterised by various sensitive analysis methods (see Table 1-1), both before and after experiments. The materials were of highest purity, and strict measures were taken as to avoid contamination during handling, including steps before chemical analysis.

Table 1-1. Acronyms and their encoding of the characterization methods that have been used.

Analysis method	Physical principles*	Application (aggregation state)
XPS	X-ray photoelectron spectroscopy	Element analysis (*s*)
AES	Auger electron spectroscopy	Element and phase analysis (*s*)
XRF	X-ray fluorescence spectroscopy	Element analysis (*s*)
XRD	X-ray diffraction (in GI mode)	Phase analysis (*s*)
LECO	Fusion analysis	Gas analysis (*s,l*)
QMS	Quadrupole mass spectrometry	Phase analysis (*g*)
ICP-MS	Inductively coupled plasma mass spectrometry	Element analysis (*l*)
ERDA	Elastic recoil detection analysis	Element analysis (*s*)
SEM	Scanning electron microscopy	Microstructure (*s*)
TEM	Transmission electron microscopy	Submicro analysis (*s*)

* For details concerning the various methods, see Boman et al. (2014).

Further experiments were at that time waiting for evaluation, in particular analyses of samples exposed to water for still longer times, including a glass blank. In addition, some issues concerning hydrogen loss or uptake with proper analysis have now been addressed. The question arose whether the surface condition (dislocations, mechanical strain and macroscopic topography) might influence the reactivity. Therefore, some tests have been made where the surface of the copper was scratched, the effects were monitored and the results evaluated.

1.2 Structure of the presentation

The report consists of two parts, the main text and appendices. The appendices present some details of apparatus, calculations or certain analysis results.

The disposition of the main text is meant to primarily illustrate the progress of the work since the previous report: Chapter 1 (Introduction); Chapter 2 (Developments); Chapter 3 (Results and comments); Chapter 4 (Discussion), Chapter 5 (Conclusions) followed by References and Appendices.

2 Developments

2.1 Additions and alterations strategy

The equipment was thoroughly described in the previous report (Boman et al. 2014). The heart of the experiments lies in having pure copper in contact with pure O_2-free water. The water is contained in a beaker made of glass with the highest class of hydrolytic resistance commercially available. The beaker rests in a vessel of stainless steel equipped with a lid where a membrane of palladium metal allows for the free passage of hydrogen through it. Such a vessel may stand freely in a glove box for a certain period while hydrogen escape through the palladium membrane, until the vessel is opened by dismantling the lid, and the contents are transported away for analysis. We have now data available for longer times than the 1, 3 and 6 months previously reported, extending the exposure time under the very same conditions as before.

As a complementary method to XPS concerning the surface analysis of copper, we also used a dedicated AES instrument with a scanning mode, using an electron beam. There are certain advantages with this approach: In the scanning mode one can see where the electron beam hits and the analysed area is definitely smaller than that probed by photons in an XPS instrument. Moreover, because only electrons are involved the surface sensitivity is enhanced. The reason for this approach was to find out whether the composition of a grain boundary was different from bulk, since contaminants have a tendency to accumulate between the grains. This instrument was not "in house" so the number of analyses was therefore limited.

A few of the vessels were used for monitoring the pressure, *i.e.* these were connected to a system with data logging facilities. On monitoring the hydrogen pressure, it had been found that the design of the fitting where the palladium membrane was clamped between the two compartments did not preclude that hydrogen gas also escaped from the system: Hydrogen was able to leave the palladium membrane through its edges. Therefore, this lateral leakage made a trustworthy estimation of the total hydrogen production difficult. Still, the attained pressure rise was more than expected from a direct chemical correspondence with the amount of observed oxidation products involving copper. Furthermore, as a complementary control of the hydrogen sources, measurements were performed to check the hydrogen content of the copper after the purification procedures previously described (Boman et al. 2014).

Thus, constructive measures were taken to ensure trustworthy readings and also to lower the hydrogen background in the pressure experiments. This strategy included changes of equipment and material properties. For establishing a certain connection between the observed hydrogen pressure and a corrosion process it must be possible to discern a net pressure increase compared to the background level. Since the observed amount of oxidized copper (predominantly expected as Cu_2O) was found to be very low (Boman et al. 2014), the corresponding reduction product (hydrogen gas) must also be very low. As a consequence, very harsh requirements were needed to bring down the hydrogen background pressure. Two main approaches were conceived, one aiming at decreasing the hydrogen background from the stainless steel and other parts involved, and one to completely ensure that hydrogen could not leave the system of interconnected compartments.

2.1.1 Modification of the vessels with new lids and pressure gauges

Two of the stainless steel vessels (SS 304L) that were meant for monitoring hydrogen pressure were machined (lathed) to an outer diameter of 70 mm so that the total volume of the steel was considerably reduced with the size of the inner void of the reaction chamber intact (see Figure 2-1). Less volume made heat-treatment possible in a UHV furnace (Figure 2-2) which was made for one of them, equipped into the setup called Main 3. A previous vessel that was not UHV-treated but treated in air (see below) was used in the Main 2 setup (see Table 2-1).

Previously we noted (Boman et al. 2014) that hydrogen most probably seeped out laterally through the palladium membrane. The leaking rate was enhanced on increasing internal pressure, and ultimately a situation was reached where the hydrogen production rate and leaking rate were more or less equal. Consequently, another technical solution had to be found.

Figure 2-1. *A new setup for pressure measurements (Main 3) equipped with a new lid including the Pd membrane (cf. Figure 2-3). The outer diameter of the lower chamber has been reduced.*

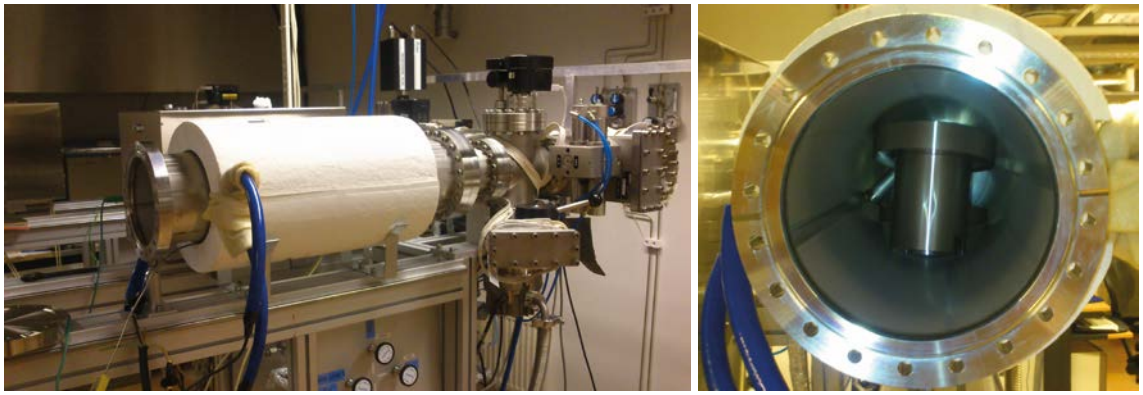

Figure 2-2. *UHV furnace with the size-reduced stainless-steel vessel for Main 3 inside.*

In the new design of the connection between the measuring and reaction chambers (*i.e.* the lid with its Pd membrane; see Figure 2-3 and details in Appendix A), no hydrogen at all can leave the system. In comparison with the former design (in Main 1 and reference setups), the diameter of the membrane is now reduced with a factor of 2. Therefore, the increase rates of the pressure curves cannot be directly compared with those of Main 1. The new design was fitted onto the vessels of Main 2 and Main 3. Testing of outgassing was made *without* Pd foil after another baking out at 150°C for 5 days ("postbakeout"). This was followed by a blank test *with* Pd foil and loaded reaction chamber but without copper.

Figure 2-3. *The new lid, here with blind VCR ¼" connection together with the outer CF-38 seal.*

New pressure gauges were connected to the Main 2 and Main 3 setups. Main 2 was equipped with one Pfeiffer CCR 374 (0–88 mTorr) and Main 3 with two, one for the 0–88 mTorr range and the other for 0–1.00 Torr (Figure 2-1). The reason for the change of pressure gauges was to strongly reduce the outgassing rate from these parts, since they may emit hydrogen themselves at a considerable rate and cannot be baked out (see Appendix A). Comparisons between the new and old setups are shown in Table 2-1.

Table 2-1. Comparisons between old and new setups.

Description*	Main 1	Main 2	Main 3	Complement
General	See Boman et al. 2014	New setup	New setup	New setup
Lower chamber	304L	304L	304L	304L
Upper chamber	304L	304L	304L	304L
Lid	304L	New: 316L	New: 316L	New: 304L
Outer diameter of chamber	114 mm	114 mm	70 mm (final wall thickness 3.5 mm)	114 mm
Diameter and weight of Pd membrane	20 mm 0.38 g	10 mm 0.10 g	10 mm 0.10 g	10 mm 0.10 g
Pressure gauges	MKS 627B	Pfeiffer CCR 374	Pfeiffer CCR 374	MKS 627B

* Including stainless steel quality.

2.1.2 Heat treatments of the setups

Two stainless-steel qualities have been used for the equipment, either 304L (upper and lower chamber) or 316L (lid). The L-suffixed qualities have lowered maximum carbon content compared to 304 and 316 with as a main effect better corrosion resistance vs. weld decay, *i.e.* especially developed for increased weldability. The European 316 qualities contain molybdenum, an alloy addition that in particular affects the tendency for pit corrosion in sea water (effects of chloride). For the application in this study, the choice between 304L and 316L is not germane in that respect (Jones 1992).

However, it is more relevant in the context of the present experimental situation to consider whether there is a pronounced difference in outgassing properties between 304L and 316L. A thorough study of the properties after proper heat treatments shows that there are no essential differences between them in that respect (Park et al. 2008). The authors also present a scheme how to reduce the outgassing by heat treatment in vacuum and air followed by postbakeout at a lower temperature.

The outgassing rate of hydrogen by the previous set-ups (Main 1 and old Main 2) were typically $2–3 \times 10^{-11}$ Torr·L·s^{-1}·cm^{-2}, yielding about 3×10^{-5} mol/year as hydrogen background. This value is two orders of magnitude larger than the hydrogen evolution corresponding to the maximum copper corrosion rate of about 3×10^{-7} mol/year, as estimated by Boman et al. (2014) from analyses of

copper-containing species. In order to significantly discern hydrogen emanating from a copper corrosion process, the hydrogen background pressure encountered in the experiment had to be reduced by at least two orders of magnitude.

For UHV steels such as 304L and 316L, an outgassing rate of about 3×10^{-11} Torr·L·s^{-1}·cm^{-2} is normal for a bakeout at 150°C for 50 h (O'Hanloon 2003). At this temperature water is efficiently baked out while hydrogen in the steel is less affected. In order to reduce the outgassing significantly, temperatures of about 400–450°C should be used (Park et al. 2008). This treatment could reduce the outgassing level down to the 10^{-13} Torr·L·s^{-1}·cm^{-2} range.

As a vital comment to the heat treatments, one must stress that some parts were not bakeable at higher temperatures. Such limitations are shown in the summary of Table 2-2. As a consequence, each component was baked individually at appropriate temperature before the assembling of the setup. All CF and VCR components, except the UHV valve, were baked out at 400°C or 440°C.

Table 2-2. Individual components and the maximum baking-out temperature.

Component	Maximal temperature
CF parts, lid and chamber	400–450°C
UHV valve (copper seal)	400°C, under vacuum
VCR-fitting	537°C
Svagelock valve VCR	315°C
Pfeiffer CCR 374 pressure gauge; MKS 627 B pressure gauge	50°C

Two different methods (see Table 2-3 for details) for more efficient bakeout than attainable at 150°C were tested:

- **Main 2**. Baking in air to oxidize the surface of the stainless steel; the high temperature is expected to reduce the hydrogen content. The oxide surface layer is also expected to increase in thickness which should reduce the outgassing from the bulk of the steel (Bills 1969). This method did not give a low outgassing rate (2×10^{-5} mol/year; see Appendix A) and an additional annealing was therefore performed at 300°C in UHV.
- **Main 3.** In this second approach a large UHV furnace was used for heat-treating the individual components under UHV conditions. A low hydrogen pressure is expected to yield a faster outgassing rate of the hydrogen (Park et al. 2008).

The chosen schemes of the heat treatments of the vessels are shown in Table 2-3. As summarized there, the treatments are fundamentally different (heating partly in air or not) for the setups used for Main 2 and Main 3. Thus, the outgassing behaviour may be different between the two, although the stainless-steel qualities and internal volumes are the very same.

Table 2-3. Heat treatment schemes for the stainless-steel compartments.

Vessel for Main 2:			Vessel for Main 3:		
Temperature	**Time**	**Atmosphere**	**Temperature**	**Time**	**Atmosphere**
150°C	overnight	argon	150°C	overnight	UHV, typically 10^{-9} Torr
400°C	96 h	argon	300–400°C	5 days	UHV, typically 10^{-9} Torr
400°C	2 h	air	440°C	3 weeks	UHV, typically 10^{-9} Torr
300°C	240 h	UHV, typically 10^{-9} Torr			

2.1.3 Complementary setup outside glove box

A special setup was designed for testing various background and pressure relaxation effects (see Figure 2-4). It was not thoroughly baked out (only kept at 150°C), being an old setup equipped with a new lid made of 304L stainless steel (see Table 2-1) to fit the new improved membrane connection. In contrast to the live experiments in the glove box, this setup was modified to allow pressure measurement also in the lower chamber (corresponding to the reaction chamber with copper and water).

Two MKS pressure gauges were attached to the upper chamber for up to 0.05 and 1.00 Torr, respectively. Another gauge (1.000 Torr) measured the pressure of the lower chamber, attached through a ¼″ tube welded to it.

This setup does not have direct bearing on the copper corrosion experiments but focuses on issues concerning the gas exchange between the reaction and measuring chambers. Furthermore, the background has not been decreased by extensive heat treatment but only at 150°C. Therefore, the hydrogen pressure regime in this setup is certainly higher than in those used in the corrosion experiments. Still, essential features of the exchange could be investigated and shed light also on the situation occurring for the setups containing copper in corrosion experiments. Since the setup deviates in many respects and all effects cannot be conveyed directly to the corrosion experiments, data concerning this setup are found in Appendix C, rather than here.

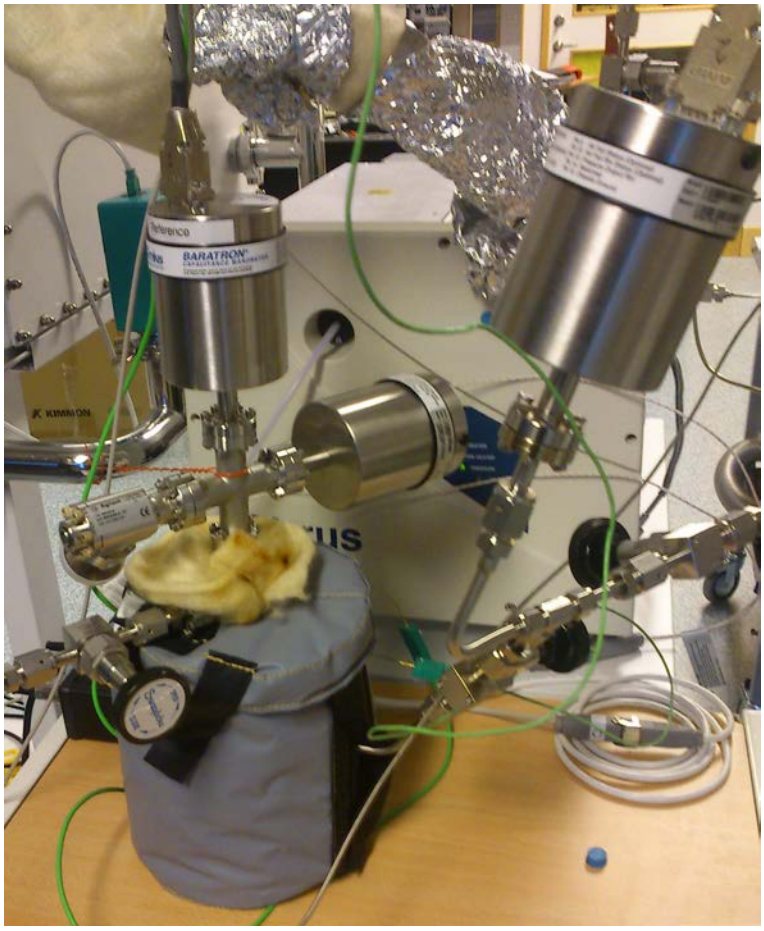

Figure 2-4. *Complementary setup for pressure measurements outside the glove box.*

2.2 Determination of hydrogen content

It has not been established whether the hydrogen content of copper itself might influence the corrosion properties, *e.g.* whether a high content of dissolved hydrogen might reduce the reactivity of the copper. This suggestion has emerged as a tentative explanation of the low corrosion rates observed by Boman et al. (2014), connected to the practised purification of copper containing a step of heat treatment in hydrogen gas. No support of that idea has been found in the literature. On the contrary, the solubility of hydrogen is low and decreases on heating in hydrogen gas, being about 90 ppb at 600°C (Martinsson and Sandström 2012). Only above 675°C may the hydrogen content increase through uptake from the gas phase (Martinsson et al. 2013). In Boman et al. (2014) the problem of establishing the concentration of dissolved hydrogen had been addressed by using two methods, ERDA and fusion analysis.

Although seemingly promising because very low contents should be detectable by ERDA, the fact that the equipment was not tuned to solving this kind of problem led to difficulties in interpretation. After the publication of the report by Boman et al. (2014), it has become clear that the technique often tends to overestimate the contents of hydrogen (and, as a further drawback, it is not able to distinguish between free or chemically bound hydrogen). In Boman et al. (2014, Section 5.2.3 and Appendix D2), an ERDA analysis was reported and its level of significance was also discussed. No direct measurement could be made, leading to analyses resting on modelling only. Therefore, it is recognised in retrospect that ERDA was not a good method to be applied to the problem of so low hydrogen contents for attaining high accuracy. As a consequence, this method was discarded for further analyses.

For hydrogen analysis, the melting analysis method (LECO) was used by the supplier (Alfa Aesar) as shown for only one of the batches of copper that were used in our experiments. However, it seems to be common practice by this technique to mechanically remove the surface layer of specimens before the metal is melted during a rather short heat run. This procedure to get rid of oxide (that would influence the apparent hydrogen content) cannot be easily applied to thin sheets, so we suspect that the analysis results quoted in the supplier's analysis certificate have in fact been performed on pieces of copper taken out of a batch before processing the copper into thin sheets. If that is the case, the value presented in the analysis certificate is not necessarily applicable for the processed copper – but the supplier has not responded to our specific questions on this issue. Moreover, the values presented in Boman et al. (2014, Section 5.2.4 and Appendix D1) were obtained on too little material (too low mass) or without repetition which precluded satisfactory statistics.

This kind of measurements was afterwards applied again under more controlled conditions in coordination with another analysing company (Degerfors Laboratorium AB), where we were also able to influence the measuring strategy since our sample deviated from what was fit for their routine procedures. Samples are – if need be – surface-polished by a diamond cloth, and transferred to the instrument, a LECO ONH-836 Elemental Analyser. The samples then get melted in a graphite crucible under He atmosphere. The hydrogen that is released reacts on a copper oxide catalytic converter to form water. The water content is determined by IR spectroscopy with calibration towards standard materials. As encountered before, problems with small sample sizes prevailed (see Appendix E for a discussion).

Considering the issue of hydrogen content of copper in connection with sample treatment, samples were also investigated in another way. In the purification process of copper described in Boman et al. (2014, Section 2.2.1 and Appendix C1–C3), the last two steps involve the reduction of superficial oxides (from electropolishing) by H_2 at 300°C followed by annealing in vacuum at 400°C. During the latter step, the outgassing of hydrogen was then monitored by mass spectrometry. The same methods were now also applied to various copper samples in order to study the outgassing, but using a broader temperature range to yield more information on the copper quality and on the processes involved.

3 Experimental results with comments

3.1 Overview

In order to make the results easier to follow, we first present an overview of the various experimental "stations" that have been operating, aiming at a complete picture of the situation. For clarity, we therefore also include measurements on samples already reported on. Appropriate data are all collected in Table 3-1.

Table 3-1. The various experiments and their evaluation.

Experiment station	Type of experiment	Chemical analysis techniques*
Free-standing, 0 months**	Oxidation products	XPS/AES, ICP-MS, XRF, LECO****
Free-standing, 3 months**	Ditto	XPS/AES, ICP-MS, XRF, LECO
Free-standing, 6 months**	Ditto	XPS/AES, ICP-MS, XRF, LECO
Free-standing, 15 months	Ditto	XPS/AES, ICP-MS, XRF, LECO
Free-standing, 29 months	Ditto	XPS/AES, ICP-MS, XRF, LECO
Free-standing, 41 months	Glass blank (no copper)	ICP-MS
Main 1 (from beginning)***	Primarily pressure measurement	XPS, ICP-MS, XRF
Main 2 (new equipment)	Ditto	XPS/AES, ICP-MS, GI-XRD
Main 3 (new equipment)	Ditto	XPS/AES, ICP-MS
Complementary setup	Ditto	*Not applicable*

* For the acronyms, see Table 1-1;
** Description and results in Boman et al. (2014);
*** Data in Appendix F.
**** All LECO data in Appendix E.

In Boman et al. (2014), data were collected and the results were reported for the exposure times 1, 3 and 6 months concerning the long-term semi-open vessels, *i.e.* those that were not connected for pressure measurement but allowed passage of hydrogen out into the glove box. Now those that were run for still longer times have been investigated, and the trend may be followed in an extended time frame. The analyses apply to copper and its near environment (water), as well as the glass in contact with that water. The analysis methods were described in Boman et al. (2014) and are discussed here only where considered appropriate. The samples from the setups for pressure monitoring (in Main 1, 2 and 3) have not been analysed to the same extent. In order to follow the extraction from glass only, a blank was included for which analysis only of the water phase was considered worthwhile.

The modified Main 2 and Main 3 setups were assembled for pressure measurements. As an interesting addition to previous procedures, two samples of purified copper (99.9999%, surface treated) were now also scratched, considering that surface morphology and mechanical strain might influence the reactivity towards water. The scratching of the copper foils was made manually on both sides inside a glove box with nitrogen atmosphere. However, the manual scratching implies inadequate reproducibility compared to the case with an automated technique. In order to conjecture possible galvanic cell formation, two materials of different electronic conductivity were chosen for the surface treatment, SiC paper (Struers, 320 grit size – 40 μm) and diamond powder (Diamantprofil AB, type MB-1-UM, 30 mesh). In the latter case, two copper foils were rubbed against each other with a small amount of diamond powder in between, *i.e.* no foreign matter that could influence the corrosion was introduced in the polishing process in that case. The surfaces of the scratched samples were investigated by SEM, the results being given in Section 3.6 (*vide infra*). However, particles might not be detected by SEM, but still their effects on topology.

That scratched samples may behave differently than untreated ones gets some support by the observation (Johansson et al. 2015) that scratched copper evolved hydrogen during a limited time (up to a few days) after immersion. In order to not confuse this possibly temporary process with longer-term hydrogen evolution, the diamond-scratched copper foils were subsequently kept in oxygen-free ultrapure water for six days prior to loading them into the reaction chamber. This measure was not taken for those scratched by SiC.

After loading Main 2 and Main 3, the setups were evacuated (only upper chambers possible) for a couple of days before starting to monitor the pressure. Both setups used the revised steel containers equipped with the new lid construction for the palladium foil, so as to not to allow any hydrogen to leave the system. The new equipment had to be thoroughly investigated with regard to the hydrogen background levels since the outgassing rate must be different from before by all the changes, not the least through the extensive heat treatments and change of pressure gauges. The contents of both setups were in due time subject to complementary chemical analyses (Table 3-1).

The complementary "bench setup" was used for testing various ideas concerning effects that might be relevant for the interpretation of the experimental outcomes of the pressure measurements of Main 2 and Main 3, with the focus on the palladium foil interface. These experiments (Appendix C) never included copper or water.

The "old" Main 1 setup has been running since the start of the experiments (Boman et al. 2014) and not undergone any instrumental changes. Pressure measurements have been made continuously over all this time. Data for this setup are given in Appendix F, where recent experiments concerning behaviour on temperature change are included. After disassembling the setup, chemical analyses were made on the copper sample, the added glassware and the water as for the other setups. Because of the temperature changes, the analytical results cannot be compared directly with the other samples as a function of time.

3.2 Pressure measurements

3.2.1 General remarks

For establishing whether there is any significant hydrogen production from copper due to corrosion in the water, the influence of the background has to be taken care of through trustworthy measurements of the pressure. It is then crucial that all important aspects of the experimental situation are taken into serious consideration. Because of the low production rate of hydrogen from the anticipated very limited corrosion process, the total hydrogen emission present in the equipment has to be evaluated properly. The geometry of the setup is principally a division into two parts, one where the corrosion may occur (the reaction chamber) and one where the pressure is measured. The interface between the two compartments is the palladium membrane through which only hydrogen can pass. One cannot neglect the influences of the Pd metal to correctly interpret the outcome of the pressure measurements.

The difference in experimental outcome of the equipment as regards hydrogen pressure measured is demonstrated in Figure 3-1. The two measurements were performed with the Main 3 setup. It is unequivocally illustrated that the pressure readings, that are supposed to yield the hydrogen gas production rate, cannot be trusted from the assembly that encompasses the Pd membrane without corrections for its intrinsic effects. (The data of Figure 3-1 were corrected only for difference in gas volume between the two cases. The measurement without Pd was made with an empty reaction chamber, while that with Pd also included the water-filled beaker.)

Hydrogen is the only gas that may pass the palladium membrane. What happens at the metal surface is a homolytic dissociation of the H_2 molecules into separate hydro-gen atoms. These are small enough to diffuse into the metal crystal structure to form a solid solution. The driving force for any diffusion process is a difference in chemical potential, in most cases as a result of different concentrations. The dissolved hydrogen atoms thus tend to distribute themselves over the available voids in the palladium crystal structure. If there is a difference in hydrogen pressure between the two sides of the membrane a steady state situation is eventually reached for the flow through it. With the present arrangement there may be different production rates for the two compartments, so the final situation reflects that fact. Before the steady state is reached, there are temperature and concentration dependent mechanisms that occur simultaneously and in succession (Ward and Dao 1999, Caravella et al. 2013). The final solubility of hydrogen within the membrane, valid in the single-phase regime found for low hydrogen contents according to Flanagan et al. (1976), is expressed by Sieverts' law:

$$X = K_s\sqrt{P} \qquad (3\text{-}1)$$

Here, the K_s factor depends on the species that are involved and on temperature.

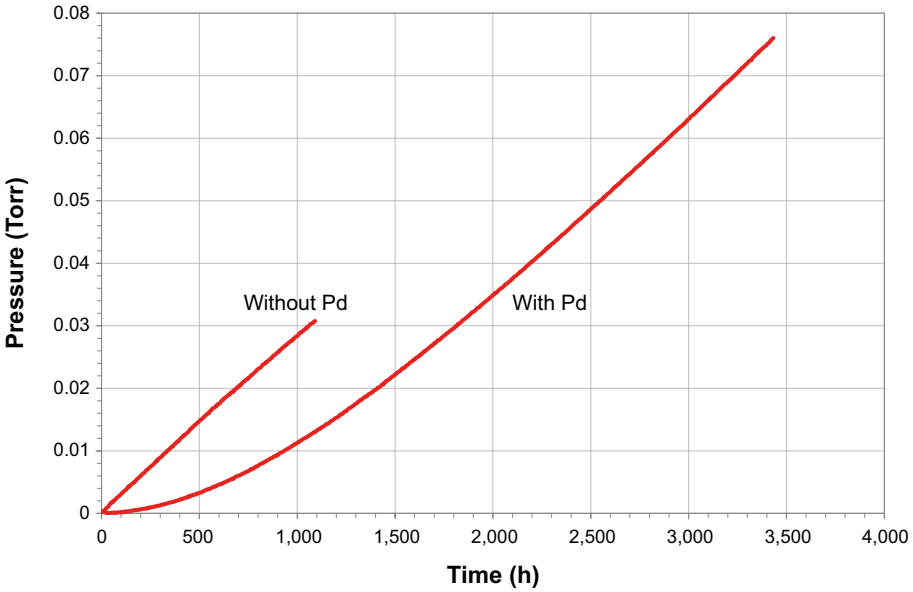

Figure 3-1. *Pressure rise in a system with or without the Pd membrane between the two compartments.*

To compensate for the fact that the membrane takes active part in the hydrogen distribution, a simple model was used (see Appendix B). The model illustrates that hydrogen is to be found in the form of H_2 gas as well as atoms within the membrane, the molar amounts being summed, but it fails to describe the situation properly at low pressures. Hence, the hydrogen production rates get underestimated. A basic assumption behind this model is that equilibrium is pertained between the two chambers and the Pd membrane. Tests concerning this aspect were performed by the complementary equipment (Appendix C), indicating relatively long times for equilibrium to establish (but there at pressures higher than in Main 2 and Main 3).

$$P_{WoPd}=P_m + K_{exp} \sqrt{P_m} \qquad (3\text{-}2)$$

where:

P_m = The measured pressure.

P_{WoPd}= The pressure without Pd.

K_{exp} = Experimental constant, including K_s and volume factor.

In order to make the results and the interpretation of the pressure experiments easier to follow, the experimental schemes are presented in connection to the illustrations of the graphs, rather than giving them in Chapter 2. All measurements (at 50°C) were started with measurement of the background before loading with respective copper sample. The old setup, Main 1, forms a special case, discussed in Appendix F.

The outgassing background was measured by two methods:

1. Vacuum outgassing, by measuring the increase in total pressure vs. time (without the palladium membrane). This was done after baking the setup for about 5 days.
2. Background under experimental conditions, *i.e.* the pressure increase in the upper chamber with the Pd membrane mounted and water/sample holder in the reaction chamber. This was performed after loading the chamber with deaerated water inside the glove box.

The outcome according to the first method (blank) applied to Main 2 and Main 3, is illustrated in Figure 3-2 with numerical data for the outgassing rate in Table 3-2. The volumes are the same, so the difference must depend on the respective treatment of the stainless steel (see Table 2-3) and the temperature. The pressure rise due to hydrogen evolution from the container materials and measuring devices is essentially linear with time.

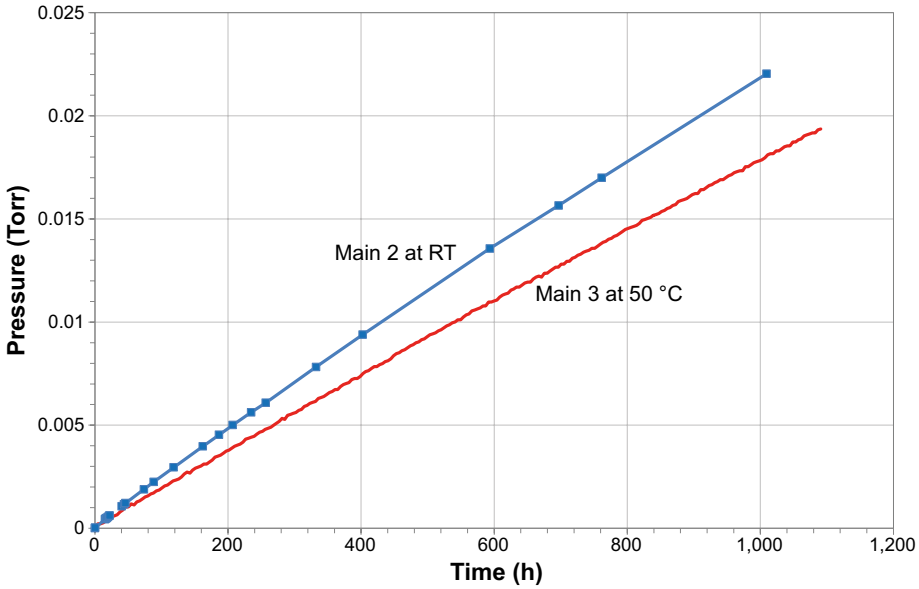

Figure 3-2. *Background measurements in Main 2 and Main 3 (at different temperatures; RT = room temperature, 25°C).*

Table 3-2. Outgassing rates for the empty* setups (no Pd foil).

System	Outgassing mol/year	Temperature
Main 2	3.4×10^{-6}	25°C
Main 3	2.5×10^{-6}	50°C
Main 1*	$2–3 \times 10^{-5}$	50°C

* For comparison, data are included from Boman et al. (2014), however, for a loaded system including Pd-foil. The values are only estimations from the maximum pressure increase.

For Main 2 the background outgassing rate (see Appendix B) was determined from pressure measurement at room temperature (*cf.* Figure 3-2) directly after baking at 300°C (*cf.* Table 2-3). Main 3 was assembled, and the upper chamber was baked out at 150–200°C for a few days before the measurement series.

Loading. After introducing the Pd membrane (see further Section 3.2.2), Main 2 was used for two series of measurements with copper residing in sample holders in water:

- SiC-scratched copper (Sample M2-SiC),
- unscratched copper (Sample M2-EPH2).

Both samples were of 99.9999% purity and first polished and purified as described in Boman et al. (2014, Section 2.2 and Appendix C).

After background tests (see further Section 3.2.3), Main 3 was similarly loaded with diamond-scratched copper of identical quality (Sample M3-diam).

For an easier overview of the various experiments performed with the new setups, Main 2 and Main 3, Table 3-1 is here complemented with details concerning the actual samples used:

Table 3-3. Experiments performed in the loaded new setups.

System	Sample	Sample characteristics
Main 2	M2-SiC	Purified copper, scratched with SiC paper (30 cm^2)
Main 2	M2-EPH2	Purified copper, unscratched (48 cm^2)
Main 3	M3-diam	Purified copper, scratched with diamond powder (48 cm^2)

3.2.2 Main 2

The background was first measured *without* Pd membrane and water (see Figure 3-2 and Appendix B). The measurements (*with* Pd membrane) followed the scheme below, where four distinct regimes (I-IV) are discerned (*cf.* Figure 3-3):

I. 1. Evacuation.
   2. Background measurements with water and sample holder.
   3. Evacuation.

II. 4. Adding of *SiC-scratched* copper foils (M2-SiC).
   5. Evacuation (roughly three days).
   6. Pressure increase.
   7. Evacuation (the maximum of 88 mTorr being reached).
   8. Pressure increase.
   9. Evacuation (the maximum of 88 mTorr being reached).

III. 10. Start of background measurements without copper samples.
   11. Pressure increase.

IV. 12. Loading of *unscratched copper* foils (M2-EPH2,without evacuation).
   13. Pressure increase.
   14. Evacuation (just before the pressure limit).
   15. Pressure increase.
   16. Evacuation (pressure limit just reached); experiment halted.

V. 17. Start of background measurement with water and sample holder.
   18. Pressure increase until pressure limit cut-off (19).

The various curves of Figure 3-3 need to be commented and analysed. Please note that the M2-SiC sample was measured twice (II, curves 6 and 8) with evacuation in between. Likewise, the background was measured three times, before (I, curve 2) and after the live samples (III, curve 11 and V, curve 18). What is directly obvious from the results is the behaviour of pressure rise immediately after evacuation. The pressure increase is strongly deviating from a linear relationship with time which is interpreted as an effect of hydrogen uptake in the Pd membrane (*cf*. Figure 3-1). This effect influences the accuracy of the pressure increase and is especially cumbersome for determining the net hydrogen evolution from copper. In order to obtain a more correct background, the application of modelling seems proper. Attempts in this respect are described in Appendix B and were used for estimations of the hydrogen outgassing rates, as illustrated in Figure 3-4 that is divided into the same regimes as Figure 3-3 since they are related.

The background rates. The first background (curve 2 in Figure 3-4, regime I) starts at about 4 μmoles per year and increases with time to about 8 μmol/year after 800 hours (at 1,100 h in Figure 3-4). These values are considerably higher than obtained for the empty setup (3.4 μmol/year in Table 3-2). The second background (III, curve 11) was measured after finishing the measurements on sample M2-SiC (regime II) and is considerably lower. After a slight increase it levels out at ~4 μmol/year. That value is in better agreement with that obtained for the empty system. The third measurement was performed after that on M2-EPH2. The rate starts at about 2.5 μmol/year and increases to about 6 μmol/year during 3,000 h (V, curve 18).

The rates are not expected to depend very much on time. The observed behaviour is an indication of an unstable system, since the rates increase for all curves. The curves of Figure 3-3 did not convey this behaviour of the system. The origin of the increase is obscure and its solution lies outside the scope of this report. It is noteworthy that the Main 3 system (Appendix B3) does not show any similar instability; one difference is that it has undergone a different heat treatment (Table 2-3).

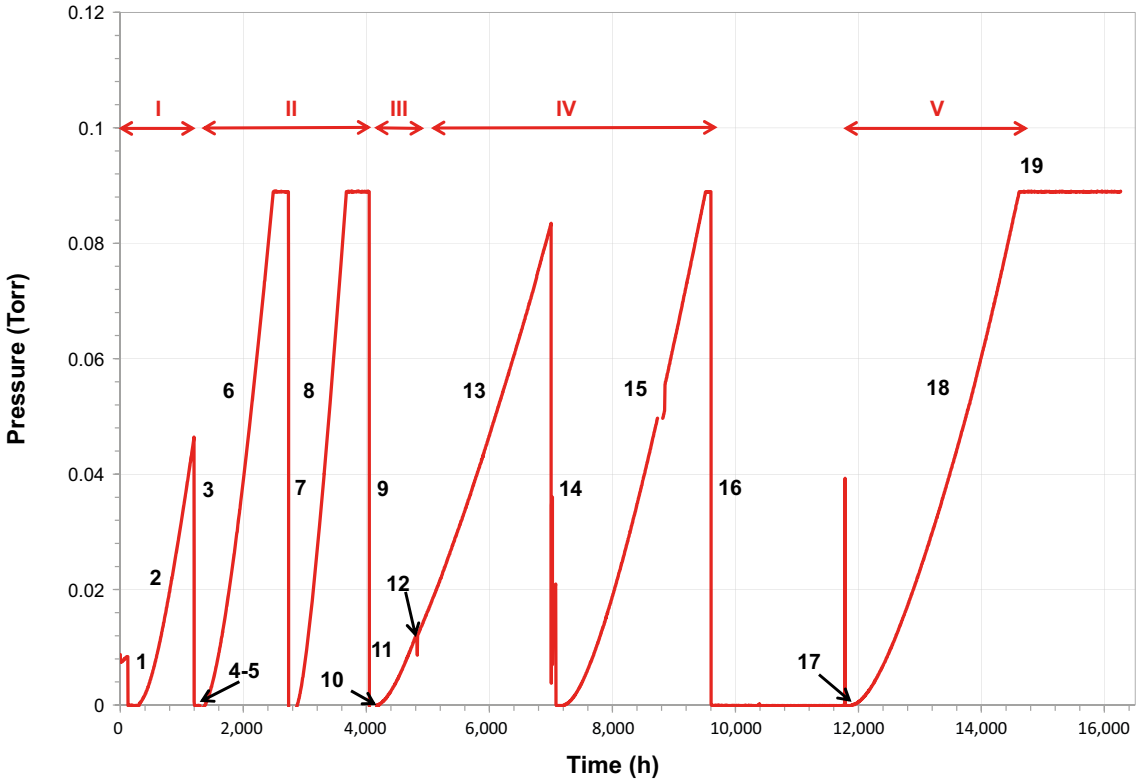

Figure 3-3. *Results of the pressure measurements for Main 2. The numbering alludes to the measuring scheme given in text. The cut-off at 0.088 Torr is an artifact due to the limitation of the pressure gauge. The imperfection at about 8,800 h is due to a flaw in the common logging system.*

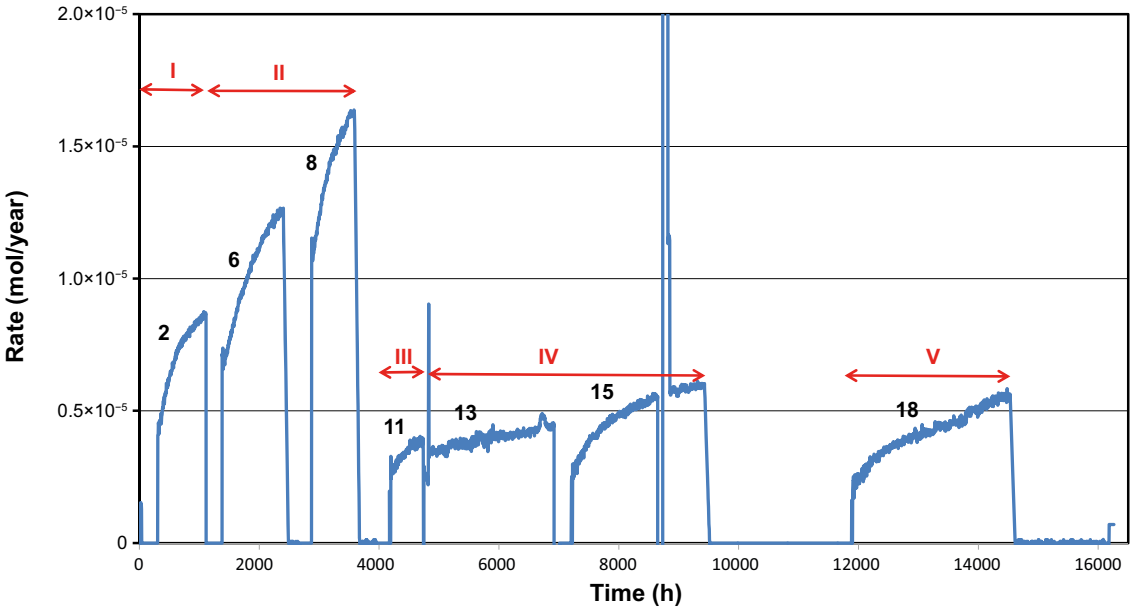

Figure 3-4. *Plot of the same data as in Figure 3-3 in the form of estimated hydrogen production rates. The irregularity in regime IV at about 8,800 h is due to a flaw in the logging system.*

System with SiC-scratched copper (M2-SiC). Like in the first background measurement, the rates observed for curve 6 and 8 (regime II) show an increase with time except when the process is interrupted. Curve 6 starts with about 7 µmol/year and ends with 13 µmol/year after 1,000 hours (at 3,600 h at the time scale) where the upper chamber was pumped out because the limit of the pressure gauge had been reached (See Figure 3-3). The monitoring of curve 8 (same regime) commenced after 200 hours of pumping, yielding values of 11–16 µmol/year during 800 hours. Again the 88 mTorr limit was exceeded and the upper chamber was pumped out, ending the measurement session of regime II.

Here also, the rate seems to increase during the experiment that had to be divided within regime II due to the limited pressure range of the gauge. Whether the pressure rate would have levelled out after a long time is impossible to tell. The rates are definitely higher than that measured for the background. This indicates an enhanced hydrogen production but we cannot exclude artefacts. Because of the unexpected behaviour of the rate curves it is not possible to deduce any reliable rates from the present data. Further investigations are needed to understand the hydrogen evolution from SiC-scratched copper, but indications were found (*vide infra*) that contaminations get introduced. The data are inconclusive as to whether that is an influencing factor here.

A QMS analysis showed about 97% hydrogen in the gas phase, an indication that the pressure increase is not due to a leak in the system. Otherwise, an enhanced nitrogen content would have been evident. The pressure increase must originate from hydrogen production somewhere within the system.

System with unscratched copper (M2-EPH2). The new sample was inserted (between III and IV) without pumping the upper chamber. A small pressure decrease was observed after the loading. The rate starts (IV, curve 13) at about 3.5 µmol/year and increases up to 4.3 µmol/year during 2,000 hours. Just before the pressure limit was to be attained, the upper chamber was pumped out. The series continued (IV, curve 15) with the rate increasing from 3 µmol/year to 6 µmol/year during 2,400 hours and was stopped at 9,500 h on the time scale.

When comparing with the background measurements (V, curve 18 and IV, curve 13), the appearance lies somewhere in between but the form also differs. The rate evaluation is probably affected by the pumping time before the loading, *e.g.* the third background starts with a rate of 2.5 µmol/year. These factors could not be taken care of in the modelling.

However, considering the values obtained, any hydrogen production with copper corrosion as its source must be very small (< 2 µmol/year). The corresponding hypothetical corrosion rate is considerably less than 7 nm/year, but the uncertainty is of the very same order of magnitude.

3.2.3 Main 3

The handling deviated little from that of Main 2, using the same temperature and copper quality. However, in this case the scratching of the purified copper was made by diamond powder instead of by silicon carbide paper. After keeping them in water for six days, the foils (Sample M3-diam) were loaded into the lower chamber (in another batch of water). After pumping for about three days, the valve was closed and the pressure increase was monitored.

A similar measuring scheme for the pressure monitoring was followed as for Main 2, only that the background was measured twice before the introduction of copper. Three distinct regimes (I–III) are discerned (*cf.* Figure 3-5):

I. 1. Evacuation.
   2. Background measurements without water and Pd foil (*cf.* Figure 3-2).
   3. Evacuation

II. 4. Background measurements with water and Pd foil.
   5. Evacuation.

III. 6. Loading of diamond scratched copper foils (M3-diam) + water.
   7. Pressure increase.
   8. Pressure gauge limit of 88 mTorr reached; the second gauge up to 1 Torr was found defective as regards data acquisition compatibility.

Background rates. The various rates for samples in the setup named Main 3 were calculated from Figure 3-5 (analogous to the procedure for Main 2) and are presented in Figure 3-6.

Background I (curve 2) does not contain any influence from the membrane. By direct measurement of the pressure increase, the outgassing background was determined from the slope of the pressure increase to 2.6 µmol /year (Appendix B).

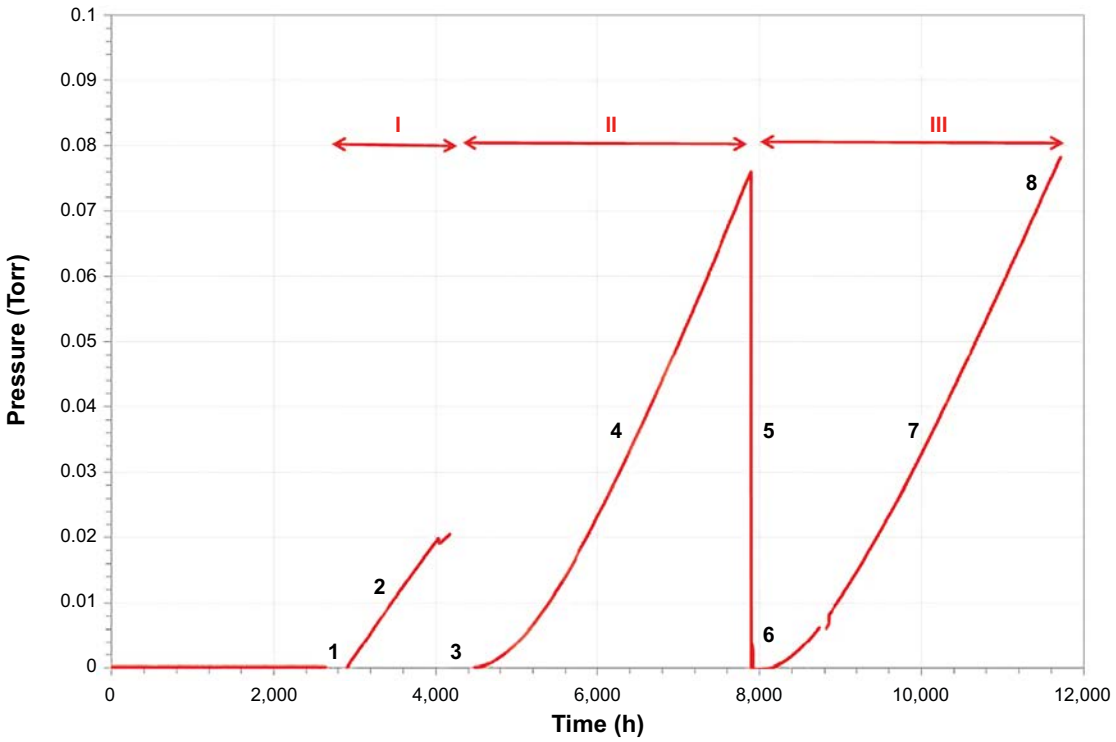

Figure 3-5. *Results of the pressure measurements for Main 3. The imperfection at about 8,800 h is a flaw in the common logging system.*

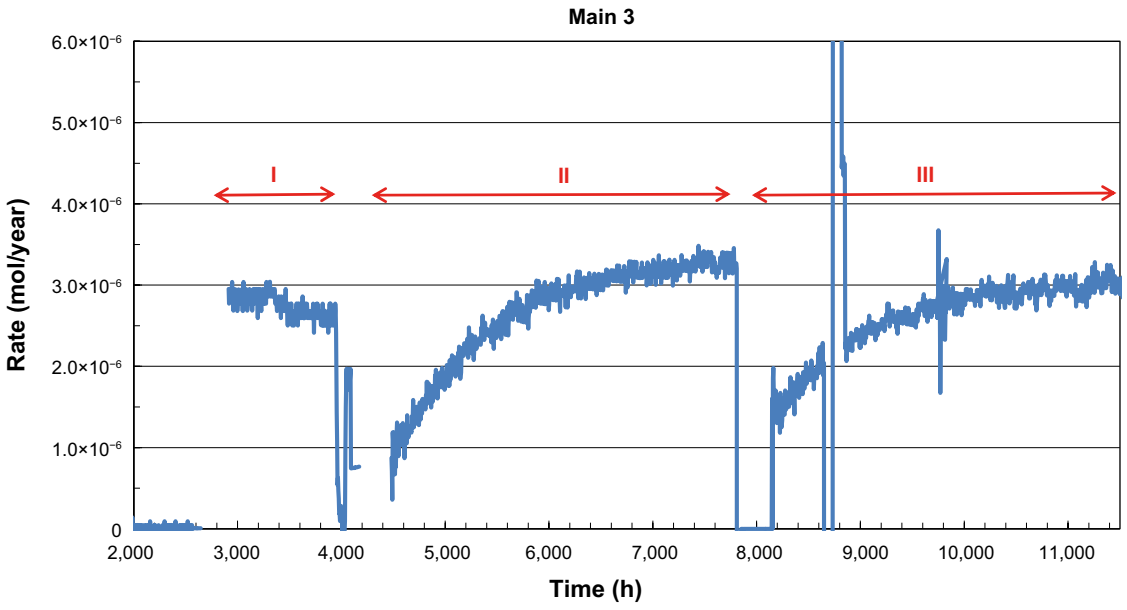

Figure 3-6. *Plot of the same data as in Figure 3-5 in the form of estimated hydrogen production rates. The irregularity in regime III at about 8,800 h is due to a flaw in the logging system.*

Background II (curve 4) had to be calculated because of the deviation from linearity, an effect of the hydrogen uptake from the Pd membrane. The modelling (as for Main 2, omitting the low-pressure part) gave 3.5 µmol/year (Appendix B3).

The diamond-scratched copper, M3-diam (III). The pressure increase is very similar to the background (II, curve 4; III, curve 7). The rate for the scratched copper starts at about 1.5 µmol/year and levels out at about 3 µmol/year which is slightly above background I and below background II.

Considering these values, any possible hydrogen production based on copper corrosion must be extremely small (<0.2 µmol/year). Again, the variation of the background makes it impossible to obtain high accuracy. From this value, considering an experimental error of the same magnitude and assuming that the hydrogen emanates from copper corrosion, the estimated corrosion rate is <1 nm/year.

3.3 Surface analyses of copper

3.3.1 Free-standing vessels

The main analysis method was XPS applied to copper. We present results obtained for samples kept for a long time in the free-standing vessels and also for copper samples taken from Main 2. Since our focus lies on oxidation products, the outcomes of XPS as to its copper Auger spectrum are the most important, and these results are presented in Section 3.3.1 and Section 3.3.2.

Figure 3-7 gives an overview of the XPS spectra obtained for the copper samples that have been exposed to water in the free-standing setups. In addition to the strong XPS peaks of copper, there are contributions by carbon, nitrogen and oxygen to be seen. Moreover, there are also Auger spectra of the most abundant elements where that of copper is the strongest. For this choice of radiation (Al $K\alpha$) these are found in the range 545–750 eV (Cu), ~980 (O) and 1,200–1,250 eV (C), respectively.

The strongest contributions from copper are found as two XPS peaks as shown in detail in Figure 3-8a. These are peaks emanating from Cu *2p* states, being split through spin-orbit coupling. Even as being deeply lying states, they are sensitive to chemical bonding to some extent. In particular, there is a "channel" to *3d*-levels if these are not completely filled. Therefore, if copper were in the Cu(II) state, with a $3d^9$ configuration, each *2p* peak would carry a broad satellite structure at higher binding energy. Thus, the presence of CuO would clearly show up in two ways; the strong Cu *2p* peaks would appear with a chemical shift towards higher binding energy (approximately by 2.3 eV) and each peak would be accompanied by a broad satellite towards higher binding energy (Boman et al. 2014). On the other hand, both Cu_2O and copper metal itself have a $3d^{10}$ configuration of copper, and their *2p* spectra differ too little to be distinguished from one another within the resolution of the instrument. Thus, these XPS spectra cannot directly reveal whether the sample is pure copper, pure Cu_2O or copper with some superficial Cu_2O.

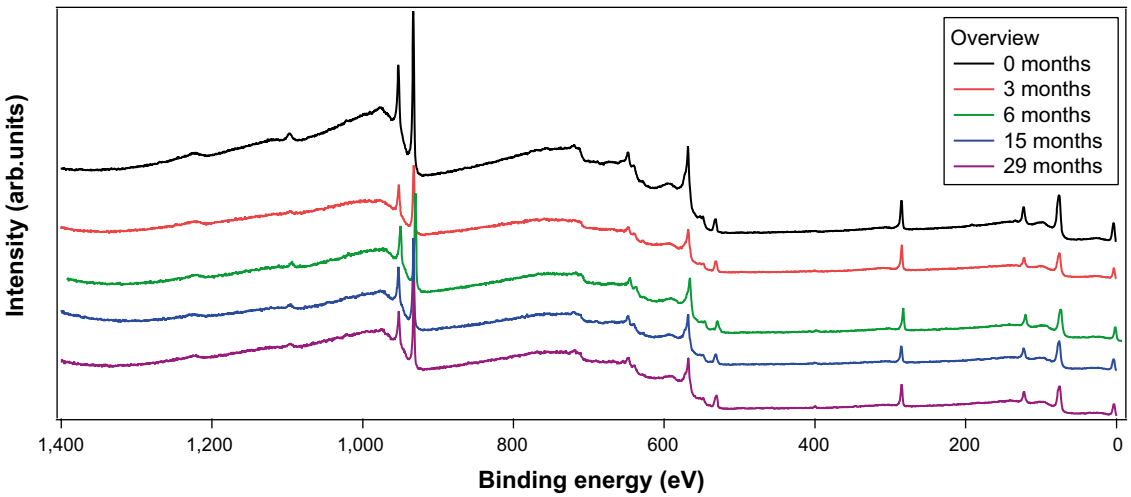

Figure 3-7. *Overview XPS spectra of the copper samples after 0, 3, 6, 15 and 29 months. The 0-month sample is copper directly from the final purification step, after which samples were stored in water for various times.*

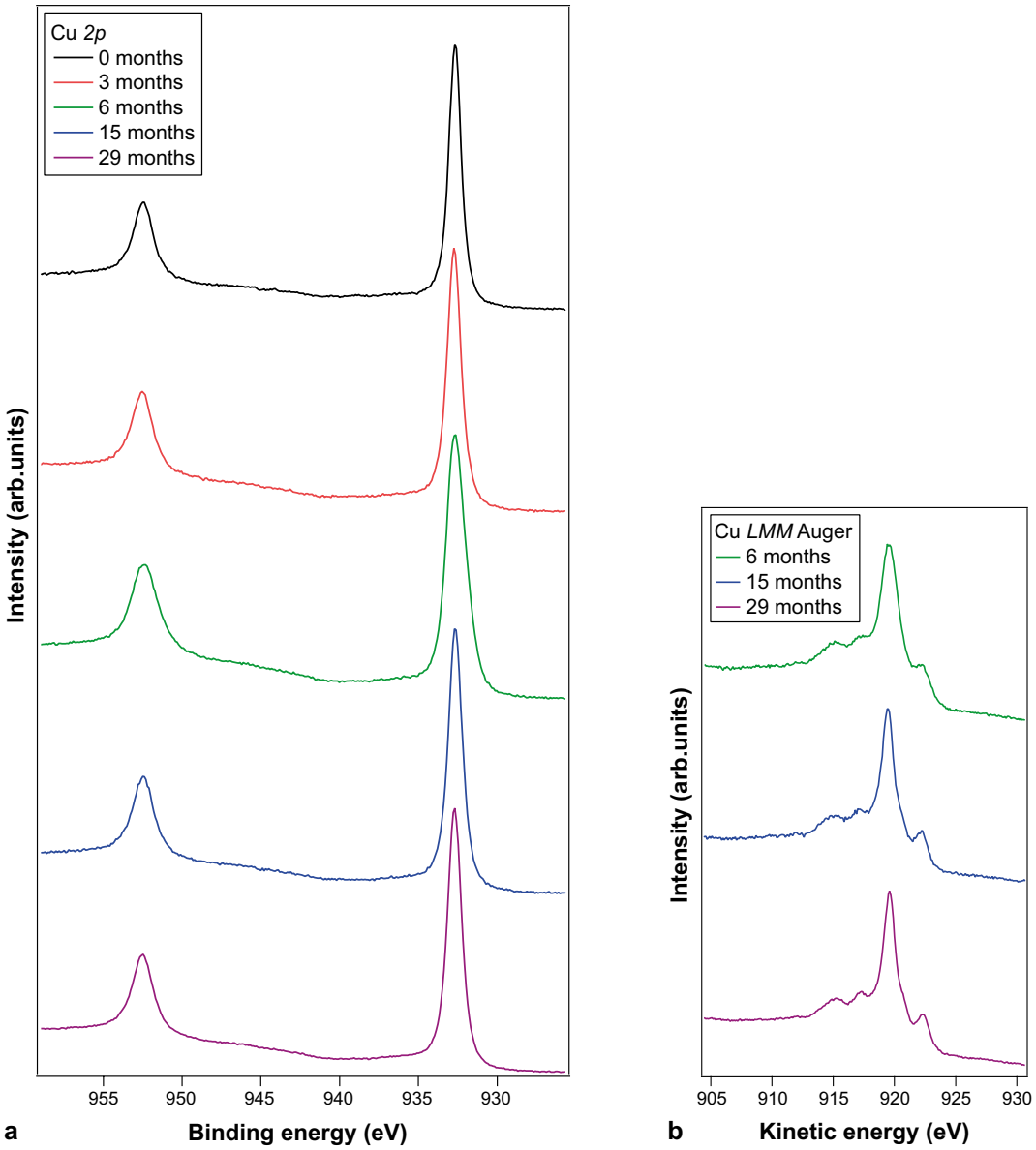

Figure 3-8 a–b. *(a) XPS Cu 2p spectra of copper samples after various exposure times. (b) Auger spectra of Cu $L_3M_{45}M_{45}$ for corresponding specimens as in Figure 3-8a (from scanning the region around 570 eV of binding energy in the XPS overview). N.B.: The energy is here expressed as increasing kinetic energy of the electrons.*

To discern Cu_2O deposited onto a copper surface, AES (spectra obtained from the XPS instrument by scanning the ~550–580 eV range of binding energy) was used. This more thorough analysis was initiated from the 6 months' sample and implemented onwards. As can be seen from Figure 3-8b, the Auger Cu $L_3M_{45}M_{45}$ spectra recorded after 6, 15 and 29 months all seem to be identical. As demonstrated in Boman et al. (2014, Figure 5-11a), the spectrum did not change after heavy sputtering where pure copper is definitely reached.

For recording all the spectra, a special transference capsule was used and care was taken for substantially decreasing the delay between opening of the experiment vessel (glove box) and making the surface analysis (spectrometer), while no contact occurred with air in between. The successful effect of these latter precautions is obvious from the quality of the spectra. As was commented upon in Boman et al. (2014) that covered samples from the first free-standing setups, the contribution of copper(I) oxide (Cu_2O) would have yielded a broad feature with its maximum in kinetic energy appearing at 917 eV (Panzner et al. 1985). Even after a couple of years there is no such indication. Figure 3-9 illustrates clearly the observable spectral changes in a series of sputterings of an oxide-covered copper surface until only pure copper is revealed (Cu L_3VV= Cu $L_3M_{45}M_{45}$).

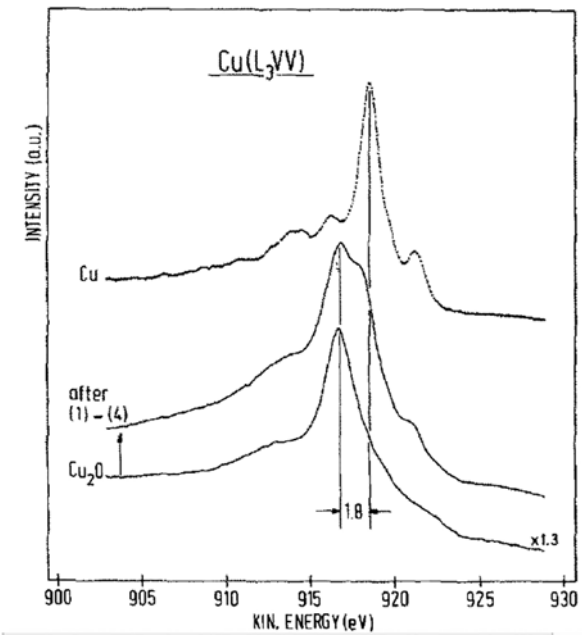

Figure 3-9. *Comparative Auger spectra of Cu_2O and Cu, the latter obtained after sputtering a copper surface covered by the oxide and eventually exposing copper (Panzner et al. 1985).*

In addition, spectra were taken in detail of the O *1s* contribution, expected for each species to appear as a single peak. Its intensity is very small, but the outcome is complicated, as illustrated in Figure 3-10a. A broad feature seems to be attributable to two dominating oxygen contributions centred at roughly 531 and 532.5 eV for all the investigated samples which indicates that oxygen is chemically bound as the electronegative part in more than one species. The 532.5 eV contribution has been attributed to superficial water (Cano et al. 2001, Yamamoto et al. 2007). That water may occur adsorbed is not surprising since the metal has been immersed in it. The claim that the 531 eV peak should belong to $Cu(OH)_2$ (Chavez and Hess 2001, Park et al. 2011) can hardly be valid here, for no Cu(II) satellites were observed in the Cu *2p* spectra. It is more likely to belong to OH_{ads} (Yamamoto et al. 2007, Andersson et al. 2008, Deng et al. 2008). An interesting aspect is that copper crystallite orientation is influential (Yamamoto et al. 2007) and might explain why the intensity ratio between OH_{ads} and H_2O_{ads} is not constant for all the samples. These two adsorbates together form a monolayer on the metal surface.

Noteable are the small peaks at 528 and 538 eV for the 6 and 15 months' samples. These might be attributed to *3d* contributions of antimony, but with energies as if in *unbound* form (Attwood 2000) which is surprising. This element denotation rests upon the peak positions and the magnitude of their spin-orbit coupling splitting. Antimony should in water rather be found as an SbO^+ species. However, while the spectra from 6 and 15 months are largely identical, there is a pronounced change found for 29 months. The first couple of peaks attributed to Sb *3d* are now gone while the new couple remain. The intensities are larger, and now it is possible to discern very weak lines at 34–35 eV, typical of Sb *4d* (Figure 3-10a, insert showing the doublet). It then seems that also the peaks at 529.5 and 539.5 eV belong to antimony, more in line with expectations for Sb(III). The splitting is almost the same, so one probable interpretation is that antimony occurs in more than one species and with different oxidation numbers. On increased time the binding energy of antimony appears higher, but we cannot exclude the effect of oxygen from the glove box atmosphere, even if the transference time to the spectrometer is short. It is natural to assume that antimony is bound to oxygen for a species in the water phase, and in Sb_2O_3 the binding energy of the *3d* states is 530.3 and 539.6 eV, respectively, being roughly 1 eV larger for Sb_2O_5 (Garbassi 1980). The O *1s* contribution of these oxide overlaps the Sb $3d_{5/2}$ peak, a note being considered in improving the fitting trials of Figure 3-10a.

An iron antimonate ($FeSbO_4$) showed similar values for the *3d* peaks of Sb(V), about 531 and 541 eV (Berry et al. 1987). It is interesting to note that in that case the oxygen O *1s* peak contribution, although the atomic ratio O:Sb is relatively larger in the antimonate than in the oxides, was not large at all. It appeared only as a shoulder of the strong Sb $3d_{5/2}$ peak, only affecting the intensity ratio between the

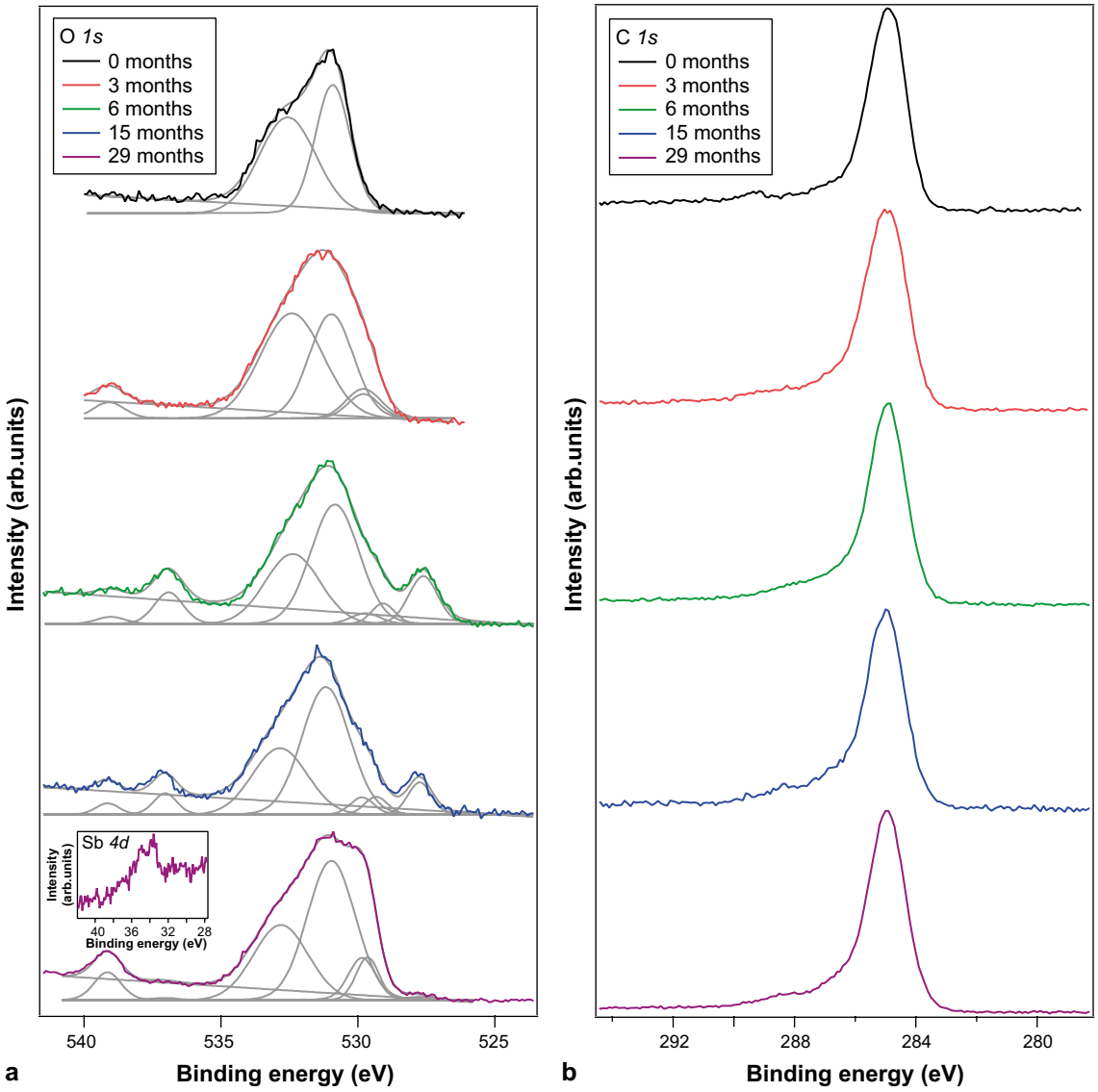

Figure 3-10 a–b. *(a) XPS peaks recorded in the vicinity of the O 1s peak. The two upper spectra are less trustworthy due to less efficient protection against air. Sketched are also suggested deconvolutions into separate contributions (see text). The insert shows a low-angle contribution attributed to antimony (b) The XPS peak of carbon for the different samples.*

contributions of Sb $3d_{3/2}$ and Sb $3d_{5/2}$ (1:2.2 instead of expected 1:1.5). This observation illustrates the inherent property that the *3d* peaks of antimony are much more intense than the *1s* peak of oxygen appearing in the vicinity. Therefore, their relative intensities by eyesight from Figure 3-10a do not at all reflect the relative abundance of the two elements. The oxygen content, having its strongest contribution illustrated by the peak from OH_{ads} at 531 eV, is very low but that of antimony must be appreciably lower still (estimated in Appendix G).

The source of the antimony in our experiments (left on the copper from a water film) is most likely the glass beaker and not only the added glass plate, deduced from the fact that these small peaks appeared also for a Main 2 experiment (sample M2-SiC, *vide infra* in 3.3.2) that was performed without an added glass plate. On the whole, the amount of antimony is very low, as deduced from XPS (*cf.* Appendix G) and considering the ppb content in the water (from ICP-MS, Appendix D), now concentrated in a thin film at the copper surface, perhaps even through enhanced chemisorption because of affinity to the metal.

A hypothesis that seems farfetched is that antimony from copper itself gets enriched at the surface. If that be true, it would explain why the binding energy is that of Sb(0), as of alloyed antimony as, for instance, found in a tin matrix (Hegde et al. 1981) or together with indium (Liu et al. 1995) with Sb $3d_{5/2}$ at 528 eV. However, such a process would need a high diffusivity of antimony in a copper matrix. Another suggestion for the occurrence of Sb(0) is a chemical reduction of Sb(III) in the beam. The question remains whether the Al$K\alpha$ source would be sufficient.

The deconvolution of spectra in XPS is an extremely delicate procedure. Specific contributions have to be determined out of a fixed sum, and the positions as well as the profile widths must be taken care of. Therefore, the choice presented in Figure 3-10a must not be considered as the only possible solution. Care has been taken to include the value of the spin-orbit coupling of Sb *3d* contributions and the theoretical relative intensities of these two peaks, but an uncertainty prevails. A contribution of oxygen bound to antimony was also considered and included. If there were an O *1s* contribution from Cu_2O, its position would be at 530.2 eV, an average value based on several measurements (Mariot et al. 1989). None of the indicated peaks seems to carry that position to yield a good fit.

As to carbon, nothing spectacular is noted. The position of the C *1s* peak correlates simply to that of adventitious carbon from hydrocarbons always present. The C *1s* spectra are given in Figure 3-10b while the small Auger contribution (C *KLL*) is found in the overview spectrum at about 1,200 eV but that contribution was not further analyzed.

3.3.2 Copper in Main 2 setup

The sample where the copper surface was first scratched by SiC paper (M2-SiC) before immersing the metal in water for 100 days was analysed by XPS.

Figure 3-11 shows the XPS spectrum of M2-SiC after exposure to water. There are no dramatic differences to the spectrum given in Figure 3-7, but some details are worth commenting on. There are some weak features (see tick-marks) between the peaks of C *1s* and Cu *3s*. The corresponding binding energies are 192 eV and 138 eV, respectively. A plausible interpretation is that both emanate from phosphorus (P *2s* and P *2p*, respectively). The spin-orbit coupling of the *p*-states is too small to allow any resolution for light elements.

In Figure 3-12 details of the total XPS spectrum are shown for an unsputtered surface. The Cu *LMM* spectrum, however not acquired with the highest resolution here, does not differ significantly from that of the unscratched samples of Figure 3-8b. The scale is here expressed as binding energy in order to include also the part around the oxygen O *1s* peak. In the Cu *LMM* spectrum, copper (I) oxide would have been revealed by a broad contribution centred near 570 eV (kinetic energy 917 eV; *cf.* Figure 3-9). Due to inferior statistics, one cannot conclude with absolute certainty that it is totally absent.

Similar to what was found in Boman et al. (2014, Figure 5-9), the now enhanced oxygen peak is again accompanied by peaks of antimony, the main source of which may be the beaker glass for two reasons: A scratched copper sample not in contact with water did not show any antimony, and there was no other possible source at hand (no added glass plate) in this experiment with water. It is peculiar that the antimony peaks have energies more similar to expectations for Sb(0) than for Sb(III) (or Sb(V)), and Sb(III) would have been accompanied by an oxygen contribution at about 530 eV (overlapping the antimony, as discussed in Appendix G).

A peculiar feature of the carbon spectrum of Figure 3-13 is that there are more than one contribution. The normal carbon peak comes from adventitious carbon (*cf.* Fig 3-10b). One explanation may be contributions from the SiC paper. Values given for SiC in the literature are 282.7 and 285 eV, the latter from C−C (Binner and Zhang 2001) as a result from contamination. Another carbon source may be from additives in the SiC paper in the form of organics containing carboxylic carbon (O−C=O). That such additives really are present was indicated in hydrogen desorption experiments where the presence of CO and CO_2 in the gas phase was established from mass spectrometry (QMS). These contributions are reflected in the high-energy shoulder and probably affect the O *1s* spectrum (Johansson et al. 2012).

These discrepancies as regards elements present compared with the spectra of polished and purified copper indicate that there are distinct additional contributions coming from the SiC paper. Another example is the detection of sulphur, as illustrated in Figure 3-14.

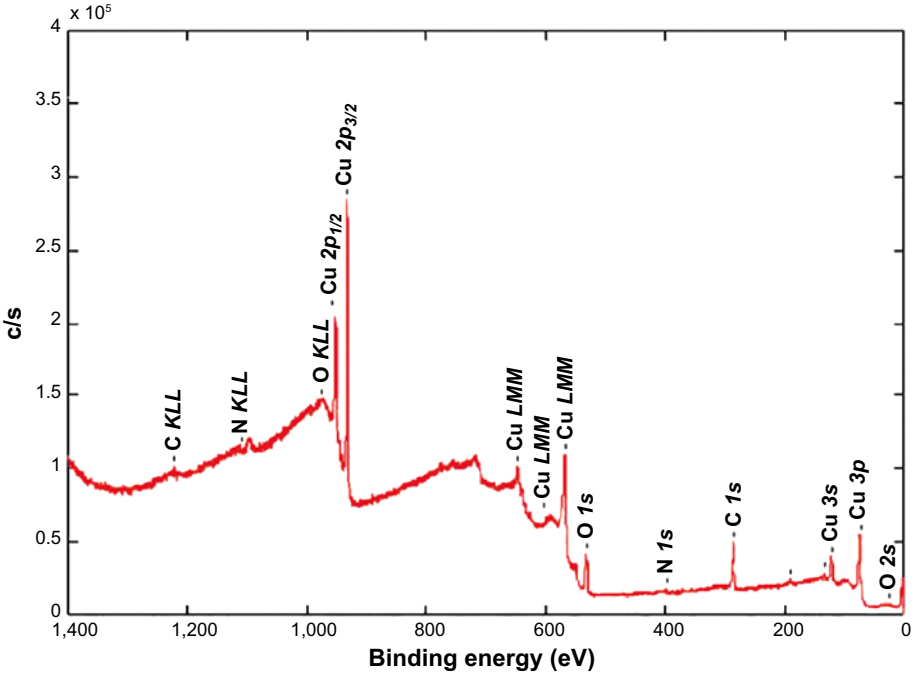

Figure 3-11. *Overview XPS spectrum of sample M2-SiC. (The weak features near O 1s emanate from the Auger Cu $L_2M_{45}M_{45}$.)*

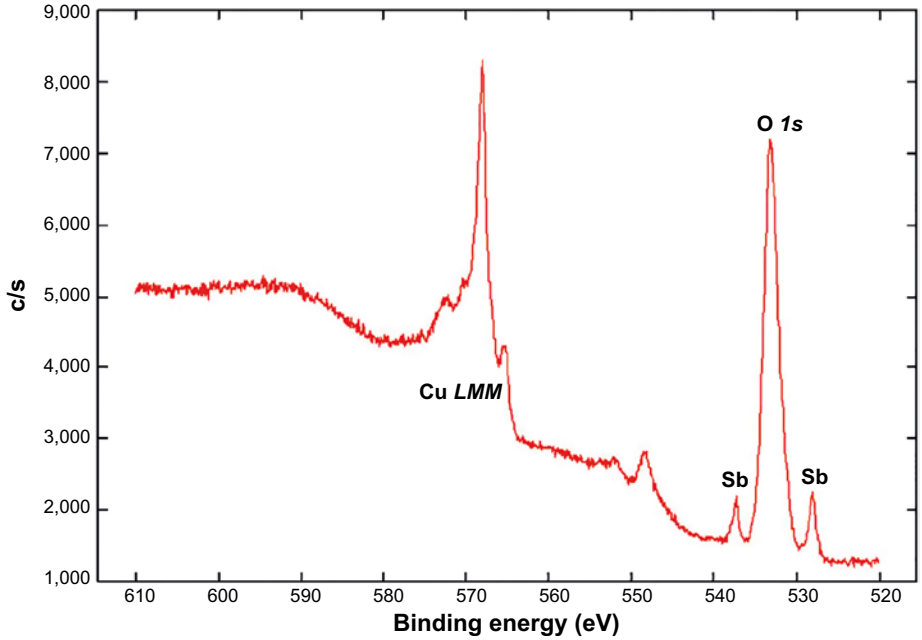

Figure 3-12. *Part of the total spectrum for sample M2-SiC. Part of the whole Auger spectrum of copper is shown together with the oxygen O 1s peak together with contributions from antimony. The whole Auger Cu LMM range is broad, covering 545–800 eV.*

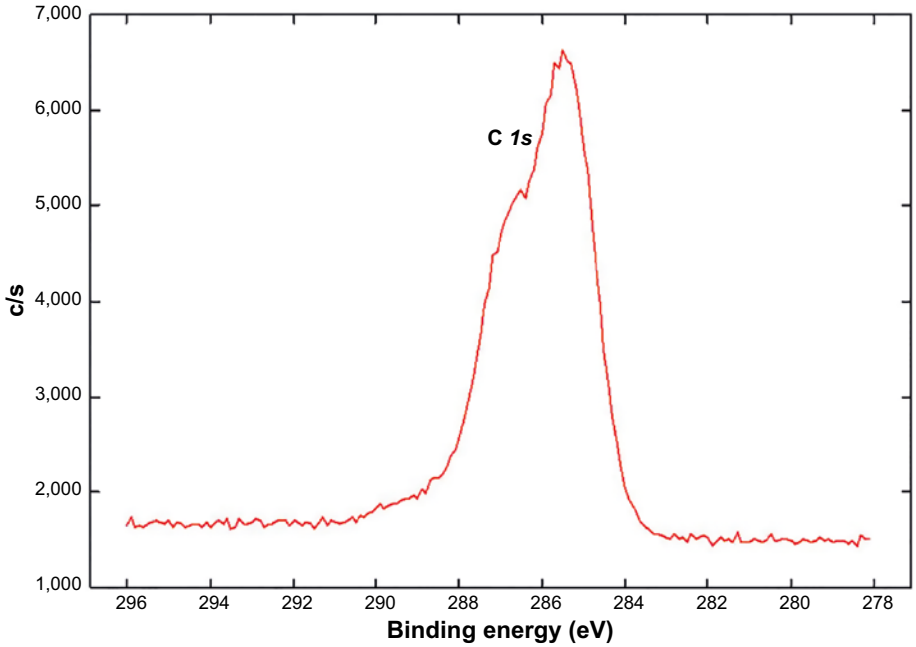

Figure 3-13. *XPS peaks of carbon from sample M2-SiC.*

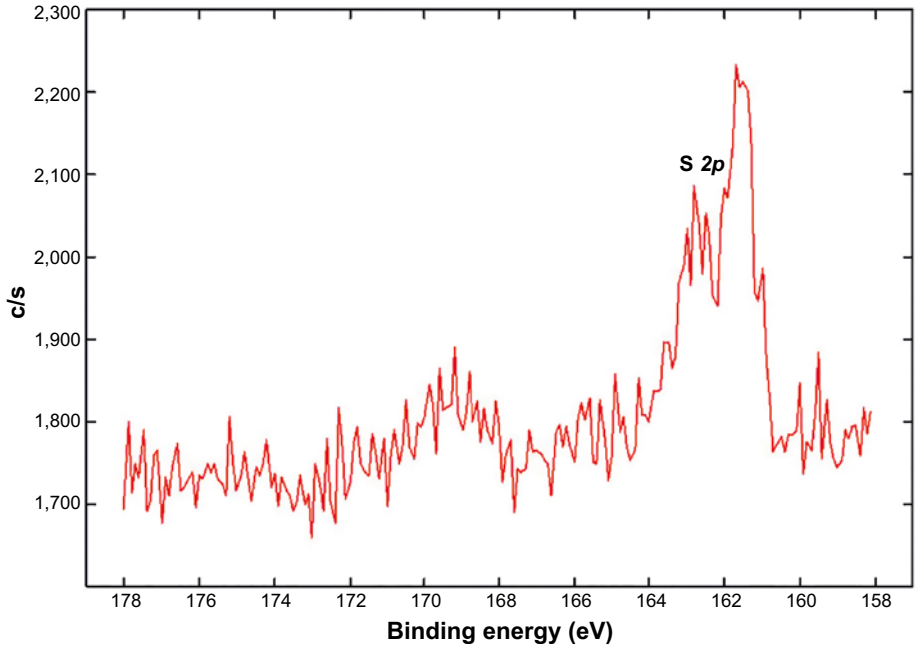

Figure 3-14. *Weak peaks of sulphur, found for sample M2-SiC.*

3.3.3 Copper in Main 3 setup

Like the copper sample in Main 2, that in Main 3 where the surface was instead first scratched by diamond powder (M3-diam) was also analysed by XPS after almost 13 months in water. Before that experiment started, the copper was resting in water for 6 days as mentioned in Section 3.2.3.

Figure 3-15 shows the XPS spectrum of M3-diam after long exposure to water. There are no dramatic differences to corresponding spectra given in Figure 3-7 but it deviates from that of Figure 3-11, taken from sample M2-SiC. The diamond-scratched sample does not show any peaks from foreign elements, such as phosphorus, but the carbon contribution is relatively stronger. However, its intensity is a function of time spent in the spectrometer, *i.e.* it depends also on the order in which all the spectra were recorded. Embedded diamond particles play a role as well. An illustrative comparison may be made between the C *1s* spectra of Figure 3-13 and Figure 3-16. In the latter figure, there is only one important carbon peak, from the hydrocarbons, emphasizing the contrast, the contamination that the SiC scratching may lead to.

From Figure 3-17 compared with Figure 3-12 it is obvious that the overlap between O *1s* and Sb $3d_{5/2}$ is different. In that respect, it seems that M3-diam is more similar to the long-term samples of Figure 3-10a. More than one O *1s* peak contribute, and the deconvolution of the total is difficult without a thorough knowledge of the constraints. Still, there is no obvious oxide contribution from Cu_2O (or CuO) as Figure 3-18 demonstrates, and the Cu *2p* spectrum (not displayed) shows the very same features of a clean copper surface as those of Figure 3-8a.

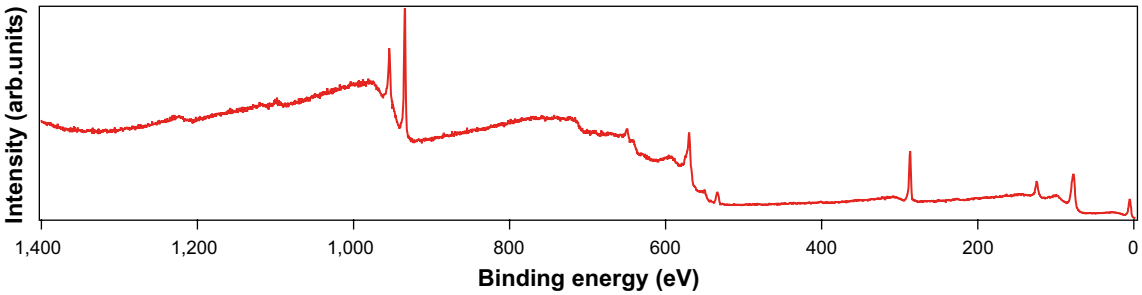

Figure 3-15. *Overview XPS spectrum of sample M3-diam.*

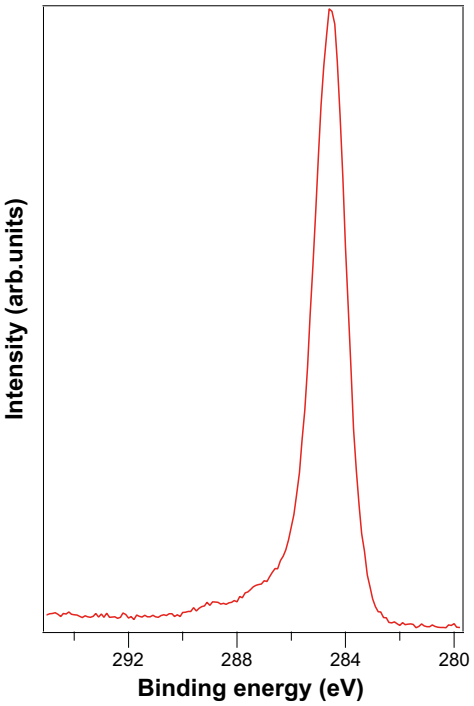

Figure 3-16. *Carbon contribution (C 1s) from sample M3-diam.*

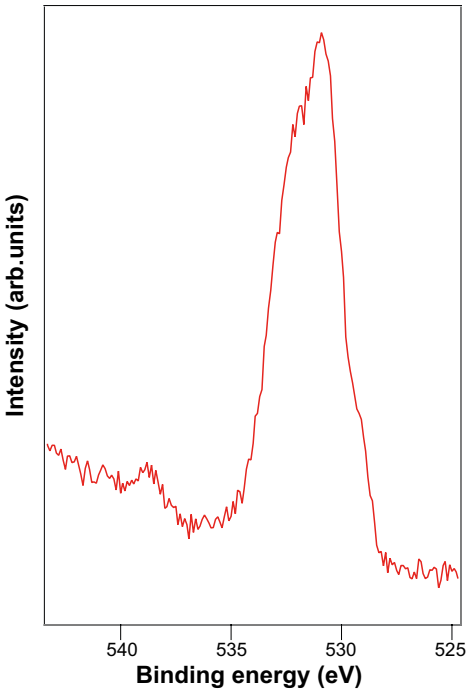

Figure 3-17. *XPS contributions from oxygen and antimony from sample M3-diam.*

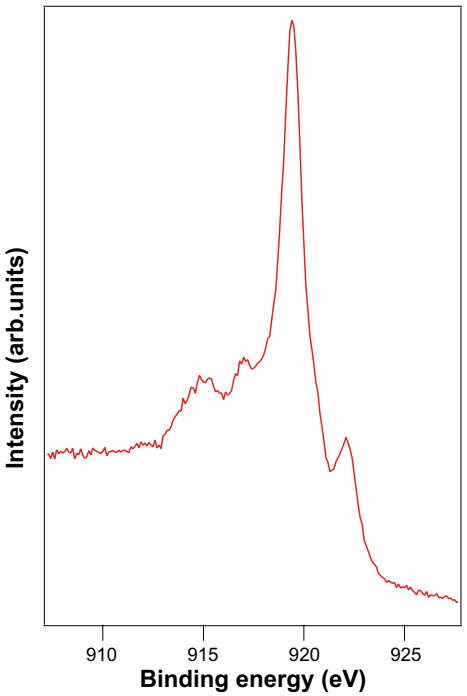

Figure 3-18. *Auger spectrum Cu $L_3M_{45}M_{45}$ from sample M3-diam.*

3.4 Bulk analyses of copper: Hydrogen content

3.4.1 Fusion analysis

The samples that were investigated (with improved accuracy) are collected in Table 3-4. The copper quality was 99.9999% as regards bulk composition (Alfa Aesar). We measured the metal as received (pristine) as well as after electropolishing (EP) and subsequent purification steps (Boman et al. 2014). We include measurement of the 29 months' water exposure sample that had undergone these purification steps. Contrary to routine procedure for removal of surface oxide, the surface was not polished for any of these samples before the melting. The analysis certificates are found in Appendix E.

Experience from previous measurements shows that a large spread in the analysis figures is obtained if the sample sizes are too small, discussed in Appendix E. It might reflect a degree of inhomogeneity of the copper sheet or be an effect of decreased accuracy of the method. That was a problem in Boman et al. (2014, Section 5.2.4) and has now been overcome by increasing the mass up to 5–6 g. With ASTM E1010 as reference, contents of the order of 0.1 ppm can be measured. The conclusions concerning procedure drawn from the analysis results of Table 3-4 are:

- Heating alone at 600°C is efficient in removing hydrogen from pristine copper, from 0.7 to 0.06 ppm.
- The content decreases from 0.7 to 0.16 ppm by electropolishing (room temperature).
- The subsequent step that encompasses heating in hydrogen reduces the content further to 0.03 ppm, a value near the limit of detection by the method.

Electropolishing is an etching oxidation process (copper is the anode). If there exists an accumulation of hydrogen in the surface layer, that gets removed even at room temperature. Larger reduction is attained by further heating in hydrogen. An important fact is that heating in hydrogen does not increase the hydrogen content but rather the opposite (Martinsson et al. 2013).

Table 3-4. Hydrogen content as determined by the LECO method (unpolished copper surface).

Copper sample	Pristine	EP	EPH_2*	EPH_2 +ht** (400°C)	Pristine +ht** (600°C)	29 months
Hydrogen content (ppm by weight)	0.7	0.16	0.03	0.03	0.06	0.09

* Hydrogen gas reduction at 300°C.
** Heat treatment at 400°C or 600°C.

3.4.2 Hydrogen desorption

Heat treatments were carried out as previously, *i.e.* first by reducing the surface oxide layer (after electropolishing the sample in a diluted H_3PO_4 solution) in order to remove all oxygen from the surface. This treatment was performed at 300°C for one hour in a hydrogen atmosphere and has proven to work for samples with an oxide layer observable to the eye. During this annealing, hydrogen is expected to partially desorb from the bulk. Then, after cooling, the tube with the sample was evacuated to low pressures (below 10^{-7} Torr), where residual gas analysis is possible, and was further annealed at 400°C while logging the partial pressures of selected species (QMS).

Two processes were observable in pristine samples ("as received"), first a desorption which gives the highest partial pressure, probably from the surface, and then another desorption from the bulk which is a more prolonged process. These are clearly seen in Figure 3-19. For comparison, data for the corresponding heat treatment of two foils having experienced surface purification (Boman et al. 2014) are shown, one directly after purification and one after 6 months in ultrapure water. The partial pressures are very low for the latter two, and the noisy appearance illustrates that they lie at the verge of resolution by the equipment. Note that the mass of the 6 months' sample is 10 times smaller than that of the others.

All qualities show a gas desorption process that commences just after 400°C has been reached. (A small delay after heating change may occur.) Annealing of copper up to 600°C has shown that hydrogen is effectively desorbed in the temperature range 300–400°C with a high evolution rate at 400°C (see Appendix E, heating rate 1 K/min.). Hence, a treatment at this temperature effectively removes dissolved hydrogen from the bulk (and surface, if present), as is corroborated by the fusion analysis results given in Section 3.4.1.

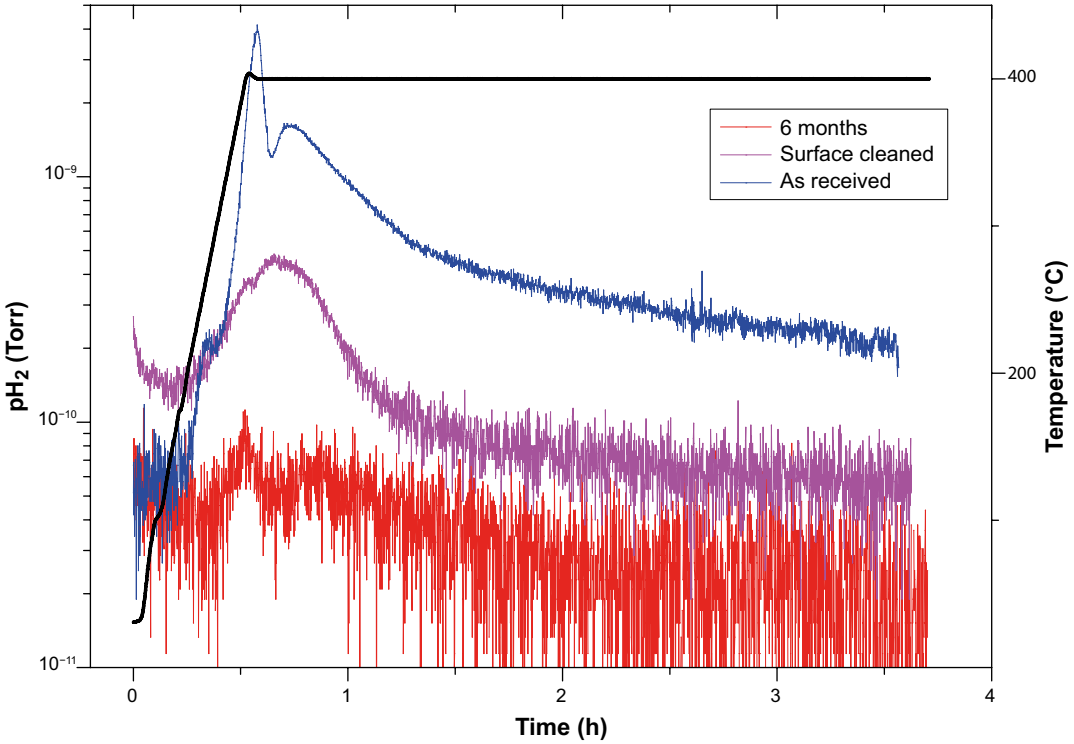

Figure 3-19. *Pressure/temperature vs. time characteristics on heat-treating Cu foils of 99.9999% purity. One sample is "as received" from the supplier (blue), one has gone through a surface purification process (EPH2, magenta), and one has after that been exposed to water for 6 months (red). The mass of the latter sample is 10 times smaller than that of the other two. The axis to the left on a logarithmic scale alludes to the data in colour. The applied temperature in black is read on the axis to the right (on a linear scale).*

3.5 Analyses on the near environment (water, glass)

3.5.1 Water phase in contact with copper

The water was analysed by ICP-MS, a method that can detect and determine very small amounts of elements dissolved. The main features of the technique were presented in Boman et al. (2014).

Six water samples representing a time span of 0–29 months (0, 1, 3, 6, 15 and 29) have now been measured using a semi-quantitative method for scanning a majority of the naturally occurring elements. Here, 0 months stands for a water sample without any copper immersed in it (cf. Boman et al. 2014). The element concentrations of the water samples generally tend to increase over time as depicted in Figure 3-20. For each element (symbols arranged in alphabetical order), the respective concentrations are shown as histograms that are fading in colour tone as a function of increasing time. Analysis was also made of the long-term sample in Main 1, since, despite a different temperature program than that of the free-standing samples, it was thought that the time aspect was valuable for disclosing artefacts concerning copper analysis. Further data are included in Appendix F.

Most elements seen in the water sample are probably a result of leaching from the glass container by the water itself or from the polymer tube used as sample vessel for measuring. The presented concentrations are rather uncertain due to the large concentration differences between several elements and the one point calibration, as well as to the problem of compensating for interferences by some elements (e.g. K, Ca and P). This uncertainty should however be equal for all samples since they were measured using the same calibration and instrumental settings and with a relatively similar matrix for all the samples. Therefore, the presented data can be used for comparison between samples in time and within each element, but it should be noted that the "real" concentration could vary substantially for elements that suffer from interferences and/or are present in very high concentrations (>100µg/L) or in very low concentrations (<0.1µg/L). A comparison to earlier measurements (see Boman et al. 2014) was also made to ensure that no substantial difference in concentration occurred due to storage. The samples exhibited quite comparable levels to those of previous measurements. Therefore, the data of Figure 3-20 most likely present a valid comparison between time points. Detailed numerical values may be found in Appendix D.

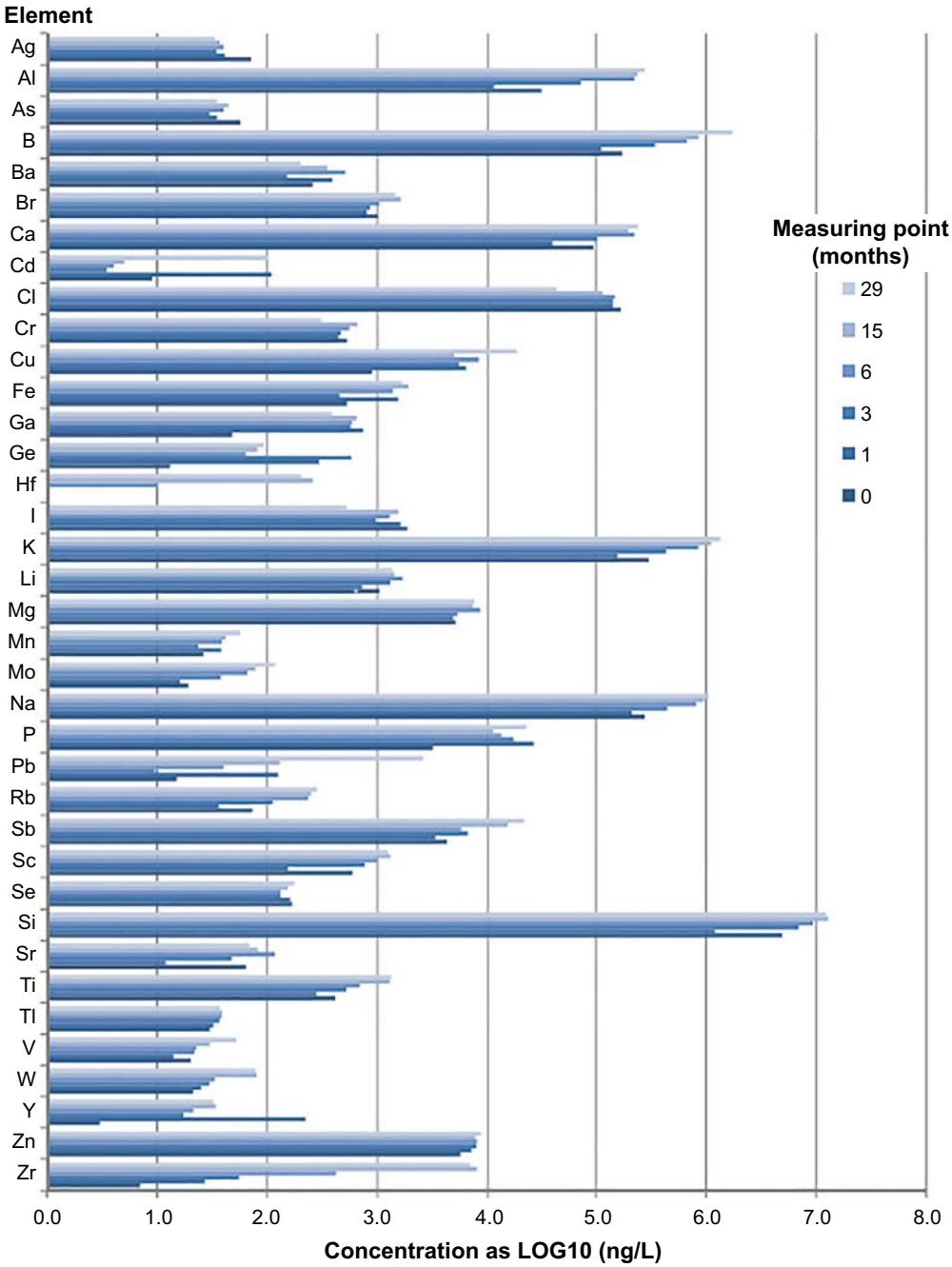

Figure 3-20. *Overview of elements in the water phase investigated by ICP-MS that have a concentration of 1 ng/L or more. The logarithmic presentation means a tenfold difference in concentration between each scale division on the horizontal axis.*

The elements that occur with the highest contents (please note the logarithmic scale) most likely emanate from leaching of the glass (*e.g.* Al, B, K, Na, Si; high-lighted in the table of Appendix D). Zinc and magnesium are borderline cases, being elements that easily may contaminate samples from the surrounding environment. All concentrations are "low", remembering that 1 ppb (= 1,000 ng/L) corresponds to the figure 3 on the logarithmic horizontal scale.

After exposure of the copper samples to water during 29 months, the measured copper concentration is roughly 25 µg/L (Table 3-5). As an illustration of the very small magnitude, that value corresponds to 4×10^{-7} M Cu which is only a factor of four times the hydrogen ion molar concentration in pure water, in other words a very low concentration.

Table 3-5 presents an example of the most recent results from ICP-MS, concerning long-term samples and samples lying in water for shorter times (see Section 3.2), including those of scratched copper. For confirmation that the values were not severely marred by systematic errors of analysis procedure, two isotopes of copper were measured and the concentrations scaled according to isotope abundance. The corresponding scaling procedure was also applied to iron, normally determined from ^{57}Fe. Even in that case, however, special care was taken to eliminate errors, in particular to avoid contamination by $^{40}Ar^{17}O$ (see Boman et al. 2014).

It may be noted that the scratched samples (*cf.* Table 3-3), although exposed a relatively short time to water, show copper contents that are comparable to that of the long-term sample or even higher, as for the one scratched by diamond. One plausible interpretation is that the scratching process yields minute copper particles that are dispersed and enter the plasma, more pronounced for scratching by diamond that is harder than SiC. The diamond-scratched sample showed a high concentration of zinc, probably because natural diamond was used. Due to the short exposure time of the glass to water, the contents of zinc and antimony are low for M2-EPH2 and M2-SiC. The antimony comes from leaching of the glass. The high content of aluminium from M2-SiC probably emanates from the polishing paper. When sintering the silicon carbide, Al_2O_3 is commonly added (Sciti and Bellosi 2000).

Table 3-5. Selected analysis results from ICP-MS of the water phase for various isotopes. Concentrations are given in µg/L (ppb).

Sample	^{24}Mg	^{27}Al	^{63}Cu	^{65}Cu	^{66}Zn	^{121}Sb	^{57}Fe
29 months	9.2	329.9	23.6	25.7	13.9	27.1	1.4
41 months, glass	7.1	497.9	0.5	0.6	20.8	31.5	4.3
M2-EPH2*	2.7	35.1	21.7	21.6	0.9	6.8	2.2
M2-SiC	9.8	248.9	18.6	20.0	1.4	0.4	1.7
M3-diam**	5.2	33.9	67.6	65.7	107.1	0.6	1.5

* Average of two measurements.
** Analysis of a sample kept in water only for six days, prior to the pressure measurement.

As described in the previous recapitulation of the technique above, a more precise method to measure Cu levels in the water samples was also used in addition to the semi-quantitative method. The results of those measurements as plotted in Figure 3-21 gives a rather erratic view of the relationship between time and Cu concentration. The first six points refer to samples of the free-standing setup, dedicated for analyses of copper and its near environment. The point from 15 months was initially considered to be ignored as an "outlier", yielding a rather linear progression by time. However, the measurement at 29 months could equally well be an outlier from which the relationship would look more parabolic instead. After dismantling the sample from the Main 1 setup, another point at 36 months was available. Despite a different thermal history (imposed deviations from 50°C during the last 8,500 h of the total exposure) and the fact that there was more metallic copper per water volume, we choose to include the corresponding data (Appendix F, Table F-3) but denoted with another symbol (red star) in the graphics.

The analysis method is very sensitive for measuring small concentrations, but it is therefore also extremely sensitive to minute disturbances. As discussed above, deliberate scratching of the surface by necessity mar the copper analysis results. However, all copper samples may experience gentle scratching of the surface from the unavoidable movements to introduce and eventually remove samples in and out of the holder. The surface effect of this involuntary mechanical scratching is seen in SEM (*vide infra*, Figure 3-26). The net result would be an uncontrollable enhanced copper content measured by ICP-MS because of some removed nanoparticles that enter the water and form a colloidal solution. The method does not distinguish between various forms of the element present in the water phase that enters the plasma. Systematic errors as enhancements are thus more likely to occur than *vice versa*. Therefore, by omitting the 29 months' sample a more collected view is obtained. The copper concentration approaches a more or less constant value of 5 µg/L by time. Analysis of a blank with only glass in water for 41 months showed a copper concentration below 1 ppb, indicating that glass does not contribute much to the measured values.

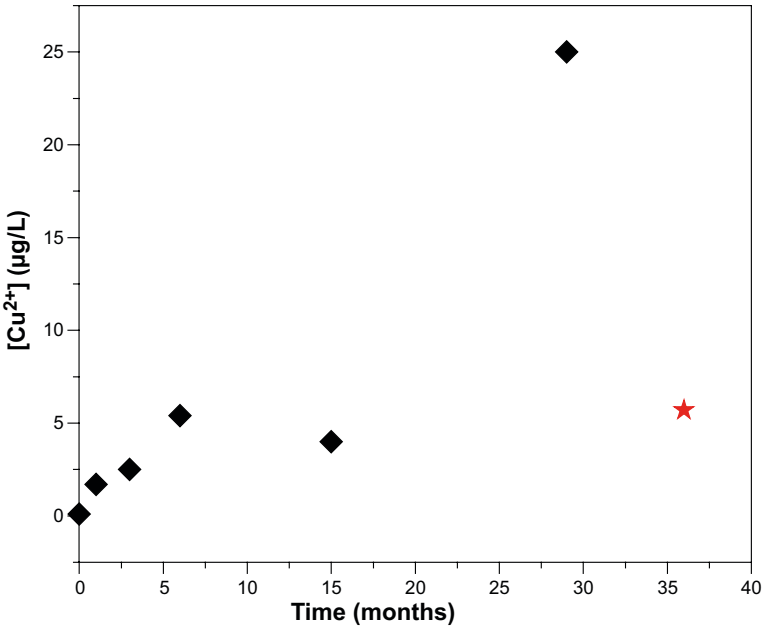

Figure 3-21. *Time dependence (discrete measurements) of the copper concentration in the water phase. The point at 36 months belongs to Main 1, with a different thermal history (see text).*

3.5.2 Glass in contact with water

The use of the XRF technique for determining copper in the glass plates that accompanied the copper in the water was described in Boman et al. (2014, Appendix D4). The beaker itself could not be analysed in the spectrometer for geometrical reasons. The XRF technique cannot determine in what form copper occurs (elemental or bound) or its distribution, *i.e.* whether the signal emanates from a surface layer or is a bulk property. Table 3-6 shows the analysis results where the amount of copper is expressed as a fictitious thickness of a copper layer that corresponds to the intensity recorded. These analyses were made for the free-standing vessels, now including previous results as well. The precision of the data is in the order of 30% and there are indications (from ICP-MS) that the spread between different glass plates is larger than that, thus affecting the accuracy. The data show no obvious trend with time, *i.e.* one cannot tell whether the copper content increases (surface deposition) or decreases (glass leaching).

Table 3-6. Copper content in glass plates exposed to water in beaker with residing copper.

Exposure time	3 months	6 months*	15 months	29 months
Thickness (nm)	0.00	0.03; 0.05	0.04	0.03

* Measured from two directions of the same plate.

3.6 Miscellaneous complementary techniques

3.6.1 Scanning AES

Copper foil that had been in water for 6 months was investigated by scanning electron beam AES. Figure 3-22a shows that the copper surface, as seen in the SEM mode of the scanning Auger spectrometer, is very smooth with very narrow grain boundaries. Figure 3-22b shows ultrapure copper after the first purification step, the electropolishing, after which the surface gets covered with a thin layer of oxides that are later removed by hydrogen treatment before the experiments.

Electron-beam AES was used in order to disclose inhomogeneity, in particular signs of corrosion attacks at the grain boundaries where then oxide would form preferentially. That could not be done by XPS where the analysing ray is much wider, goes deeper and cannot be controlled as to where it

hits. The experimental strategy is illustrated in Figure 3-23 where spots were chosen, either on a grain boundary or at adjacent areas. The spectra corresponding to these very spots are given in Figure 3-24, showing that the copper surface is fairly clean (sample container was opened in air before loading). More important, there is no accumulation of contaminants at the grain boundary (middle trace in black from point 1). The peaks are attributed to carbon, nitrogen, oxygen and copper. The peak shapes and background characteristics are different from those in XPS because only electrons are involved with this technique, not X-ray photons.

The measurement procedure showed that adventitious contamination by carbon was continuously introduced within the spectrometer (explaining the abnormal intensity of the C *1s* peak), easily monitored on waiting some minutes directly after a short sputtering. Since the extra amount is minute, the strong response illustrates the high sensitivity of the method. Iterative sputtering tests showed the same phenomenon concerning the spectra, and the corresponding SEM mode showed (no pictures available) how the etching of the copper proceeded by consecutive sputtering operations, creating pronounced edges of the grains.

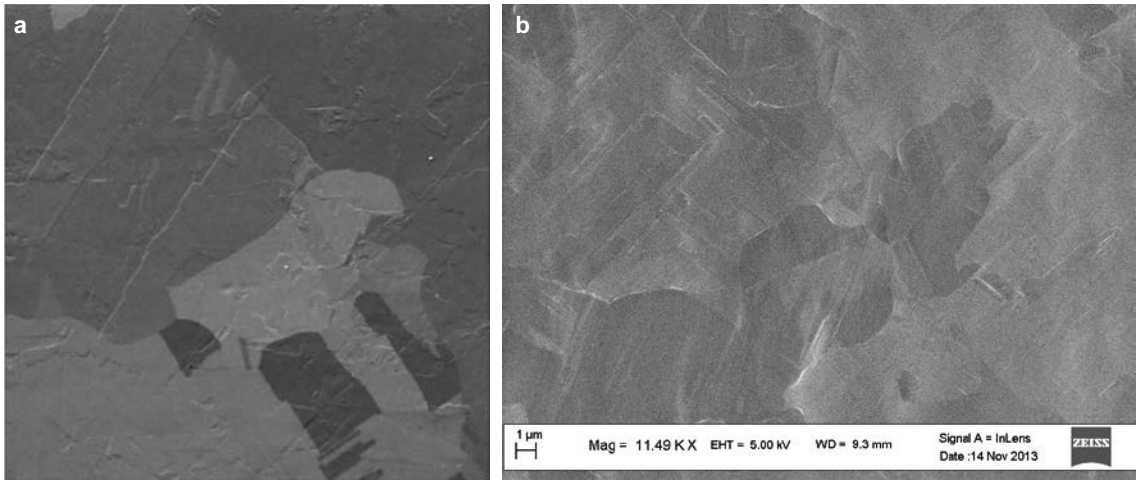

Figure 3-22 a–b. *(a) A SEM micrograph of the surface of the 6 months' sample from the scanning Auger spectrometer; (b) SEM picture of ultrapure copper after electropolishing, before the experiments. Different orientations of the copper grains yield the contrast.*

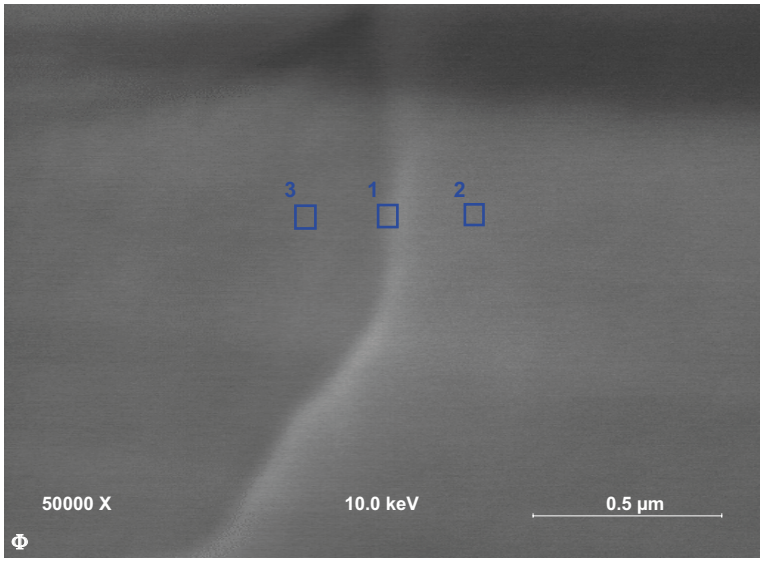

Figure 3-23. *SEM picture from the Auger spectrometer showing the copper microstructure with spots where the surface was analysed.*

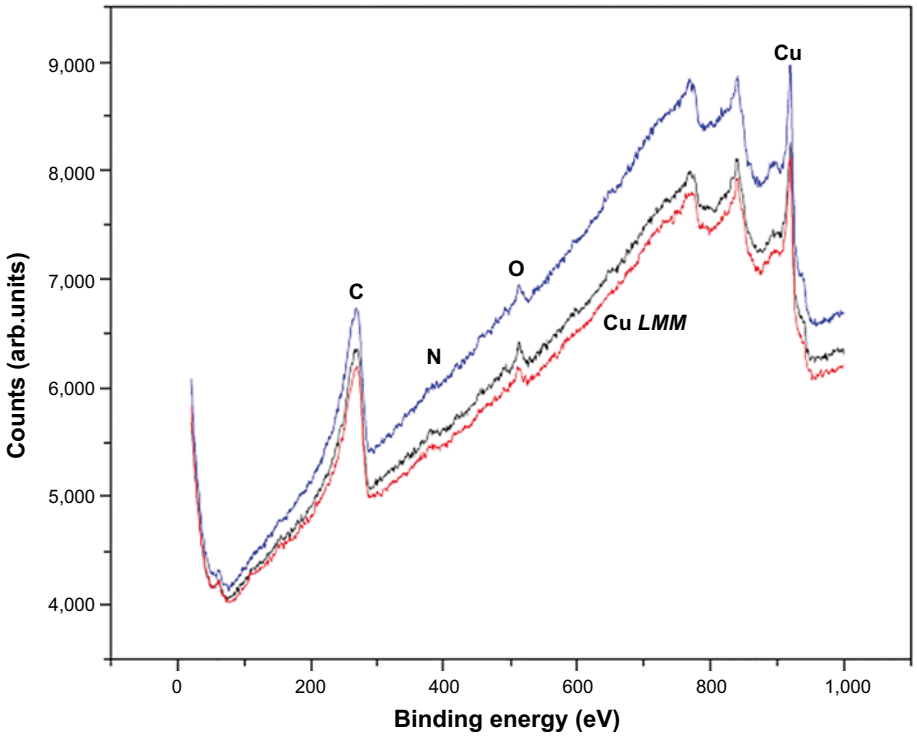

Figure 3-24. *Corresponding AES data from the spots 3-1-2 chosen in Figure 3-19 (number 3-blue, 1-black, 2-red). The middle curve (1-black) comes from the point at the grain boundary. The energy is here given as binding energy for an easier comparison with values from XPS spectra (see Figure 3-11 for proper denotations).*

3.6.2 Profilometry, SEM, GI-XRD

The investigation of the copper surface is not so straightforward, since the foils are thin and the metal very soft, so that deformation and scratching are likely to occur. The macroscopic surface topology was investigated by a profilometric analysis. SEM was performed in a dedicated microscope for in particular studying the effects of polishing the copper surface by SiC or diamond. Since the surface of the electropolished and hydrogen reduced copper is so smooth, it is difficult to obtain pictures with good contrast. On the other hand, scratches are immediately optically well resolved. XRD in grazing incidence mode was applied for disclosing possible contaminants at the surface, introduced from mechanical treatment of the surface.

Some macroscopic aspects are depicted in Figure 3-25. The softness of the metal is obvious, directly showing how delicate the handling of the thin copper samples is with respect to deformation. The samples have to be introduced into the silica glass holder within the glass beaker and eventually again removed after finishing an experimental period of continuous water immersion. Some surface effects of this handling, however cautiously performed, can be seen in Figure 3-26.

The deliberate scratching by SiC paper or diamond powder introduces irregular much deeper scratches where particles may be caught in the soft matrix and may plough through the soft upper surface and deform it radically. These effects are demonstrated in Figures 3-27 to 3-30. One may note various differences in the outcome because of the ways that the scratching was performed and the properties of the particles.

Figure 3-27 gives an overview of a surface directly after being scratched with SiC paper. The scratches run in a few main directions effectuated by the manual treatment. The samples are very thin and difficult to handle which makes it difficult to avoid some preferred directions, and some parts are not scratched at all. There are a few dark spots that may emanate from SiC particles, the contrast being due to the fact that SiC is a semiconductor where the particles may be charged (and can discharge). Figure 3-28 gives information on a more detailed level, showing trenches and loose particles.

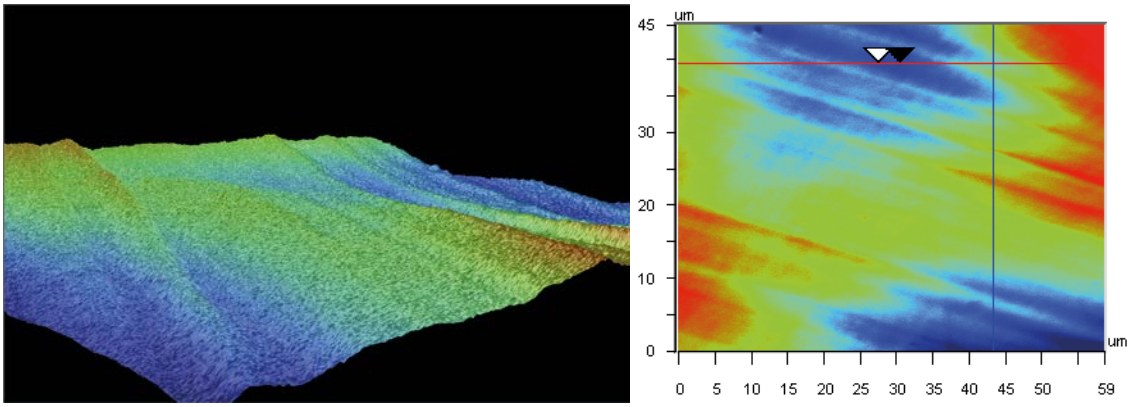

Figure 3-25. *Illustrations of the macroscopic undulating character of a soft copper surface as measured with a profilometer. The false colours have been introduced to emphasize the topology. The difference between the lowest "valleys" and highest "ridges" is 0.5–0.6 µm.*

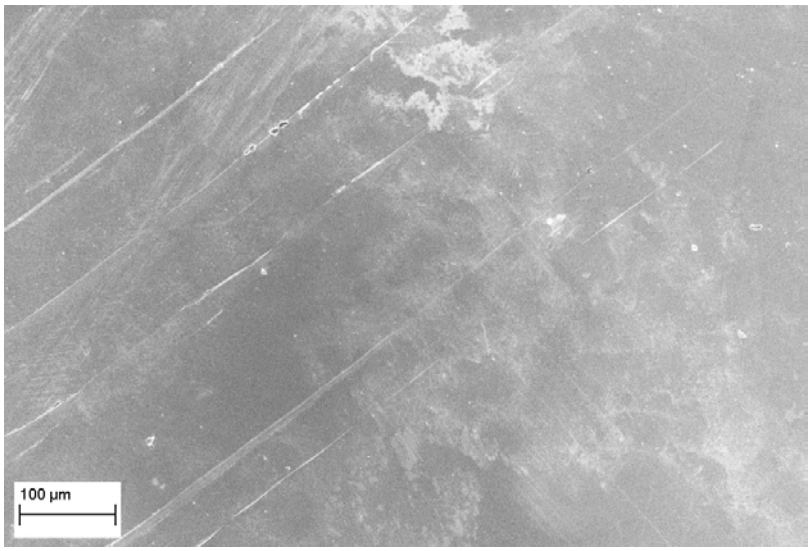

Figure 3-26. *SEM micrograph illustrating the parallel scratches that are introduced on removal of a copper sample from its holder by lifting it out by tweezers.*

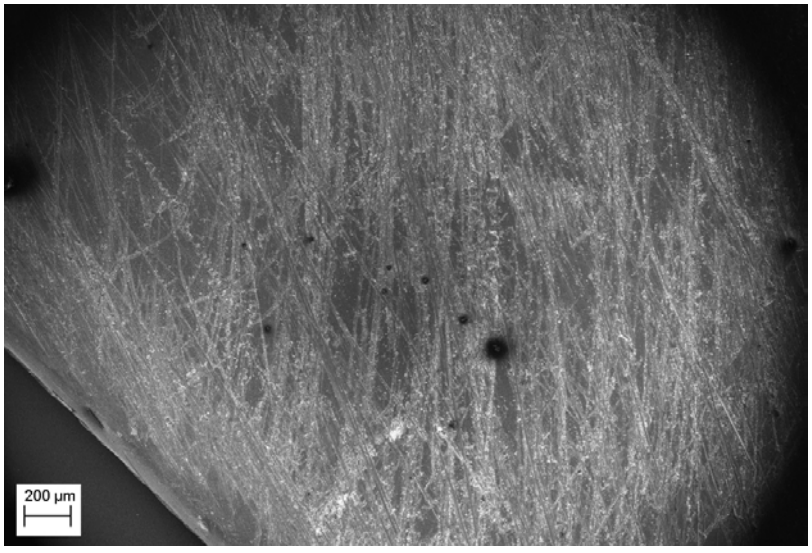

Figure 3-27. *Copper surface after scratching with SiC (as sample M2-SiC).*

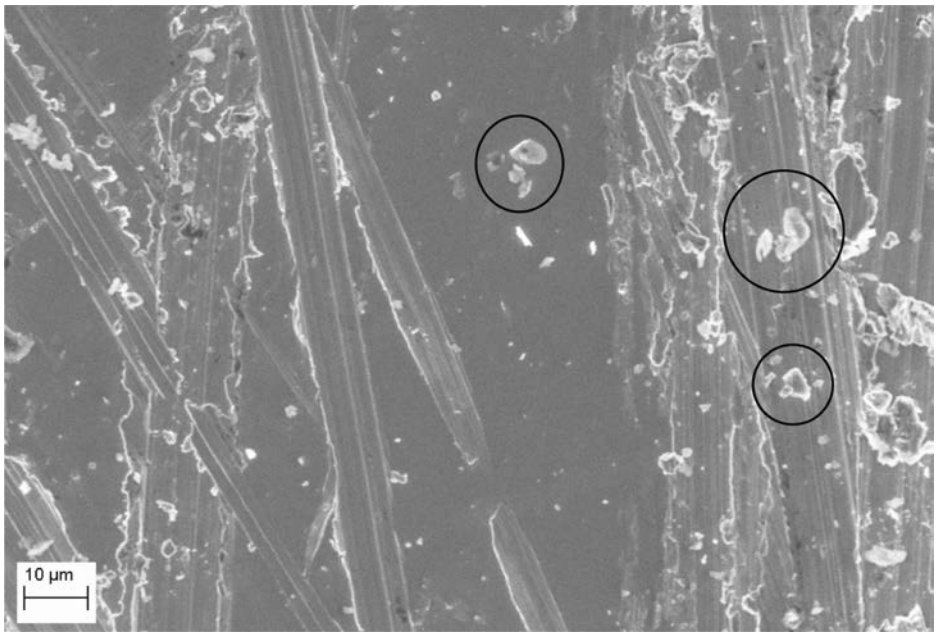

Figure 3-28. *Detail of a SiC-scratched copper surface. Some copper particles are marked out.*

The polishing procedure using diamond powder was quite different because the particles were not bound by a medium. Hence, the particles acted between two pieces of copper and were able to move around freely within that interface. Because diamond is very hard and copper is soft, this procedure has created a situation where the diamond particles may get pressed into the metal. This seems to be what Figure 3-29 illustrates, a large number of small diamond particles that have been residing at the copper surface, disturbing the smoothness. Still, some particles do move in the scratching process to create deep furrows with metallic material spilling over the edges (Figure 3-30). The microstructure of copper is then severely changed, dislocations have been created, and to some extent small metal particles have been chipped off. Again, as for the sample scratched with SiC, the sample has not experienced any water environment as yet.

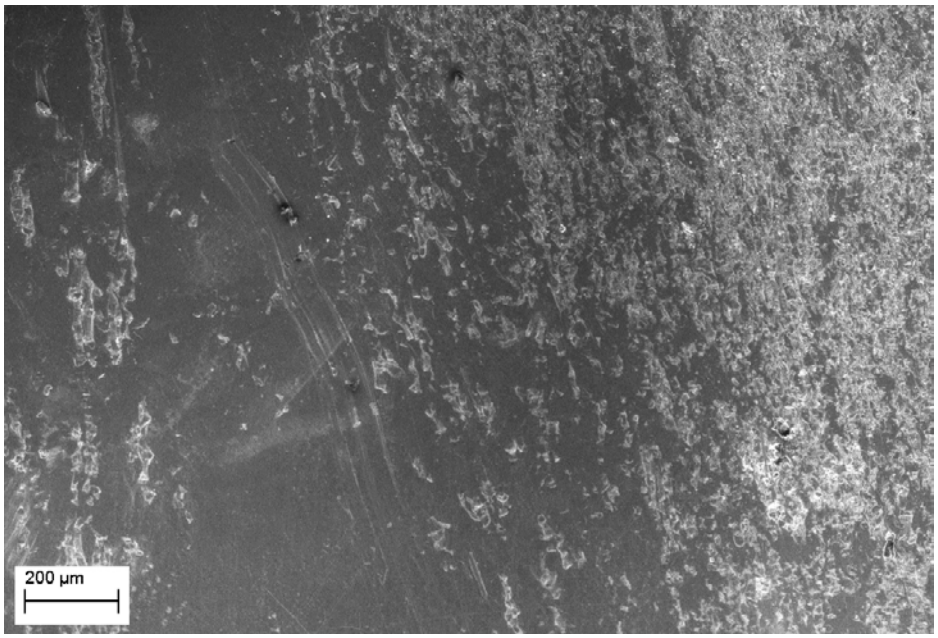

Figure 3-29. *Copper surface after scratching with diamond (as in sample M2-diam). The right side with a heavily disturbed surface might show the effect of impressions by diamond particles, not detectable themselves in SEM.*

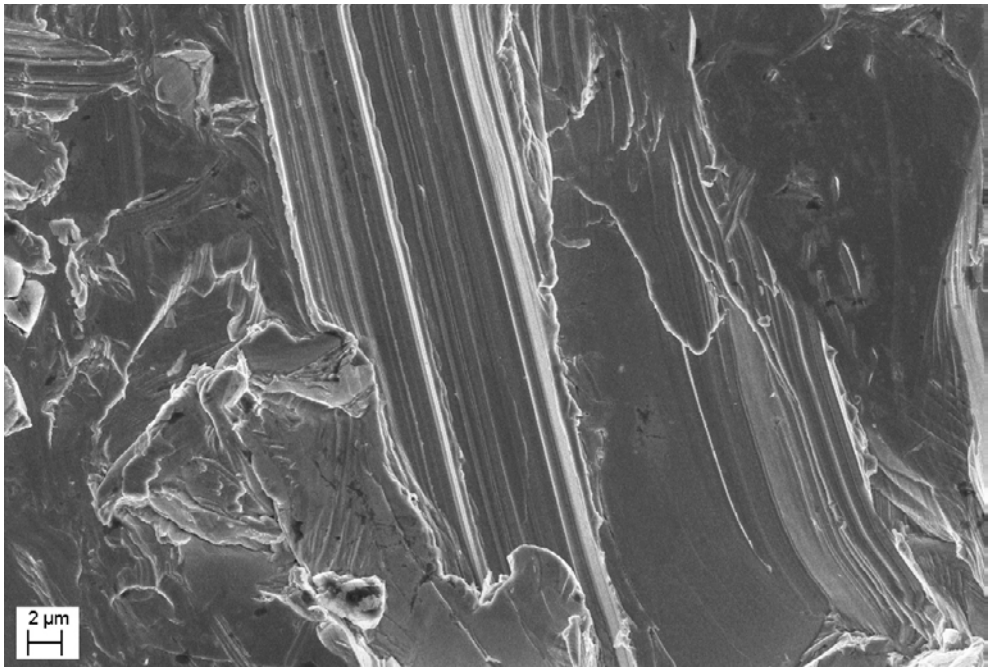

Figure 3-30. *Detail of a copper surface scratched by diamond powder.*

The sample M2-SiC (after 100 days in water) was also investigated by XRD, using a grazing incidence (GI) mode. By GI-XRD the sample surface is scanned under a very small angle, where only the phases of the topmost part are contributing. Obviously, the diffracting volume is then small, demanding long exposure time. The result of a GI-XRD experiment (incidence angle of 1 degree) during 60 hours using Cu$K\alpha_1$ radiation is shown in Figure 3-31 together with a pattern taken from the SiC paper. The latter scan was made with a θ–2θ scan mode with the same radiation. The two patterns have been put on the same angular scale, the one from GI-XRD coloured in blue and the one from the polishing paper in red at the bottom.

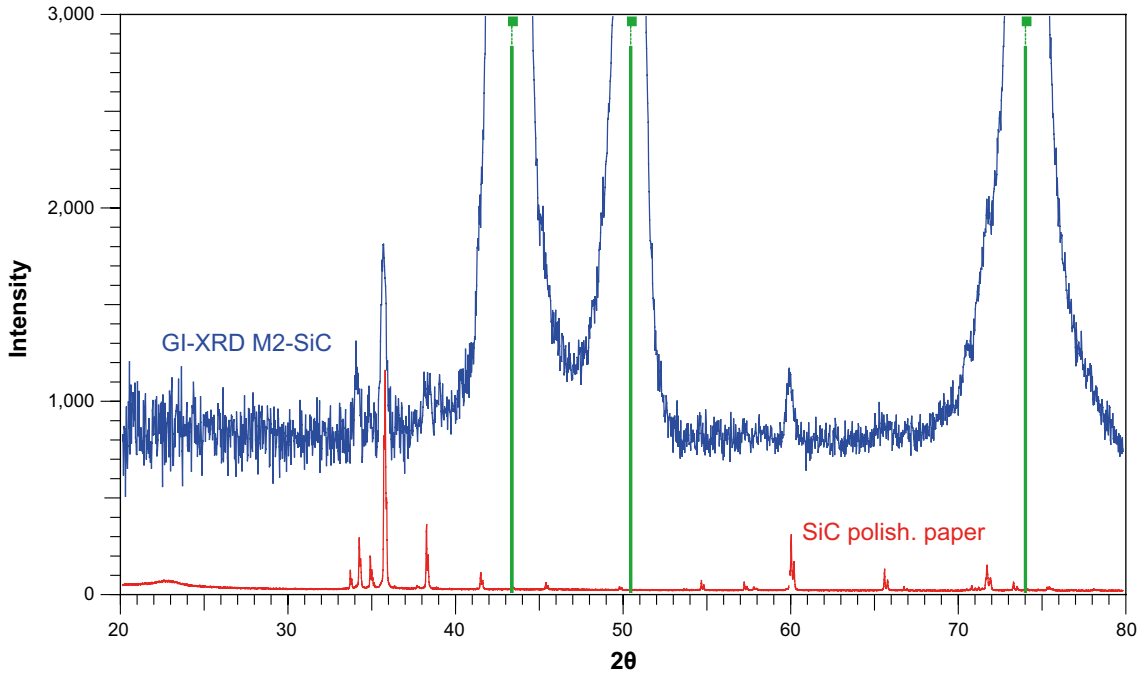

Figure 3-31. *GI-XRD on M2-SiC together with conventional XRD on SiC polishing paper.*

The three strong peaks on the blue pattern emanate from metallic copper. Their positions are accentuated by green vertical lines. The red pattern obtained from the polishing paper by conventional XRD has not been compared to any standard file for a proper phase analysis. The important issue here is the fact that its strongest lines reveal themselves as part of the blue total pattern, exemplified by the coincidences at (roughly) 34.4, 35.7, 38.3, 60.2, 65.6 and 71.8 degrees (2θ). This yields unequivocal evidence that crystalline phases present in the SiC paper appear at the copper surface, not having been washed away. Therefore, it is without doubt concluded that polishing of pristine copper with abrasive paper of this kind is detrimental for the true interpretation of any corrosion process of pure copper, since contaminations are introduced. Their surface fraction is estimated to be of the order of 0.2%, particles that according to SEM are stuck in the soft malleable copper matrix.

3.6.3 Transmission electron microscopy

Transmission electron microscopy (TEM) may be used in two different ways, either for studies of the absorption through thin samples or for electron diffraction. In both cases very thin samples are needed because of the strong absorption by electrons. In the absorption mode, very high resolution may be obtained and the grade of crystallinity and occurrence of dislocations can be studied.

For making a TEM micrograph (Figure 3-32), a thin slice of copper was ion-beam milled out of a foil of the 99.9999% quality used. It was thin enough to make it electron-beam transparent, but platinum was deposited on the copper as a backing before the thinning process which protects the copper surface from ion damage. The surface shown is the interface Cu/Pt. Voids that could contain H_2 were neither observed nor expected, considering the low hydrogen content.

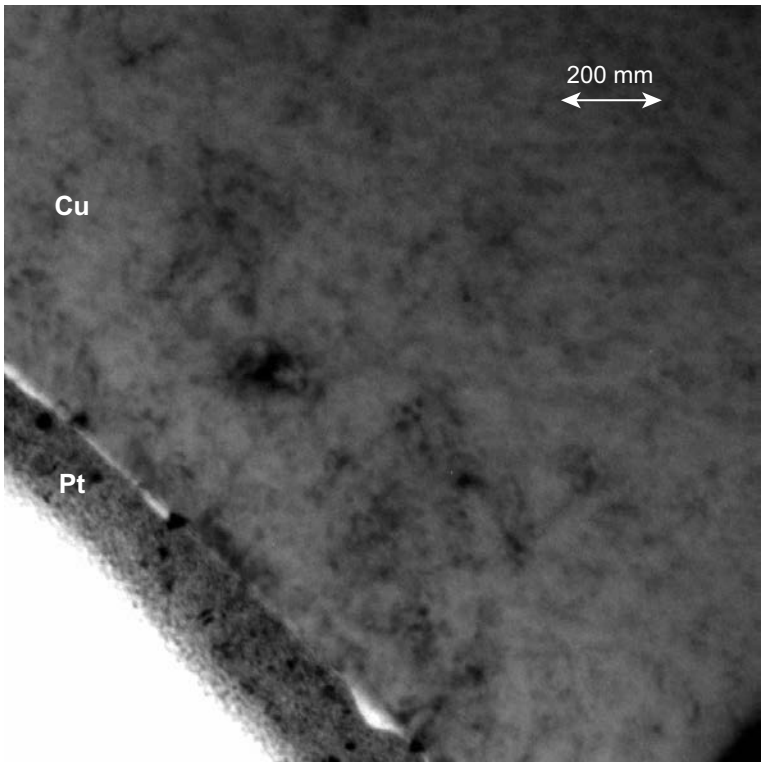

Figure 3-32. *A TEM micrograph of ultrapure copper, purified in steps as described in Boman et al. (2014). The thin copper slice is situated on a platinum backing.*

4 Discussion

4.1 Examination of possible contaminations

As before, the copper has been investigated by XPS and AES, but in one case also by XRF (Main 1 in Appendix F) and GI-XRD. Electron spectroscopic methods are extremely sensitive as a probe of surface composition and XRF less so, but that method has the advantage that it is easier to get a reasonable quantification of various elements. The Auger Cu *LMM* spectrum showed, after exposure of the copper to water for even a couple of years, only the features of pure copper. In fact, there is no evolution in time compared to the previous samples (up to 6 months' exposure) when aiming at the only probable surface product, Cu_2O, which is unambiguously detectable by this technique. Neither were there any sign of contaminants accumulated in the grain boundaries as established with an electron Auger spectrometer designed for spot analysis. On the other hand, incorrect handling of the samples, such as the use of SiC abrasive paper, seems to introduce contaminations.

4.1.1 Antimony

Species containing antimony and oxygen at the surface were detected by XPS. As for the oxygen, we may identify these contributions as belonging to adsorbed species from the water environment, namely H_2O_{ads} and OH_{ads}. Due to the low pressure in the spectrometer, these oxygen-containing adsorbents can at the most cover one monolayer together. The peaks from antimony are much less intense than the oxygen peak (Figure 3-10a). In fact, the amount of antimony is very low, being much less than a monolayer as demonstrated by calculations based on the electronic cross-sections (Appendix G). Examples are given for other cases with antimony and oxygen together, in comparison with experiment (Berry et al. 1987, Garbassi 1980). The conclusion of a very low coverage by antimony is corroborated from XRF on the sample left in the Main 1 setup for three years (Appendix F).

It is a well-known observation that species containing foreign elements may in some cases influence corrosion rates. It has been found that antimony species work as inhibitors in the case of steel corrosion, but only in concentrations of 0.10% or more (Le et al. 2008). As for copper, the effect of various adsorbed atoms (adatoms) has been investigated (Hourani and Wedian 2000). It was shown that the surface coverage by antimony was at the most only 20%, and its presence increased the corrosion rate of copper by approximately 10% compared to standardized conditions. It is difficult to translate these claimed corrosion properties to the environment of only water, but the proposed low surface coverage factor is quite in line with what our study shows (XPS and XRF), and the data give at least a valuable hint towards what to expect from this element combination. If superficial antimony does carry any considerable role in changing the corrosion properties of copper, it would act as a promoter rather than an inhibitor.

Antimony is an additive to glass to reduce the formation of bubbles (Atkarskaya and Bykov 2003). That the glassware does contain antimony was shown by XRF (Appendix F). While the glass is being leached by the water, it leads only to a low concentration (ppb level) in the water phase, even after three years of immersion (Appendix F, Table F-2). The antimony species are probably not deposited onto the copper but only dragged out in a thin water film that adheres to the metal surface all the way into the spectrometer where a monolayer forms from evaporation. This leads to an increased concentration in the surface layer, but the antimony coverage is still extremely low. All the adsorbents are easily removed by gentle sputtering.

A question remains whether antimony inherent in the metal also takes part. In the copper quality used (Cu 99.9999%) there is less than 0.005% Sb (Boman et al. 2014, Appendix A2). A notable observation is that the value of the binding energy is peculiar to Sb(0), and its shift on time is larger than the shift reported in the literature by the oxidation from trivalent to pentavalent antimony.

It must be emphasized that this study of copper in O_2-free water (in part reported by Boman et al. 2014) is the first one to actually also take the whole local environment (water, glass) into account and measure even these small amounts. Antimony is by necessity present as a leaching product in

all experiments where glassware with added Sb is used in contact with water. As a consequence, assuming that similar glass qualities were used, it must have been present to some extent also in all previous experiments where hydrogen evolution from corrosion by copper in water was claimed (Hultqvist 1986, Szakálos et al. 2007, Hultquist et al. 2009, 2011). However, those investigations neither included any thorough chemical analysis nor any discussion of contamination effects (from SiC-scratching treatment or from other materials) that might affect the results. It is noteworthy that no factors of this kind were included that might influence the validity of the interpretation that the observed hydrogen production had to be due only to copper corrosion. No XPS overview spectra have been presented to give a hint concerning trace elements, for instance phosphorus and sulphur, as well as other signs of contamination from SiC-scratching.

It is also unfortunate that XPS data presented cannot show the presence (or absence) of antimony because of overlap of Sb $3d_{5/2}$ by the CuO oxygen O *1s* peak or because the high-energy part of the spectrum near O *1s* (for Sb $3d_{3/2}$) has been omitted (Hultquist et al. 2015). However, the layers of copper oxide or hydroxide would overshadow its presence.

4.1.2 Contamination from the scratching process

A few short-term experiments (described in sections 3.2.2 and 3.2.3) were made with the modified equipment (Main 2 and Main 3) where the surface was treated by manual scratching, with the idea that copper that had been roughened at the surface might change its reactivity through the introduction of dislocations or even by the creation of nanoparticles. Some effects were observed that influence the conclusions to be drawn. First of all, investigations by SEM clearly indicate that copper particles might appear. Their implications are indicated from the results found by ICP-MS from scratched surfaces, where the copper contents were found far higher than in comparable samples, for example from an immersion of only six days (diamond scratching) than found even after three years of exposure to water (Main 1). Copper residues are thus corrupting the results of the method, in fact meaning that ICP-MS cannot be trustworthy when applied to water where scratched copper samples have resided.

SiC scratching influenced the copper ICP-MS analysis to less extent. On the other hand, this treatment introduced foreign elements, phosphorus and sulphur, that were found at the copper surface as well as enhanced aluminium levels in the water phase. Moreover, the oxygen O *1s* contribution was much larger than coming from adsorbates, and the carbon C *1s* indicated species at the surface containing bonds between carbon and oxygen.

No unequivocal explanation could be offered why the SiC-scratched copper (M2-SiC) would influence the hydrogen production as indicated in Figure 3-4. The instability of the stainless steel system of Main 2 might introduce artefacts, but we cannot rule out effects of the inferred contamination. If only a changed surface microstructure were to determine the outcome, the diamond-scratched sample (M3-diam) should yield the same enhancement effects – but it showed none. On the other hand, the Main 3 system behaved in a more consistent way also as regards the background.

The examination of a SiC-scratched copper surface by GI-XRD presented solid evidence that the composition of the surface is changed through residues of the polishing paper. This contamination level is larger by far than any antimony partial coverage discussed above. The reactivity of the copper surface may be altered so as to influence the corrosion properties from the SiC particles if they somehow take active part. Features interpreted as particles caught in the matrix were observed by SEM also for diamond scratched samples, but diamond in itself must be quite inert and cannot take an active role in any corrosion process. The formation of local galvanic cells where SiC is involved (as the anode) is one alternative that we have not been able to investigate.

4.2 Effects from hydrogen treatment

As mentioned in Section 2.2, previous measurements of hydrogen content in copper (Boman et al. 2014) were hampered by inferior handling. The main drawbacks with the LECO method of fusion are that it craves gram-size samples and cannot use the very same sample again for analysis. Renewed LECO measurements of bulk hydrogen, complemented by desorption studies, showed that

the hydrogen content is low. Contrary to speculation concerning the effects of heating in hydrogen gas, the purification steps (electropolishing + hydrogen reduction) strongly reduce the hydrogen content. The final treatment at 400°C, where most of hydrogen desorption occurs, obviously guarantees a continued low hydrogen content. Studies by TEM corroborated these findings.

4.3 Effects from scratching

The attempts to change the macroscopic surface structure of the copper by scratching have yielded different results in the pressure monitoring, depending on substance (SiC, diamond). Whereas the scratching by diamond did not yield a pressure different from the background, the experiment with silicon carbide showed a pressure increase. Since SiC paper introduces contamination of the copper surface through remaining particles, the influence of scratching itself cannot be properly interpreted in that case. The scratching by diamond did influence the outcome of the ICP-MS analysis but not the pressure evolution.

The scratching of copper by SiC probably changed the outcome of various experiments, presumably through heavy contamination:

- Concentrations in water of aluminium and copper get enhanced, and both phosphorus and sulphur appear on the copper surface (contaminations).
- Carbon species containing carbon-oxygen bonds appear.
- Particles from the abrasive paper are caught in the copper matrix.
- The hydrogen evolution appears enhanced but yet no Cu_2O can be discerned.

The scratching of specimens by diamond yielded less dramatic effects:

- Concentrations in water (immersed for six days) of copper and zinc get enhanced, interpreted as artefacts from the handling.
- The hydrogen evolution does not significantly deviate from the background.

5 Conclusions

We have continued the work already reported on (Boman et al. 2014) along two lines: First of all, the time for the long-term experiments of copper in water has been extended considerably. These samples were kept for the study of *copper oxidation* by various chemical methods, a well-defined way to establish a true picture of a corrosion process since the existence of hydrogen production alone may be misleading, other sources being at play.

Secondly, renewed experiments have been performed concerning the pressure measurements, urged from the fact that hydrogen as a product of *water reduction* (from a corrosion process) had to be distinguished from other sources of production. The kernel of the problem was how to bring down the background level of hydrogen, knowing that stainless steel is a source that cannot be circumvented except for totally redesigning the equipment – which is outside the scope of the project. Considering the low degree of oxidation products, we encountered a challenging problem how to decrease the background so much that the corresponding calculated hydrogen contribution from a corrosion process could be discerned. Extensive heat-treatments have brought down the hydrogen emission from the steel to a very low level, in line with the best values reported in the literature. In addition to the work on reducing the background, a new design was adopted for the palladium membrane fitting so that no hydrogen flow was possible other than between the reaction chamber and the compartment with the pressure gauges. These latter were changed to improve the accuracy because of much lower outgassing, meaning a decreased background level from this exchange as well.

Some experiments were performed while changing the copper surface through scratching. The treatment is not reproducible; it does not imply any improvement and is even quite dubitable, forming a source of contamination that affects the results.

For the purified copper (electropolishing followed by hydrogen reduction) that has undergone exposure to water for a prolonged time span – up to a few years – the following facts may be summarized as the outcome of analyses:

- The copper Auger spectra from long-term experiments are identical and show no detectable Cu_2O, only pure metallic copper.
- There is a slight tendency of increased copper concentration by time in the water (although levelling off). The final value is very low ($\sim 10^{-7}$ M).
- There is no measurable tendency of changed copper content in (or on) the added glass plates by time.
- The low hydrogen content of the copper obtained through the purification does not increase on exposure to water.
- The hydrogen pressure increase is hardly discernible from the background that, compared to Boman et al. (2014), has been lowered considerably through the new design and harsher heat treatments.
- The diamond scratching does not alter these experimental findings, while scratching by SiC introduces heavy contamination and must be discarded as a method of cleaning a copper surface.
- The very minute antimony content is of no importance for the corrosion properties; no expected promotion effects were noted.

Since copper corrosion is revealed unambiguously only from its oxidation products, either by a deposition onto the copper or into the water phase, the conclusion prevails from the previous report (Boman et al. 2014) that there are no obvious signs of a significant corrosion process involving copper even after a couple of years at 50°C. The corresponding Auger spectra from the longest exposures have the best quality of them all, after the insight that a very rapid transference of the sample to the spectrometer is crucial for reliable results. The copper concentration in the water has increased to a minor extent with increasing residence time, and we can now, from separate measurement on a blank sample, rule out the simultaneous leaching from the glassware as part of the observed enhancement. That seems to strongly deviate from linearity by time, tending towards a constant low value.

Autocatalytic dissociation of water on a copper surface has been claimed (Andersson et al. 2008) that might be able to yield evolution of hydrogen on the simultaneous formation of a surface OH-species as a monolayer. In a first stage, such dissociation leaves adsorbed OH and H that very well may recombine and leave the surface before a monolayer is built up. There is also a small probability that H atoms migrate and combine to molecules yielding a pressure hardly discernible from the background. That study operated with gaseous water which means that the surface energy term would be relatively more important than in liquid water. Cu_2O is thermodynamically more stable under such conditions and would be expected to form. Even less than a monolayer of this oxide is without doubt easily detectable by Auger spectroscopy; none was found.

6 Acknowledgments

This work was financed by the Swedish Nuclear Fuel and Waste Management Company but our strategy, experimental solutions and conclusions have not been influenced or restricted by that fact.

The work rests to a large extent on the possibility to have the equipment refurnished and the analyses made with the highest accuracy. Moreover, we have relied on the easy access of the facilities of the Ångström Laboratory. We thank Jonas Ångström for the skilful help with preparation of copper samples and Jan Bohlin for excellent workmanship in machining the stainless steel equipment.

Finally we are indebted to Ingvar Bernhardsson and coworkers at the Degerfors Laboratory for their willingness to deviate from routine practice in their hydrogen analyses to conform to our wishes concerning sample preparation.

References

SKB's (Svensk Kärnbränslehantering AB) publications can be found at www.skb.se/publications.

Andersson K, Ketteler G, Bluhm H, Yamamoto S, Ogasawara H, Pettersson L G M, Salmeron M, Nilsson A, 2008. Autocatalytic water dissociation on Cu(110) at near ambient conditions. Journal of the American Chemical Society 130, 2793–2797.

Atkarskaya A B, Bykov V N, 2003. Clarification of glass using arsenic and antimony oxides. Glass and Ceramics 60, 389–391.

Attwood D T, 2000. Soft X-rays and extreme ultraviolet radiation: principles and applications. Cambridge: Cambridge University Press.

Berry F J, Holden J G, Loretto M H, Urch D S, 1987. Iron antimonate. Journal of the Chemical Society, Dalton Transactions, 1727–1731.

Bills D G, 1969. Ultimate pressure limitations. Journal of Vacuum Science and Technology 6, 166–173.

Binner J, Zhang Y, 2001. Characterization of silicon carbide and silicon powders by XPS and zeta potential measurement. Journal of Materials Science Letters 20, 123–126.

Boman M, Ottosson M, Berger R, Andersson Y, Hahlin M, Björefors, F, Gustafsson T, 2014. Corrosion of copper in ultrapure water. SKB R-14-07, Svensk Kärnbränslehantering AB.

Cano E, Torres C L, Bastidas J M, 2001. An XPS study of copper corrosion originated by formic acid vapour at 40% and 80% relative humidity. Materials and Corrosion 52, 667–676.

Caravella A, Hara S, Drioli E, Barbieri G, 2013. Sieverts law pressure exponent for hydrogen permeation through Pd-based membranes: couples influence of non-ideal diffusion and multicomponent external mass transfer. International Journal of Hydrogen Energy 38, 16229–16244.

Chavez K L, Hess D W, 2001. A novel method of etching copper oxide using acetic acid. Journal of the Electrochemical Society 148, G640–G643.

Deng X, Verdaguer, Herranz T, Weis C, Bluhm H, Salmeron M, 2008. Surface chemistry of Cu in the presence of CO_2 and H_2O. Langmuir 24, 9474–9478.

Flanagan T B, Lynch J F, Clewley J D, Von Turkovich B, 1976. The effect of lattice defects on hydrogen solubility in palladium: I. Experimentally observed solubility enhancements and thermodynamics of absorption. Journal of the Less Common Metals 49, 13–24.

Garbassi F, 1980. XPS and AES study of antimony oxides. Surface and Interface Analysis 2, 165–169.

Hegde R I, Sainkar S R, Badrinarayanan S, Sinha A P B, 1981. A study of dilute tin alloys by X-ray photoelectron spectroscopy. Journal of Electron Spectroscopy and Related Phenomena 24, 19–25.

Holleck G L, 1970. Diffusion and solution of hydrogen in palladium and palladium–silver alloys. Journal of Physical Chemistry 74, 503–511.

Hourani M, Wedian F, 2000. The effect of adatoms on the corrosion rate of copper. Corrosion Science 42, 2131–2144.

Hultquist G, 1986. Hydrogen evolution in corrosion of copper in pure water. Corrosion Science 26, 173–177.

Hultquist G, Szakálos P, Graham M J, Belonoshko A B, Sproule G I, Gråsjö L, Dorogokupets P, Danilov B, AAstrup T, Wikmark G, Chuah G-K, Eriksson J-C, Rosengren A, 2009. Water corrodes copper. Catalysis Letters 132, 311–316.

Hultquist G, Graham M J, Szakálos P, Sproule G I, Rosengren A, Gråsjö L, 2011. Hydrogen gas production during corrosion of copper by water. Corrosion Science 53, 310–319.

Hultquist G, Graham M J, Kodra O, Moisa S, Liu R, Bexell U, Smialek J L, 2015. Corrosion of copper in distilled water without O_2 and the detection of produced hydrogen. Corrosion Science 95, 162–167.

Johansson J, Blom A, Chukharkina A, Pedersen K, 2015. Study of H_2 gas emission in sealed compartments containing copper immersed in O_2-free water. SKB TR-15-03, Svensk Kärnbränslehantering AB.

Johansson L-S, Campbell J M, Hänninen T, Ganne-Chèdeville C, Vuorinen T, Hughes M, Laine J, 2012. XPS and the medium-dependent surface adaptation of cellulose in wood. Surface and Interface Analysis 44, 899–903.

Jones D A, 1992. Principles and prevention of corrosion. New York: Macmillan.

Le D P, Ji W S, Kim J G, Jeong K J, Lee S H, 2008. Effect of antimony on the corrosion behavior of low-alloy steel for flue gas desulfurization system. Corrosion Science 50, 1195–1204.

Liu W K, Yuen W T, Stradling R A, 1995. Preparation of InSb substrates for molecular beam epitaxy. Journal of Vacuum Science & Technology B 13, 1539–1545.

Mariot J-M, Barnole V, Hague C F, Vetter G, Queyroux, F, 1989. Local electronic structure of Cu_2O, CuO and $YBa_2Cu_3O_{7-\delta}$. Zeitschrift für Physik B Condensed Matter 75, 1–9.

Martinsson Å, Sandström R, 2012. Hydrogen depth profile in phosphorus-doped, oxygen-free copper after cathodic charging. Journal of Materials Science 47, 6768–6776.

Martinsson Å, Sandström R, Lilja C, 2013. Hydrogen in oxygen-free, phosphorus-doped copper: charging techniques and modelling of the hydrogen diffusion and depth profile. SKB TR-13-09, Svensk Kärnbränslehantering AB.

O'Hanloon J F, 2003. A user's guide to vacuum technology. 3rd ed. Hoboken, NJ: Wiley.

Panzner G, Egert B, Schmidt H P, 1985. The stability of CuO and Cu_2O surfaces during argon sputtering studies by XPS and AES. Surface Science 151, 400–408.

Park C D, Chung S M, Xianghong Liu, Yulin Li, 2008. Reduction in hydrogen outgassing from stainless steels by a medium-temperature heat treatment. Journal of Vacuum Science and Technology A26, 1166–1171.

Park J-Y, Lim K-A, Damsier R D, Kang Y-C, 2011. Spectroscopic and morphological investigation of copper oxide thin films prepared by magnetron sputtering at various oxygen ratios. Bulletin of the Korean Society of Chemistry 32, 3395–3399.

Sciti D, Bellosi A, 2000. Effects of additives on densification, microstructure and properties of liquid-phase sintered silicon carbide. Journal of Materials Science 35, 3849–3855.

Scofield J H, 1976. Hartree–Slater subshell photoionization cross-sections at 1254 and 1487 eV. Journal of Electron Spectroscopy and Related Phenomena 8, 129–137.

Szakálos P, Hultquist G, Wikmark G, 2007. Corrosion of copper by water. Electrochemical and Solid State Letters 10, C63–C67.

Ward T L, Dao T, 1999. Model of hydrogen permeation behavior in palladium membranes. Journal of Membrane Science 153, 211–231.

Yamamoto S, Andersson K, Bluhm H, Ketteler G, Starr D E, Schiros T, Ogasawara H, Pettersson L G M, Salmeron M, Nilsson A, 2007. Hydroxyl-induced wetting of metals at near-ambient conditions. The Journal of Physical Chemistry C 111, 7848–7850.

Appendix A

Details concerning the modification of the assemblies

A1 Design of the new lid

The lid was made from a solid rod of 316L steel with a CF-63 connection to the lower chamber. The upper part has a CF-38 connection to the vacuum chamber. Inside the CF-38 there is a Swagelok VCR ¼″ fitting for the Pd membrane. The membrane was mounted in the gasket retainer assembly. When the gasket is tightened, the Pd membrane gets pressed towards the body welded on the lid. The VCR assembly was leak-detected with helium. This VCR–Pd fitting acts as a hydrogen filter. The external CF-38 is the outer seal. This design gives no air contact of the Pd membrane.

A2 Outgassing rates

A2.1 Non-bakeable components

The valves and the pressure gauges were tested by the pressure-rise method. Each gauge was connected to a Swagelok valve and pumped down during 24 h under baking at 150–200°C. The pressure increase was measured, and from the gas volume the outgassing rate was calculated.

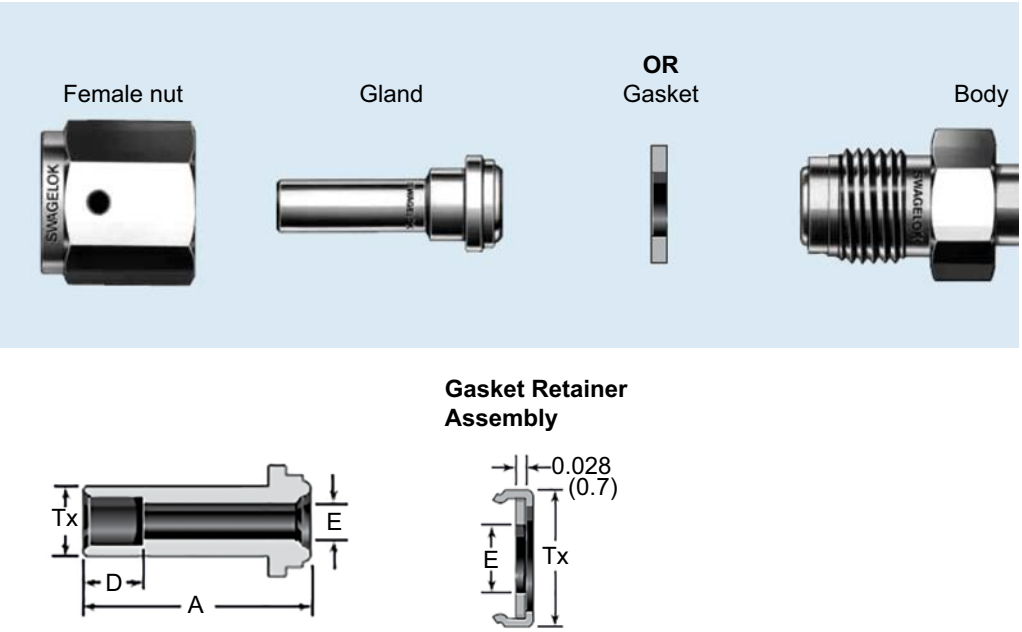

Figure A-1. *The principle of the he VCR fitting from Swagelok.*

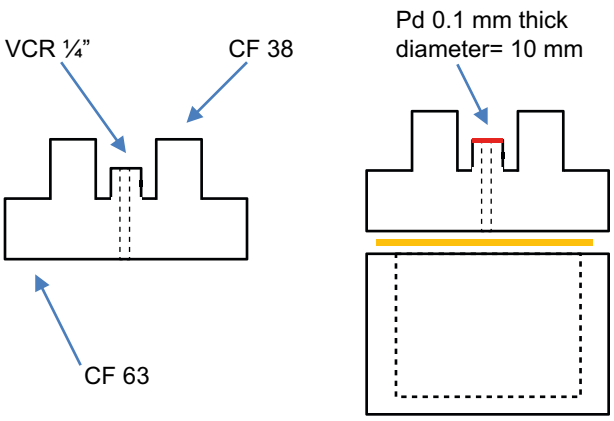

Figure A-2. *A sketch of the lid with the membrane connection.*

MKS627B pressure gauge

Pressure increase: 20 mTorr/24 h (5 cm^3) at RT.

This corresponds to an outgassing of $20 \times 365 \times 5/(760 \times 1{,}000 \times 24{,}465^*) = 2.0 \times 10^{-6}$ *mol/year.*

This value is a relatively high outgassing rate, which suggests that one possible source is the Inconel pressure membrane used in all MKS Baratron pressure gauges.

Pfeiffer CCR 374 pressure gauge

This has ceramic membranes that cannot give off hydrogen.

Pressure increase: 0.30 mTorr/24 h (18.4 cm^3).

This corresponds to $0.30 \times 365 \times 18.4/(760 \times 1{,}000 \times 24{,}465) = 1.1 \times 10^{-7}$ *mol/year.*

This gauge gives a much lower outgassing rate. Consequently, the pressure gauges for the new set-ups, Main 2 and Main 3 were exchanged to Pfeiffer CCR 374 gauges.

A2.2 Main 2 with new pressure gauges

Baking partly at 400°C

Calculated surface area about 600 cm^2 (lid 1 side + chamber = 214×1.5); Gas volume 350 cm^3.

Pressure increase: 3 mTorr/24h at RT.

This corresponds to $3 \times 365 \times 350/(760 \times 1{,}000 \times 24{,}465) = 2.1 \times 10^{-5}$ *mol/ year.*

Outgassing / surface area is:

$$\frac{0.003 \times 0.350}{24 \times 3{,}600 \times 600} = 2.0 \times 10^{-11}\ \text{Torr} \cdot \text{L} \cdot \text{s}^{-1} \cdot \text{cm}^{-2}$$

Baking an assembled system further at 300°C for 240 h

Pressure increase: 0.5 mTorr/24 h at RT.

This corresponds to $0.5 \times 365 \times 350/(760 \times 1{,}000 \times 24{,}465) = 3.4 \times 10^{-6}$ *mol/ year.*

Outgassing / surface area is:

$$\frac{0.0005 \times 0.350}{24 \times 3{,}600 \times 600} = 3.4 \times 10^{-12}\ \text{Torr} \cdot \text{L} \cdot \text{s}^{-1} \cdot \text{cm}^{-2}$$

* 24,465 cm^3/mole is the molar volume of the gas at 760 Torr and 25°C.

Appendix B

Measurements of hydrogen pressure, general aspects

B1 Sieverts' law and data background.

For the equilibrium of the gas phase and the solid solution of H in Pd the following is valid:

$$Pd(s) + ½\ H_2(g) \rightleftharpoons PdH_x(s) \quad \text{(B-1)}$$

Since $PdH_x(s)$ forms the same phase as Pd(s), only differing in composition, the hydrogen pressure depends on the composition of the solid solution. The Sieverts' law constant (K_s) is defined as the equilibrium constant, K_s for $X << 1$.

$$K_S = \frac{P_{H2}^{½}}{X}, \quad \text{(B-2)}$$

where X= H/Pd atomic ratio.

The constant depends on the temperature, enthalpy and entropy (Ward and Dao 1999):

$$K_S = e^{\left(\frac{\Delta\overline{H}_H^0}{RT} - \frac{\Delta\overline{S}_H^0}{R}\right)} \quad \text{(B-3)}$$

Ward and Dao (1999) quote data published by Holleck (1970), experimentally determined in the temperature range 260–640°C:

$\Delta\overline{H}_H^0 = 2000\ \frac{cal}{mol}$ (The relative partial molar enthalpy of dissolution at infinite dilution.)

$\Delta\overline{S}_H^0 = 11.65\ \frac{cal}{mol \cdot K}$ (The relative partial molar entropy of dissolution at infinite dilution.)

From these data Ward and Dao (1999) calculate $K_s = 351.6e^{\left(\frac{-1007}{T}\right)}$ $atm^{½}$.

Most of the experiments in this report is at a palladium temperature of 55°C, yielding:

K_s (55°C) = 16.32 $atm^{½}$ and

K_s (25°C) = 12.00 $atm^{½}$.

By using Torr as the pressure unit (conversion factor $760^{½}$), the relation is rewritten as:

K_s (55°C) = 449.903 $Torr^{½}$ respectively,

K_s (25°C) = 330.85 $Torr^{½}$.

The constant can also be expressed with the unit mol/(cm^3 $Torr^{½}$).

For Pd, with density = 12 g/cm^3 and atomic mass = 106.4 g/mol,

K (55°C) = 2.51×10^{-4} mol/(cm^3 $Torr^{½}$) and

K (25°C) = 3.41×10^{-4} mol/(cm^3 $Torr^{½}$).

N.B. All these data were validated at higher pressures than in our experiments, typically at 1 atm. Moreover, the temperatures were higher. Both these aspects maybe influence the value of the equilibrium constant (that has been determined experimentally) to be used in other regimes of temperature and pressure.

B2 A model for pressure correction.

The pressure corrections to the data of Main 2 and Main 3 must take care of the different volumes of the two compartments (lower and upper chamber) and the membrane, the hydrogen solubility in the membrane and must also handle the different temperatures. Since the lower chamber is heated to 50°C for most of the experiments and at room temperature for one background measurement, while the palladium is held at 55°C, different combinations have to be considered:

I. All parts at room temperature (RT) in an *empty system* (background) [Main 2].

II. Lower chamber at 50°C and the upper chamber at 25°C. The system is *empty* (background) [Main 3].

III. Lower chamber at 50°C, palladium at 55°C and the upper chamber at 25°C. The system is *empty* (background) [Complementary setup].

IV. Lower chamber at 50°C, palladium at 55°C and the upper chamber at 25°C. The system is *loaded* (background and corrosion rates) [Main 2, Main 3].

The volumes of the system parts:

Upper chamber (above the lid): 100 cm^3.

Lower chamber (reaction chamber): 250 cm^3.

Lower chamber with water, holders and Cu: 120 cm^3.

Volumes for the calculations:

1. Empty system: 100 (RT) + 250 (RT or 50°C) = 350 cm^3.
2. Loaded system: 100 (RT) + 120 (RT or 50°C) = 220 cm^3.

The Pd membrane:

Diameter: 10 mm; Thickness: 0.1 mm; Volume: 7.86×10^{-3} cm^3.

Mass: 0.094 g (density is 12 g/cm^3).

The amount of hydrogen within the Pd membrane

The amount of hydrogen in Pd:

$$C_{Pd} = K(55°C) \cdot \sqrt{p} \cdot 7.86 \times 10^{-3} \text{ mol} \quad \text{(B-4)}$$

$$C_{Pd}\ (55°C) = \sqrt{p} \cdot 1.97 \times 10^{-6} \text{ mol} \quad \text{(B-5)}$$

$$C_{Pd} = K(25°C) \cdot \sqrt{p} \cdot 7.86 \times 10^{-3} \text{ mol} \quad \text{(B-6)}$$

$$C_{Pd}\ (25°C) = \sqrt{p} \cdot 2.68 \times 10^{-6} \text{ mol} \quad \text{(B-7)}$$

However, since the gaseous form of hydrogen is a diatomic molecule,

the amount H_2 in Pd (55°C) is $\sqrt{p} \cdot 1.00 \times 10^{-6}$ mol (B-8)

the amount H_2 in Pd (25°C) is $\sqrt{p} \cdot 1.34 \times 10^{-6}$ mol (B-9)

The pressure yielded by the hydrogen in Pd

N.B. The standard temperature is 50°C in the lower chamber.

The molar volume for 25°C = 24,465 cm^3 (760 Torr).

The molar volume for 50°C = 26,517 cm^3 (760 Torr).

The different cases (I-IV) are treated using the following nomenclature:

P_m= Measured pressure.

P_{WoPd}= Calculated pressure including effect of hydrogen in palladium.

Since molar amounts are being considered, the pressures can only be compared if they are multiplied with an experimental factor that involves the volume of the space and the molar volume of the gas.

Empty systems:

The volume factor for an empty system at RT (25°C) is:

$$\frac{24{,}465}{350} \cdot 760 = 53{,}124 \text{ Torr/mol } H_2 \quad \text{(B-10)}$$

The pressure correction at 25°C is obtained from combining (B-9) and (B-10):

$$P_{WoPd} = P_m + 0.0712\sqrt{P_m} \text{ (at 25°C)} \quad \text{(B-11)}$$

The volume factor for an *empty* system with hydrogen at 25°C and 50°C is:

$$\left(\frac{26\,517\left(\frac{250}{350}\right)}{350} + \frac{24\,465\left(\frac{100}{350}\right)}{350}\right) \cdot 760 = 56{,}307 \text{ Torr/mol } H_2 \text{ (at 25°C resp. 50°C)} \quad \text{(B-12)}$$

The pressure correction including the Pd at 55°C is obtained from combining (B-8) and (B-12):

$$P_{WoPd} = P_m + 0.0563\sqrt{P_m} \text{ (at 25°C, 50°C resp. 55°C)} \quad \text{(B-13)}$$

Loaded systems:

Here, part of the space is taken by the introduction of the copper samples.

The volume factor for *loaded* system with hydrogen at 25°C and 50°C is:

$$\left(\frac{26\,517\left(\frac{120}{220}\right)}{220} + \frac{24\,465\left(\frac{100}{220}\right)}{220}\right) \cdot 760 = 88{,}383 \text{ Torr/mol } H_2 \text{ (at 25°C resp. 50°C)} \quad \text{(B-14)}$$

Pressure correction for a loaded system including Pd from combining (B-8) and (B-14):

$$P_{WoPd} = P_m + 0.0884\sqrt{P_m} \text{ (at 25°C, 50°C resp. 55°C)} \quad \text{(B-15)}$$

For comparing of outgassing between an empty and a loaded system, the volume difference between the two has to be compensated for by the ratio 1.570. That factor can be multiplied to the measured pressure and used.

The applied model has obvious limitations. It is solely based on a situation of equilibrium, and as indicated above, even the equilibrium constant (Sieverts' law) is approximated since these experiments deal with other pressures and temperatures. In the model it is not possible to introduce parameters that involve the dynamics of the system, considering hydrogen production in both the lower and the upper chamber and processes at the palladium surface. Equilibrium models can never include the time aspect, *i.e.* how long it takes before equilibrium is attained. These problems are most certainly reflected in the outcome of the experiments, making it difficult to extract exact values since the model is faltering.

B3 Evaluation of the pressure measurements

In order to determine the pressure increase rate, data from both from the backgrounds and the corrosion experiments have to be included. The pressure increase is the slope of the pressure curve.

$$Rate = \frac{\partial P}{\partial t} \approx \frac{\Delta P}{\Delta t} \quad \text{(B-16)}$$

The data are evaluated in the Excel software; the slope is calculated by taking the pressure difference in an interval of approximately 83–85 h.

In order to arrive at comparable rates, Torr/h is transformed to *mol/year*.

The transformation formula is:

$$\frac{Volume\ (cm^3) \cdot 24h \cdot 360\ days}{molar\ volume\left(\frac{cm^3}{mol}\right) 760} \quad \text{(B-17)}$$

In this expression, the input pressure is measured in Torr and the time in hours. The molar volume at 760 Torr is 24,465 cm^3/mol at 25°C and 26,517 cm^3/mol at 50°C (See Section B2 above).

At RT (25°C), the factor is 0.1649.

At 50°C, the factor is 0.1556 for an empty system and 0.09911 for a loaded system.

The rates may be plotted vs. time in order to check whether a constant rate is obtained. This kind of analysis is practised in connection with Figure 3-4 and Figures C-3 and C-4.

Determination of the rates for Main 3:

Data from the pressure measurements for Main 3 (Figure 3-5) were corrected for the influence by the Pd membrane (see Appendix B2), from which hydrogen rates were calculated (*cf.* Figure 3-4 for Main 2). The result for Main 3 is given in Figure B-1 below:

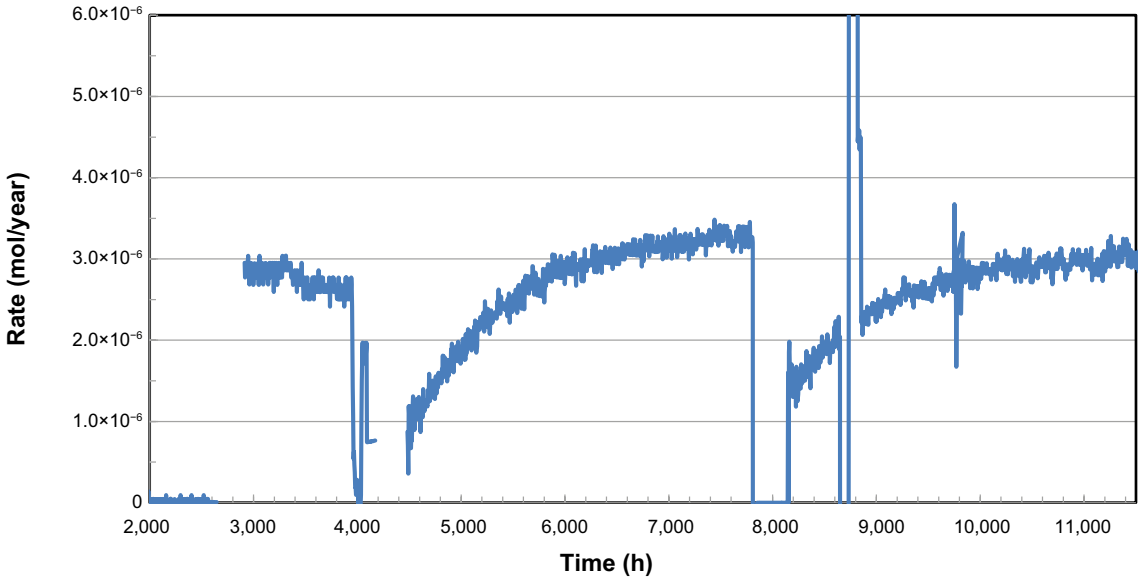

Figure B-1. *Estimated hydrogen production rates for Main 3. (Note the logging system flaw.)*

Appendix C

Complementary equipment

C1 Influence by oxygen

One test with the equipment outside the glove box concerned the possibility of interference from oxygen. With this equipment pressure could be measured in both chambers, and the equalization of pressure between the chambers after any perturbation could be monitored by time.

A scheme was followed where the equipment only had a Pd membrane between the compartments but contained no water:

1. Evacuation.
2. Addition of 0.1 Torr air (0.021 Torr O_2) to the lower chamber.
3. Further addition of 0.85 Torr air.
4. Evacuation.

Monitoring was made of the equalization rate between the chambers as presented in Figure C-1.

The stainless steel and other parts of the system act as the only emitting sources of hydrogen. It was thus important at start to remove as much as possible of the background gas by thoroughly evacuating. The inserted numbers in the figure allude to those of the experimental scheme above, but the first step is illustrated by several evacuations during the first 1,500 hours.

After about 1,500 hours the evacuations were stopped. A continuous almost linear increase of pressure in the lower chamber (red line) is accompanied by the same in the upper chamber (green line – N.B. different scales). At about 1,750 h, at point 2, the first addition of air is made. The rate of pressure increase in the upper chamber is altered somewhat as a result, a small lowering occurs. The pressure in the upper chamber is due to hydrogen only while there is now a gas mixture in the lower one.

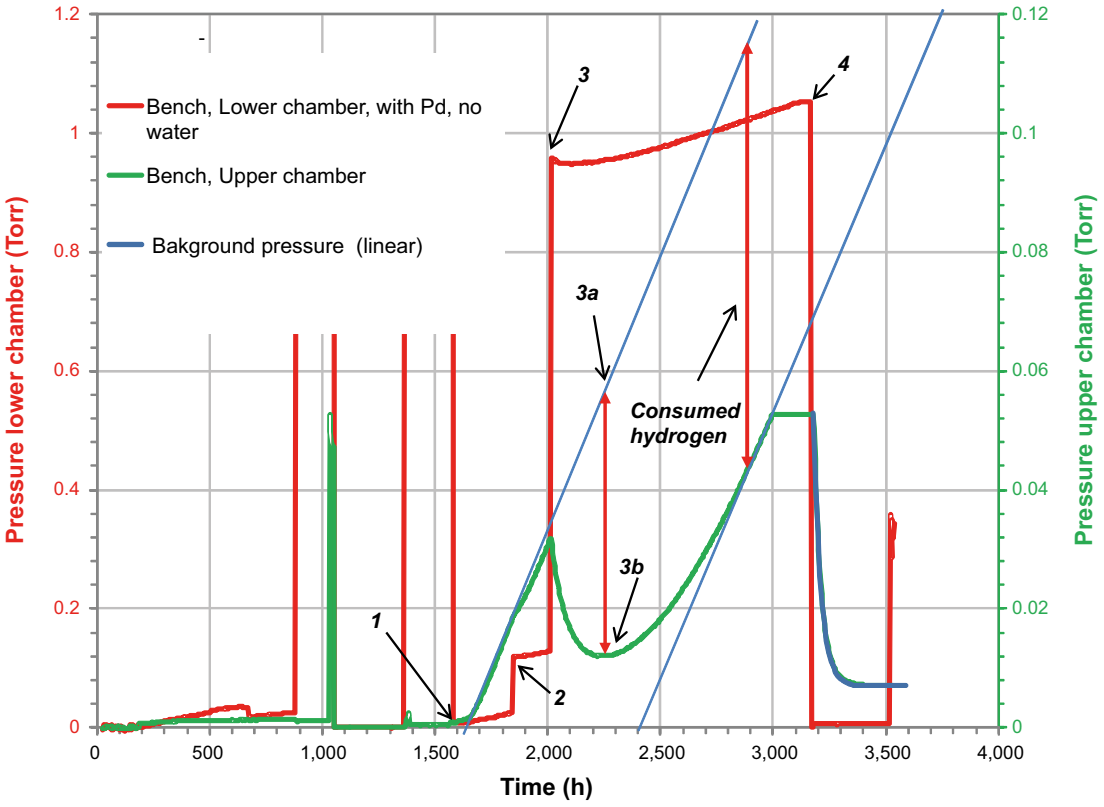

Figure C-1. *Pressure characteristics of the experiment are described in text. Pressures may be followed in lower as well as upper chamber, these being connected through a Pd membrane for hydrogen exchange.*

At 2,000 h a much larger addition of air is made (point 3) to the lower chamber, with a pronounced effect also in the upper one: Now both pressures go down and then rise again. The minimum of the hydrogen pressure in the upper chamber occurs at point 3b while point 3a denotes the pressure that would have occurred if there had not been any perturbation, assuming that the linear increase just continued. The pressures increase up to about 3,200 h when (at point 4) another evacuation occurs of the lower chamber. The plateau in the green curve before that stage is an artefact created from the readings of the pressure gauge. Just after point 4 when the evacuation of the lower chamber is seen as very efficient, there is a slow response at the upper chamber, and the pressure goes to a fixed value just below 0.01 Torr.

The direct qualitative interpretation of the outcome of introducing air in the lower chamber is that the oxygen consumes hydrogen with the palladium catalysing that reaction. At the minimum in hydrogen pressure (upper chamber) the pressure has dropped from the unperturbed expected pressure of 0.054 Torr (point 3a) to 0.012 Torr (point 3b). After the minimum, there is again an increase in pressure with a rate that is approaching that of the unperturbed system (slope of tangent at 3,000 h), a value of ~0.12 Torr/1,500 h. The displacement of the tangent in comparison with the extrapolated rate before the perturbation is a measure of the amount of hydrogen taking part in the reaction with oxygen. This corresponds to a pressure difference of 0.070 Torr (*e.g.* at arrows at ~2,900 h in the figure).

The amount of consumed hydrogen relates to 0.070 Torr in 350 cm^3 (= 24.5 Torr·cm^3). The amount of added oxygen from the air was 0.95 Torr × 0.21 × 250 cm^3 = 49.9 Torr·cm^3. The found molar ratio of H_2 and O_2 is then roughly 1:2.

The important conclusion from this experiment series is that the palladium membrane seems to take an active part as a catalyst so that water forms. However, this experiment cannot elucidate the role that the membrane itself takes as it dissolves hydrogen (that would otherwise have reacted further with oxygen). This effect of forming a solid solution, PdH_x, affects the determination of the background.

C2 Determination of background outgassing rates

The background of the complementary setup was investigated through a series of measurements with intermittent pumping. The pressure curves are shown in Figure C-2, the left part of which constitutes Figure C-1. The same nomenclature is used, *i.e.* green curves and scale belong to the upper chamber, and red ones to the lower chamber.

The outgassing rates could be calculated from the pressure curves using the model described previously in Appendix B. Specifically, the model III of Section B2 (Equation (B-13) there) is to be used. The connection between the pressures is expressed by

$$P_{WoPd} = P_m + 0.0563\sqrt{P_m}. \qquad \text{(C-1)}$$

The transformation to molar amounts of hydrogen gas (H_2) from the relation $\frac{P_m \cdot 350 \cdot 24 \cdot 365}{26\,517 \cdot 760}$ yields a production of $P_{WoPd} \cdot 0.1552$ mol/year (pressures in Torr).

The background pressures were measured in the time period 4,000–5,400 hrs but also before the inlet of air (see Table C-1). The transformation into rates is displayed in Figures C-3 and C-4. “Stable” and “unstable” figuratively describe whether a fair value could be obtained or not.

Table C-1. Estimations of outgassing rates (mol/year) from measurements and modelling.

Time period	Upper chamber	Comment	Lower chamber	Comment
1,800–1,900	1.9×10^{-5}	Unstable	1.7×10^{-5}	Unstable
4,000–4,700	2.0×10^{-5}	Stable	1.9×10^{-5}	Stable
4,900–5,400	2.3×10^{-5}	Unstable	2.2×10^{-5}	Stable

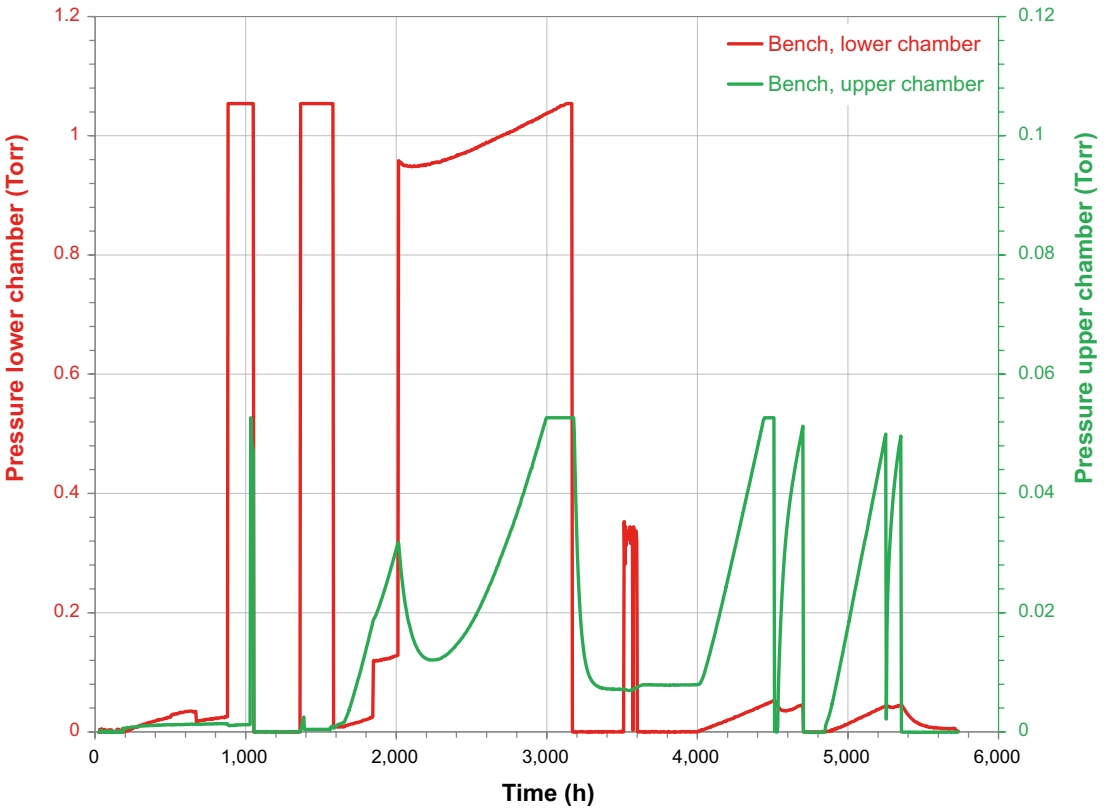

Figure C-2. *Supplemented data of Figure C-1. The background measured after 4,000 hrs are only due to the outgassing from the stainless steel.*

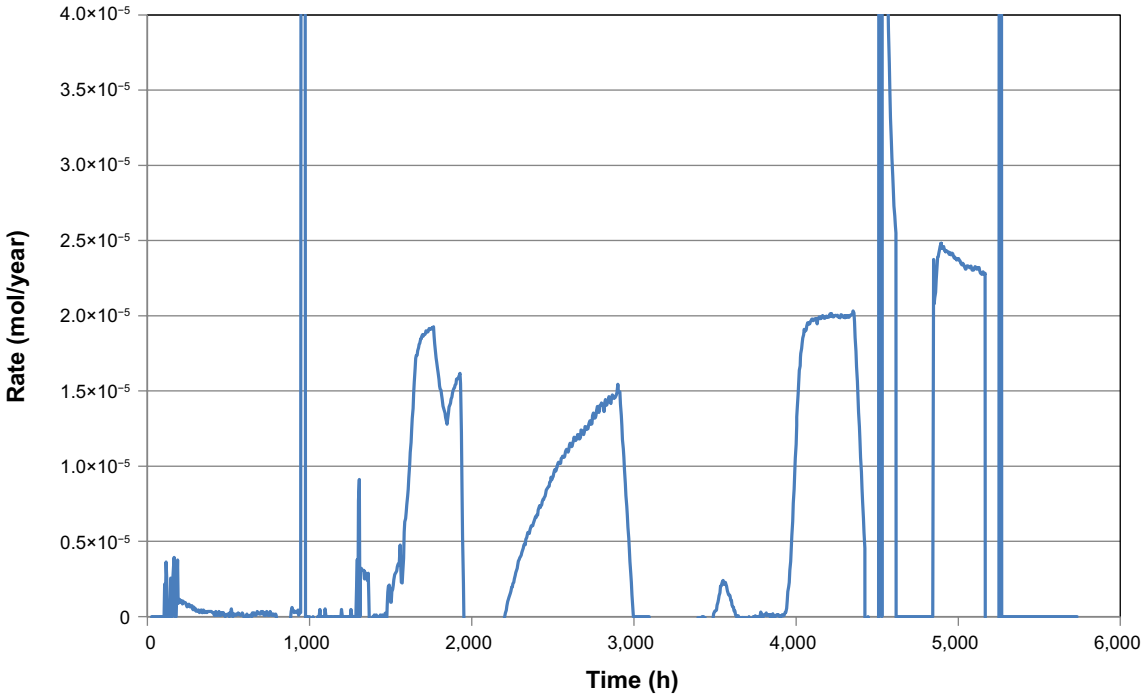

Figure C-3. *Calculated outgassing rates from data of the upper chamber (green curves of Figure C-2) using the relations given in text.*

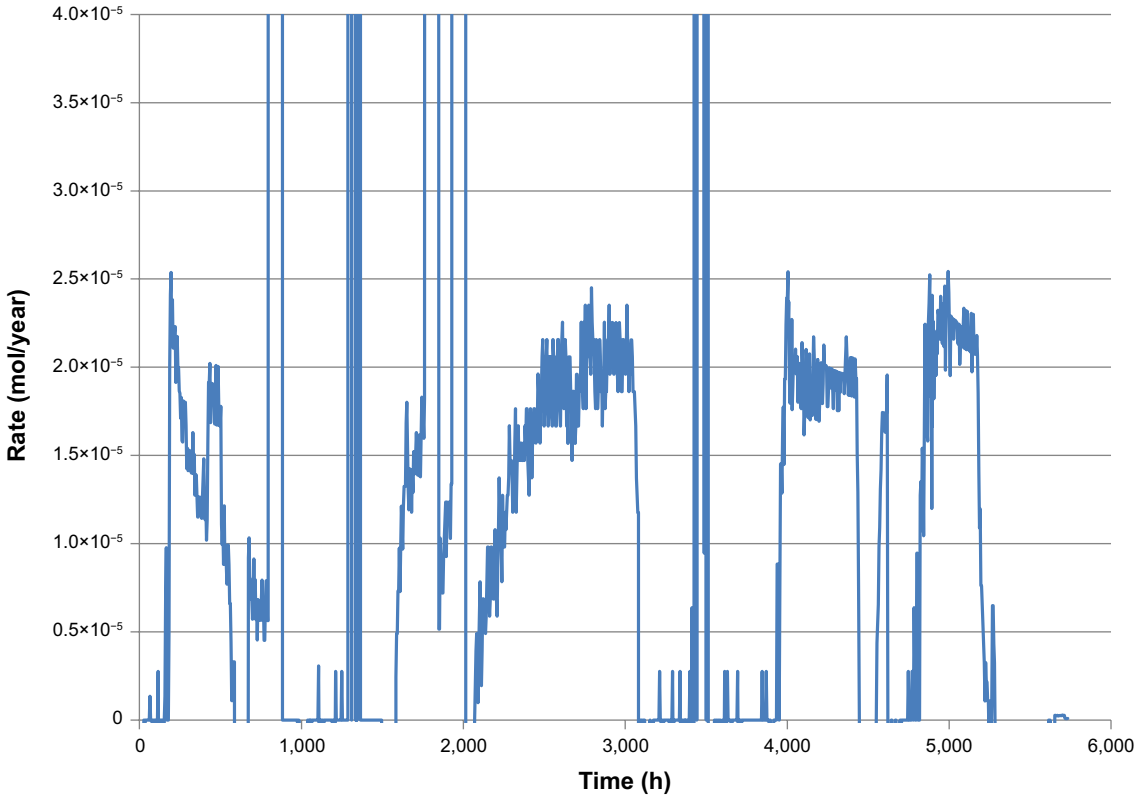

Figure C-4. *Calculated outgassing rates from data of the lower chamber (red curves of Figure C-2) using the relations given in text.*

C3 Pressure equilibration between the chambers

C3.1 Addition of an H_2/N_2 mixture

In order to investigate the response time between the lower reaction chamber (of volume 250 cm^3) and the pressure gauges in the upper chamber (100 cm^3), an H_2/N_2 mixture was added to the lower chamber. The question raised was whether nitrogen in excess (that is present because of the glove-box environment) would hamper the exchange to any considerable extent. A gas mixture with very low hydrogen content was chosen, but the situation is not directly comparable with that in Main 1–3, in the sense that the pressure difference between the two chambers is roughly ten times higher than in any of the experiments concerning copper corrosion.

1. Both chambers were pumped down during about 30 h.
2. The lower chamber (250 cm^3) was filled to 752 Torr by a H_2/N_2 mixture (1,000 ppm H_2).
3. The pressure increase in the upper chamber (100 cm^3) was measured.

The pressure without any Pd in the total system volume (350 cm^3) would be:

$752 \times 1.00 \times 10^{-3} \times 250\ cm^3/350\ cm^3 = 0.537$ Torr,

P_m= the expected (real/measured) pressure would be = 0.496 Torr, as indicated in Figure C-5 (see Appendix C3.2, Appendix B2, Equation (B-13)).

C3.2 Calculation of the pressure increase with the Pd foil

The relation $P_{WoPd}=P_m + K_{exp} \sqrt{P_m}$ (See Section 3.2.1), where

P_m = The measured pressure.

P_{WoPd}= The pressure without Pd.

K_{exp} = Experimental constant, including K_s and volume factor,

may be rewritten as on a quadratic form as

$$P_m^2 - (2P_{WoPd} + K_{exp}^2)P_m + P_{WoPd}^2 = 0 \qquad \text{(C-2)}$$

Its solution is

$$P_m = ½K_{exp}^2 + P_{WoPd} - ½K_{exp}\sqrt{K_{exp}^2 + 4P_{WoPd}} \qquad \text{(C-3)}$$

K_{exp}= 0.0563 for a system temperature of 50°C, Pd temperature of 55°C (Appendix B2, (B-13)).

In this case one may arrive at the approximation

$$P_m = P_{WoPd} - K_{exp}\sqrt{P_{WoPd}} \qquad \text{(C-4)}$$

C3.3 Relaxation time

By plotting the pressure increase rate, the relaxation time can be determined.

In order to arrive at comparable rates, Torr/h is transformed to mol/year.

The transformation formula is:

$$\frac{Volume\ (cm^3)\cdot 24h\cdot 360\ days}{molar\ volume\left(\frac{cm^3}{mol}\right)760}$$ (Appendix B3, (B-17)). (C-5)

In this expression, the input pressure is measured in Torr and the time in hours. The molar volume at 760 Torr is 26,517 cm^3/mol at 50°C (From Appendix B2).

When the rate decreases to the value of the outgassing (2×10^{-5} mol/year; *cf.* Table C-1), the relaxation should be complete. From Figure C-6, this rate is obtained at 6,175 h or 355 h after the addition of the hydrogen/nitrogen mixture.

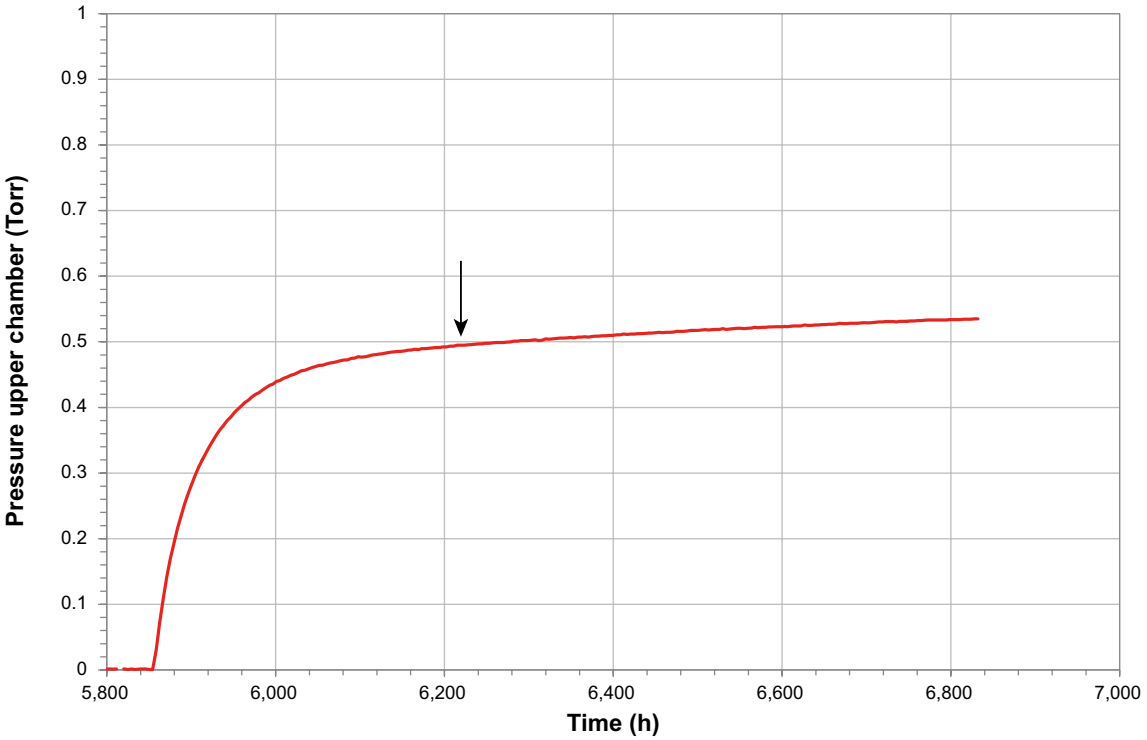

Figure C-5. *Pressure equilibration after addition of gas mixture. The expected pressure (see text) of 0.496 Torr is marked with an arrow.*

From this behaviour, the conclusions are that the relaxation time is several hundred hours for attaining equilibrium between the two chambers. The important thing is that the nitrogen is not preventing an exchange of hydrogen between the chambers and that full equilibrium is obtained. In this respect this experiment has bearing on the experimental setups Main 1–3 where the lower chambers are loaded in the nitrogen atmosphere in the glove box.

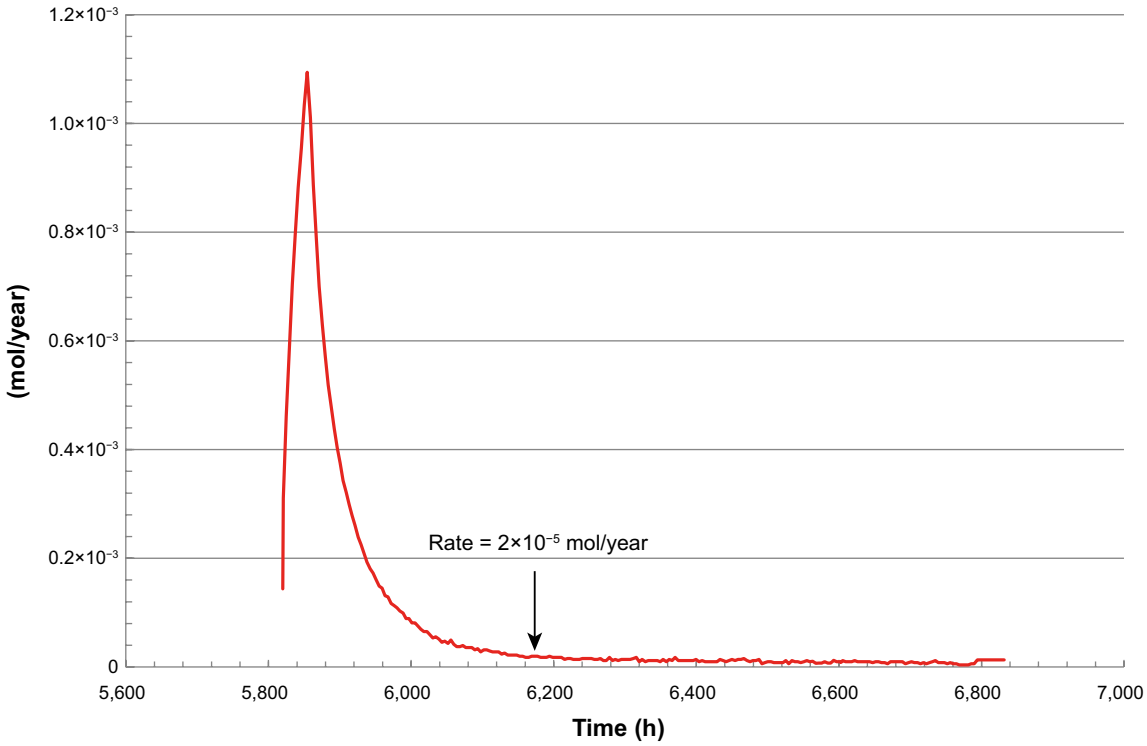

Figure C-6. *Rate evolution from Figure C-5.*

Appendix D

Details of ICP-MS analyses (semi-quantitative)

The results presented in Figure 3-20 are here given in numerical form:

Element\months		0	1	3	6	15	29
Ag	(µg/l)	0.07	0.04	0.03	0.04	0.04	0.03
Al	(µg/l)	32	12	73	222	239	275
As	(µg/l)	0.06	0.04	0.03	0.04	0.04	0.04
B	(µg/l)	*172	112	341	672	854	1,734
Ba	(µg/l)	0.26	0.39	0.15	0.51	0.35	0.20
Br	(µg/l)	1.00	0.79	0.85	1.04	1.61	1.43
Ca	(µg/l)	94	40	103	223	197	241
Cd	(µg/l)	0.01	0.11	0.00	0.00	0.01	0.10
Cl	(µg/l)	167	143	142	146	115	44
Cr	(µg/l)	0.53	0.44	0.46	0.55	0.66	0.31
Cu	(µg/l)	0.90	6.29	5.53	8.33	4.95	19.0
Fe	(µg/l)	0.53	1.55	0.45	1.37	1.91	1.67
Ga	(µg/l)	0.05	0.74	0.57	0.58	0.65	0.39
Ge	(µg/l)	0.01	0.29	0.57	0.06	0.08	0.09
Hf	(µg/l)	0.00	0.00	0.00	0.01	0.26	0.20
I	(µg/l)	1.86	1.61	0.95	1.27	1.55	0.52
K	(µg/l)	300	157	431	854	1,104	1,344
Li	(µg/l)	1.03	0.72	1.29	1.67	1.41	1.38
Mg	(µg/l)	5.09	4.84	5.31	8.53	7.27	7.56
Mn	(µg/l)	0.03	0.04	0.02	0.04	0.04	0.06
Mo	(µg/l)	0.02	0.02	0.04	0.07	0.08	0.12
Na	(µg/l)	273	211	446	811	953	1,057
P	(µg/l)	3.21	27.11	17.79	13.81	11.68	23.32
Pb	(µg/l)	0.02	0.13	0.01	0.04	0.13	2.58
Rb	(µg/l)	0.07	0.04	0.11	0.23	0.25	0.28
Sb	(µg/l)	4.26	3.33	6.62	5.68	15.85	22.22
Sc	(µg/l)	0.60	0.15	0.76	0.99	1.30	1.24
Se	(µg/l)	0.17	0.16	0.13	0.13	0.15	0.17
Si	(µg/l)	4,883	1,187	6,939	9,282	12,679	12,151
Sr	(µg/l)	0.06	0.01	0.05	0.12	0.08	0.07
Ti	(µg/l)	0.41	0.28	0.52	0.69	1.27	1.33
Tl	(µg/l)	0.03	0.03	0.04	0.04	0.04	0.04
V	(µg/l)	0.02	0.01	0.02	0.02	0.03	0.05
W	(µg/l)	0.02	0.03	0.03	0.03	0.08	0.08
Y	(µg/l)	0.00	0.22	0.02	0.02	0.03	0.03
Zn	(µg/l)	5.62	7.11	7.76	8.00	7.67	8.62
Zr	(µg/l)	0.01	0.03	0.06	0.42	7.95	6.89

* The most abundant elements (from the glass) are high-lighted in yellow.

Appendix E

Hydrogen analyses

E1 Hydrogen desorption experiments

E1.1 Testing of procedure

Experiments were also performed on other copper material for testing the purification procedure concerning hydrogen desorption, namely the efficiency to remove dissolved hydrogen as a function of temperature. Pristine copper samples from Goodfellow (99.95%) and from Alpha Aesar (99.9999%) were heated up to 600°C at a rate of 1°C/min. At this heating rate, there is no difference between sample and furnace temperature. The outcome of this treatment, from the hydrogen signal in a mass spectrometer (QMS), is illustrated in Figure E-1. As may be noted from this figure, the base pressures of the system were different. Hydrogen is effectively desorbed within a temperature range of 350–500°C with a maximum evolution at 400°C for moderate heating rates. This temperature was chosen *ad hoc* for the final purification step of the ultrapure copper used in this investigation as well as in Boman et al. (2014), in that case after electropolishing and hydrogen reduction. The outcome of heat treatment at that temperature was followed by QMS as illustrated in Figure 3-19. The peak in Figure E-1 occurring at about 300°C, irrespective of purity grade, may emanate from hydrogen bound near the surface.

E1.2 Studies of samples sent for fusion analysis (LECO)

The following figures illustrate the desorption of hydrogen and other selected species from copper samples that were later sent for fusion analysis of the hydrogen content to Degerfors Laboratorium AB (Analysis certificates under Appendix E3), the results of which are quoted. The sample masses were 5–6 g and the surfaces were not polished before the analyses.

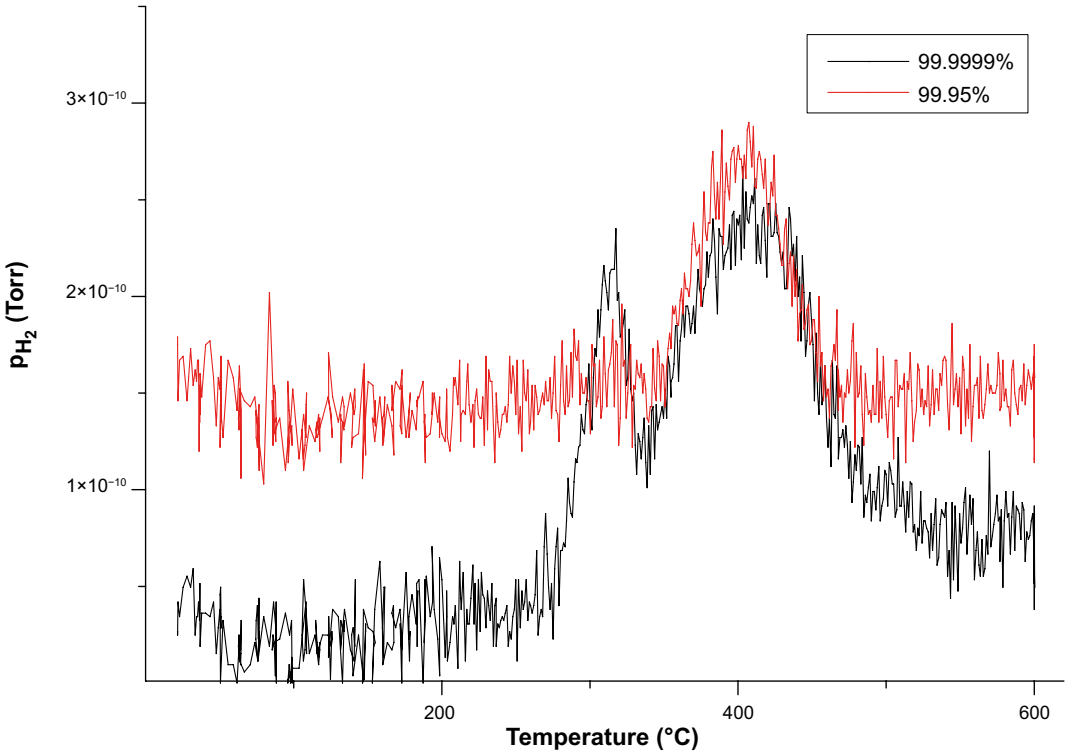

Figure E-1. *The hydrogen pressure as a function of temperature from copper samples of different purities. The mass of the 99.9999% pure sample (black curve) is 6 times larger than that of the less pure copper (red).*

The various species that were recorded (QMS) are colour coded. For each sample there are pairs of figures, where the right-hand figure shows the same data as the one at the left, only that the contribution by water (blue) has been removed and the data are rescaled so that the contributions of the rest appear larger in size. Hydrogen is marked by deep red, and the area under the red curve correlates to the amount of hydrogen in the sample.

Sample Cu1, "as received"

The hydrogen content before heating to 600°C is 0.7 ppm and after 0.06 ppm, see Figure E-2a–b.

Sample Cu2, after electropolishing

Hydrogen content after electropolishing is 0.16 ppm. As shown in Figure E-3a–b, most of the hydrogen is removed from the surface layer during the electropolishing process.

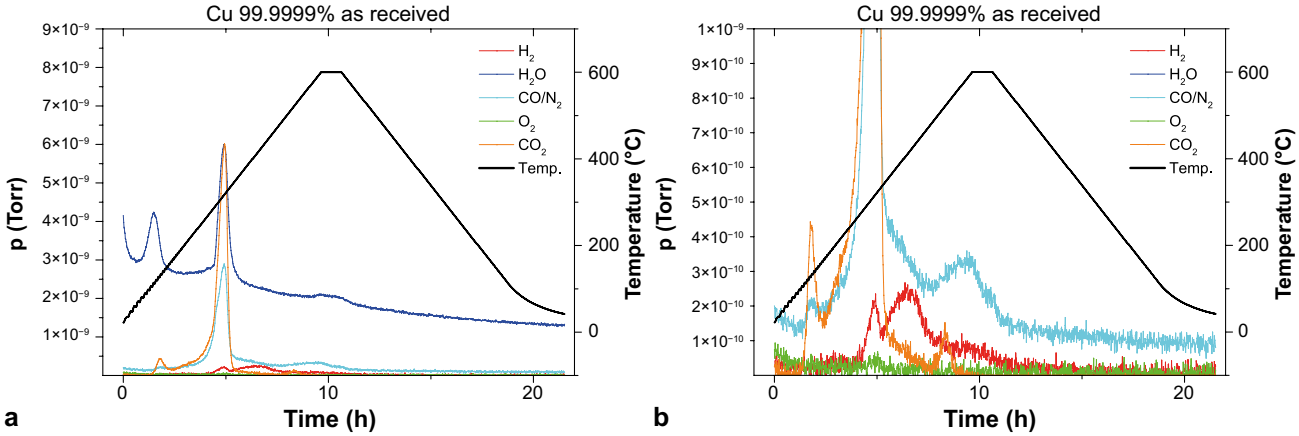

Figure E-2 a–b. *Measured pressures of the gas species vs. time/temperature obtained on heating/cooling for Cu 1. The signal marked CO/N_2 belongs to CO.*

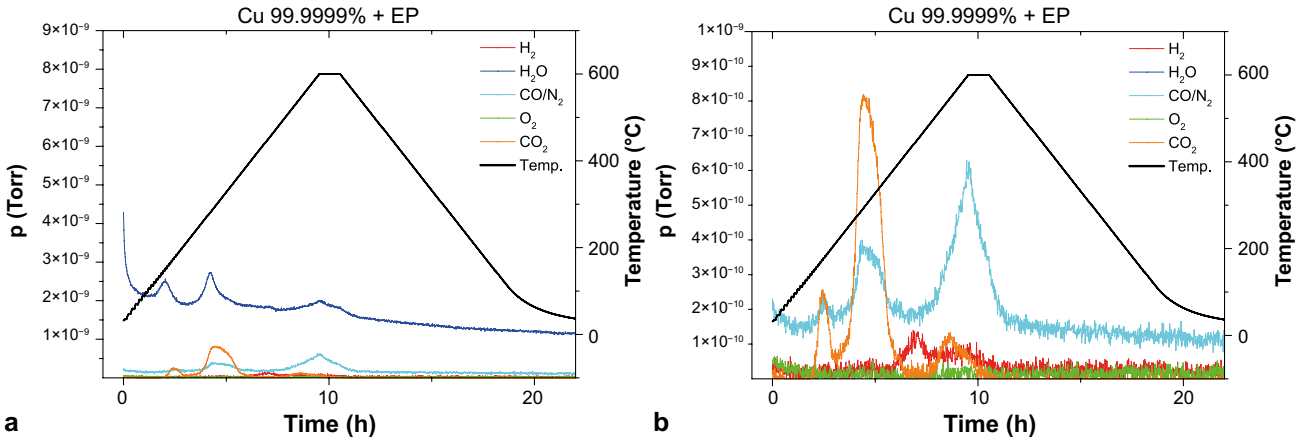

Figure E-3 a–b. *Measured pressures of the gas species vs. time/temperature obtained on heating/cooling for Cu 2.*

Sample Cu4, after electropolishing and hydrogen treatment

The hydrogen content remained low (0.03 ppm) after this treatment". (Figure E-4a–b.)

Because of different molecular properties, the areas under the curves cannot be used for a direct comparison between different species. None of the samples were kept under inert conditions prior to the analysis. Hence, the surface is contaminated to a certain degree. Water first disappears at about 100°C which may be an effect of chemisorption or the decomposition of superficial copper(II) hydroxide. Harder bound water is removed at about 300°C together with CO_2, possibly from a hydroxide carbonate of copper. A detailed analysis lies outside the scope of this study.

E2 Fusion analysis, previous trials

As alluded to in Section 3.4.1, samples were earlier sent for fusion analysis where normal procedure was followed, *i.e.* the specimens were polished before analysis. As seen from Table E-1, there is a large spread in the values obtained. This was interpreted as an effect either of inhomogeneity or of small sample size. All analysis methods have their optimum, and in a second attempt larger sizes were used, and the surface was left intact. As seen in Section 3.4.1 these instructions rendered significantly smaller values and better precision.

The differences in procedure and sample size are probable reasons for the still higher contents obtained from the analyses reported in Boman et al. (2014).

Values from the new attempt (no polishing, larger size – 5–6 grams) are found in Section 3.4.1 and the corresponding analysis certificates (values being an average from two measurements) in Appendix E-3.

Table E-1. Hydrogen content as determined by the LECO method after surface polishing.

Copper sample	As received	Electropolished	15 months' sample
Hydrogen content (ppm)	0.1–1.9	0.2–1.2	0.3

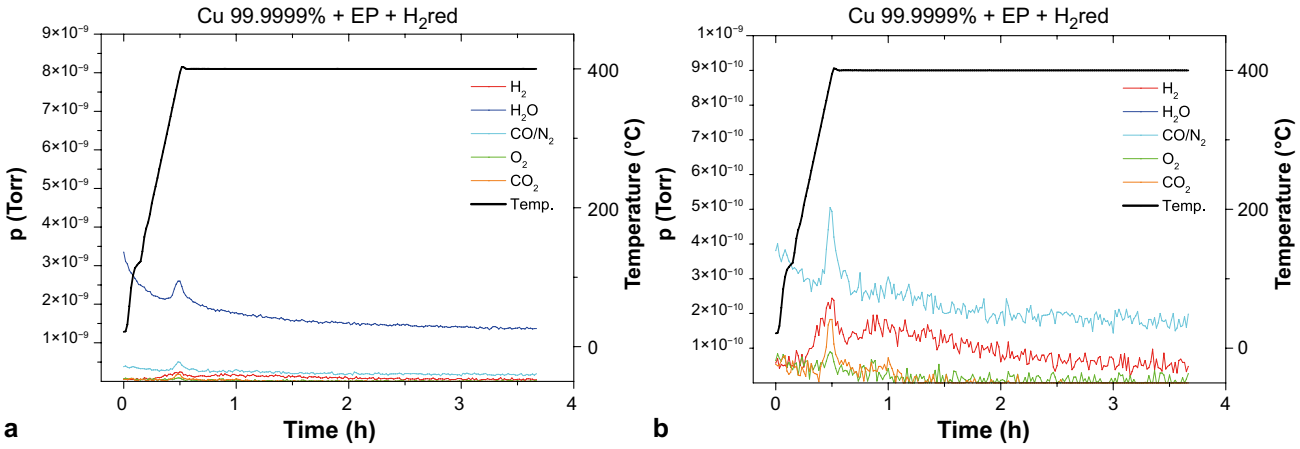

Figure E-4 a–b. *Measured pressures of the gas species vs. time/temperature obtained on heating/cooling for Cu 4*

E3 Fusion analysis certificates from new trials

D-LAB
DEGERFORS LABORATORIUM AB

Provningsresultat / Test Results:

Ordernr / Ordernо: DL-33872

Beställare / Client	Referens / Reference
Uppsala Universitet	**Pedro Berastegui**
Adress / Address: Box 538, 751 21 UPPSALA	

Er beställning / Your order No	Ankomstdag / Sample Registration Date	Utskriftsdatum / Date of issue	DL ID
139EVL Pedro Berastegui	2015-01-19	2015-01-19	533132

Provbeteckning / Sample identity: Cu1 As received (AR)

Noteringar / Notes:

Resultat/Results

H	0.7 ppm

DEGERFORS LABORATORIUM

Ingvar Bernhardsson
Kvalitetschef

Degerfors Laboratorium AB
Box 54
SE-693 21 DEGERFORS
SWEDEN

Phone +46 586 47406
Fax: +46 586 47005

Web: www.degerforslab.se
Email: sebackman@degerforslab.se
VAT no.: SE 556609044401

Bankgiro: 5735-6784
Bank: Foreningssparbanken, Degerfors
IBAN: SE8480000815629833744494
BIC/SWIFT: SWEDSESS

D-LAB
DEGERFORS LABORATORIUM AB

Provningsresultat / Test Results:

Ordernr / Ordemo
DL-33872

Beställare / Client	Referens / Reference
Uppsala Universitet	**Pedro Berastegui**

Adress / Address
Box 538, 751 21 UPPSALA

Er beställning / Your order No	Ankomstdag / Sample Registration Date	Utskriftsdatum / Date of issue	DL ID
139EVL Pedro Berastegui	2015-01-19	2015-01-19	533133

Provbeteckning / Sample identity
Cu2 AR + Elektropolerat I H3PO4

Noteringar / Notes

Resultat/Results

H	0.16 ppm

Note: Not responsible for electronically transferred reports due to changes of data during transmission. Please contact us in doubtful cases.

DEGERFORS LABORATORIUM

Ingvar Bernhardsson
Kvalitetschef

Degerfors Laboratorium AB
Box 54
SE 693 21 DEGERFORS
SWEDEN

Phone +46 586 47406
Fax. +46 586 47005

Web. www.degerforslab.se
Email: sebackman@degerforslab.se
VAT no.: SE 556609044401

Bankgiro. 5735-6784
Bank: Foreningssparbanken, Degerfors
IBAN: SE8480000815629833744494
BIC/SWIFT: SWEDSESS

D-LAB
DEGERFORS LABORATORIUM AB

Provningsresultat / Test Results:

Ordernr / Ordernr: DL-33872

Beställare / Client	Referens / Reference
Uppsala Universitet	**Pedro Berastegui**
Adress / Address: Box 538, 751 21 UPPSALA	

Er beställning / Your order No	Ankomstdag / Sample Registration Date	Utskriftsdatum / Date of issue	DL ID
139EVL Pedro Berastegui	2015-01-19	2015-01-19	533134

Provbeteckning / Sample identity: Cu3 AR + EP + Reducerat I H2 I 300C

Noteringar / Notes:

Resultat/Results

H	0.03 ppm

Note: Not responsible for electronically transferred reports due to changes of data during transmission. Please contact us in doubtful cases.

DEGERFORS LABORATORIUM

Ingvar Bernhardsson
Kvalitetschef

Degerfors Laboratorium AB
Box 54
SE-693 21 DEGERFORS
SWEDEN

Phone +46 586 47406
Fax: +46 586 47005

Web: www.degerforslab.se
Email: sebackman@degerforslab.se
VAT no.: SE 556609044401

Bankgiro: 5735-6784
Bank: Foreningssparbanken, Degerfors
IBAN: SE8480000815629833744494
BIC/SWIFT: SWEDSESS

D-LAB
DEGERFORS LABORATORIUM AB

Provningsresultat / Test Results:

Ordernr / Ordernr: DL-33872

Beställare / Client	Referens / Reference
Uppsala Universitet	**Pedro Berastegui**

Adress / Address: Box 538, 751 21 UPPSALA

Er beställning / Your order No	Ankomstdag / Sample Registration Date	Utskriftsdatum / Date of issue	DL ID
139EVL Pedro Berastegui	2015-01-19	2015-01-19	533135

Provbeteckning / Sample identity: Cu4 AR + EP + RH2 Värmebehandlat 400C

Noteringar / Notes:

Resultat/Results

H	0.03 ppm

Note: Not responsible for electronically transferred reports due to changes of data during transmission. Please contact us in doubtful cases.

DEGERFORS LABORATORIUM

Ingvar Bernhardsson
Kvalitetschef

Degerfors Laboratorium AB
Box 54
SE-693 21 DEGERFORS
SWEDEN

Phone +46 586 47406
Fax: +46 586 47005

Web: www.degerforslab.se
Email: scbackman@degerforslab.se
VAT no.: SE 556609044401

Bankgiro: 5735-6784
Bank: Foreningssparbanken, Degerfors
IBAN: SE8480000815629833744494
BIC/SWIFT: SWEDSESS

D-LAB
DEGERFORS LABORATORIUM AB

Provningsresultat / Test Results:

Ordernr / Ordernr: DL-33872

Beställare / Client	Referens / Reference
Uppsala Universitet	**Pedro Berastegui**
Adress / Address: Box 538, 751 21 UPPSALA	

Er beställning / Your order No	Ankomstdag / Sample Registration Date	Utskriftsdatum / Date of issue	DL ID
139EVL Pedro Berastegui	2015-01-19	2015-01-19	533136

Provbeteckning / Sample identity: Cu5 AR+Värmebehandlat I 600C

Noteringar / Notes:

Resultat/Results

H	0.06 ppm

Note: Not responsible for electronically transferred reports due to changes of data during transmission. Please contact us in doubtful cases.

DEGERFORS LABORATORIUM

Ingvar Bernhardsson
Kvalitetschef

Degerfors Laboratorium AB
Box 54
SE-693 21 DEGERFORS
SWEDEN

Phone +46 586 47406
Fax: +46 586 47005

Web: www.degerforslab.se
Email: sebackman@degerforslab.se
VAT no.: SE 556609014401

Bankgiro: 5735-6784
Bank: Foreningssparbanken, Degerfors
IBAN: SE8480000815629833744494
BIC/SWIFT: SWEDSESS

D-LAB
DEGERFORS LABORATORIUM AB

Provningsresultat / Test Results:

Ordernr / Ordemo
DL-33872

Beställare / Client	Referens / Reference
Uppsala Universitet	**Pedro Berastegui**
Adress / Address	
Box 538, 751 21 UPPSALA	

Er beställning / Your order No	Ankomstdag / Sample Registration Date	Utskriftsdatum / Date of issue	DL ID
139EVL Pedro Berastegui	2015-01-19	2015-01-19	533137

Provbeteckning / Sample identity
28Mån prov

Noteringar / Notes

Resultat/Results

H	0.09 ppm

DEGERFORS LABORATORIUM

Ingvar Bernhardsson
Kvalitetschef

Degerfors Laboratorium AB
Box 54
SE-693 21 DEGERFORS
SWEDEN

Phone +46 586 47406
Fax: +46 586 47005

Web: www.degerforslab.se
Email: sebackman@degerforslab.se
VAT no.: SE 556609044401

Bankgiro: 5735-6784
Bank: Foreningssparbanken, Degerfors
IBAN: SE8480000815629833744494
BIC/SWIFT: SWEDSESS

Appendix F

Investigations of the Main 1 setup

F1 Pressure evolution at 50°C

In Figure F-1 the whole logging of the Main 1 setup is given (together with two reference systems). Part of this, up to 6,700 hrs, was included in Boman et al. (2014, Section 5.1) and analysed there. Recent experiments include changing of temperature of the lower chamber (after 18,000 h). The upper chamber was held at approximately 25°C (room temperature).

F2 The influence of temperature on the steady-state pressure

The temperature of the membrane was kept 5 degrees higher than the new settings.

Overview for clarifying Figure F-1:

1. 1,500 h: Steady state pressure (0.065 Torr).
2. 4,000 h: Pumping and QMS analyses.
3. 9,000 h: Pumping.
4. 10,000 h: Ditto.
5. 11,700 h: Ditto.
6. 18,000 h: Temperature was set to 30°C.
7. 21,000 h: Temperature was set to 40°C.
8. 23,800 h: Temperature was set to 70°C.
9. 26,500 h: Ending of the experiment.

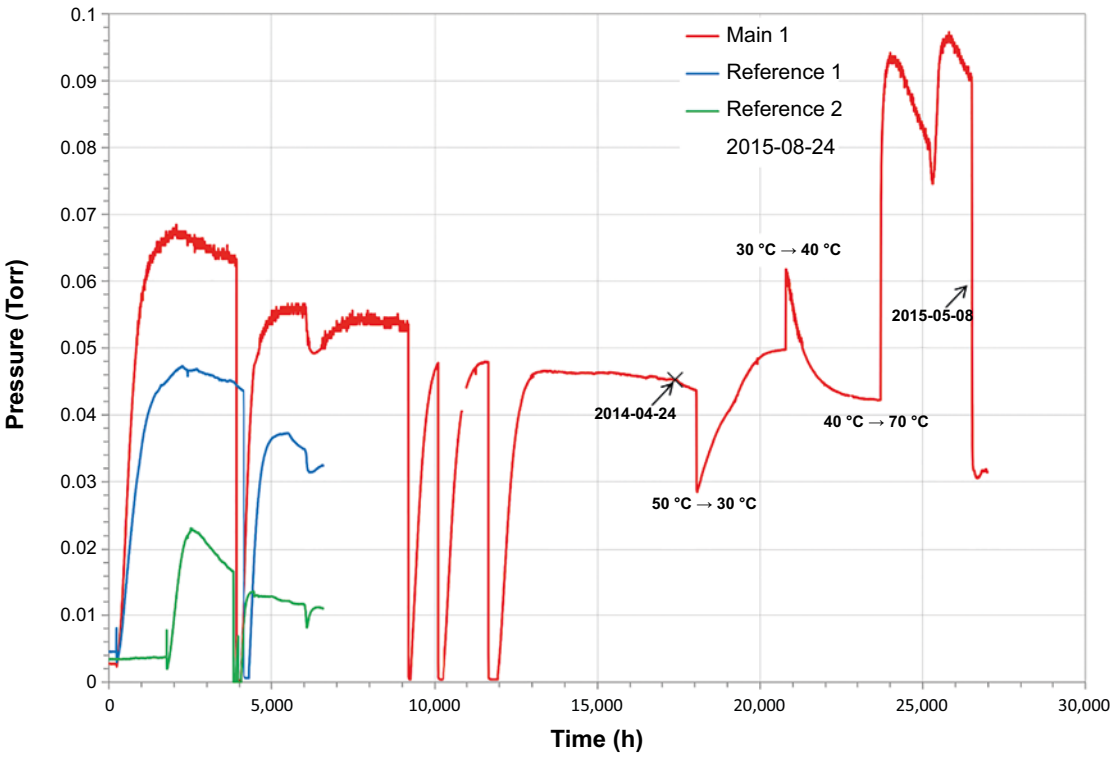

Figure F-1. *Gas pressure as a function of time (and temperature) in the upper compartment of Main 1 (and up to 6,700 hrs also in reference systems).*

The temperature change *vs.* pressure response can be divided into three different steps:

1. Palladium releases or takes up hydrogen from the gas phase. This is an effect of the temperature dependence of hydrogen solubility in palladium. On temperature decrease (*e.g.* 50°C → 30°C) the solubility increases. This is a fast reaction leading to a sharp vertical change in pressure downwards in the diagram. The opposite is true for a temperature increase when hydrogen is released from the membrane.
2. The pressure changes as to create a steady state between the hydrogen outgassing/production and the lateral diffusion out through the Pd membrane (Old system). This is a relatively slow process that takes up to 3,000 h.
3. Steady-state pressure may be attained, *i.e.* towards a constant value of the pressure.

Table F-1. Analysis of the data in Figure F-1.

Temperature System	Temperature Palladium	Initial pressure Fast change (Torr)	Steady-state pressure (Torr)
50°C	55°C	–	0.065–0.045
30°C	35°C	0.028	0.048
40°C	45°C	0.063	0.043
70°C	75°C	0.085–0.093	*Not attained*

The time to obtain a steady-state (about 3,000 h) for 30°C and 40°C can be compared with the time for steady-state after pumping the system, about 1,000–500 h. The outcome after the rise to 70°C is not interpretable. The expected pressure decrease after the hydrogen release from the membrane did not follow a pattern according to mainly diffusion relaxation. Maybe the temperature of the upper chamber was no longer stable when the lower part was so much warmer (also influencing the lateral leakage) and, moreover, artefacts occurred through failure of the glove-box atmosphere regulation. The continued pressure decrease starting at about 26,000 h did not improve the situation, and the experiment was stopped.

The measurements illustrate two important facts (Figure F-1, Table F-1). First of all, the effect of hydrogen in the Pd membrane is evident from the fast changes of pressure from the strong dependence with temperature of the solid solubility. Secondly, the attaining of a steady-state condition after a change takes considerable time.

Because of the competition between responses that carry different temperature dependence (different activation energies), there is no evident trend to read from the temperatures and the steady-state pressure eventually obtained. The situation is too complex to make modelling feasible without a more thorough analysis of all factors involved.

F3 Chemical analyses

The copper samples of Main 1 spent a very long time in water (26,500 h) but the outcome of the chemical analyses cannot be directly translated to the situation concerning the free-standing steel containers. The reason is that there is another parameter involved: Besides the time aspect the temperature was not constant but changed (see Table F-1). Still, the analysis results are valuable, especially since also a higher temperature (70°C) rather than 50°C was used for some time, which would increase the expected reaction rates of various chemical processes. Similar to the free-standing samples, the analysis methods were applied to the copper, the water and the accompanying glass plate that was initially included (Boman et al. 2014).

F3.1 Surface analysis of the copper metal

The results from XPS presented here are focussed on the most interesting energy ranges, that of oxygen and its vicinity as well as the copper spectrum. Figure F-2 shows that the copper surface gives a weak broad O *1s* peak in addition to sharp peaks belonging to antimony, all of which are removed on gentle sputtering leaving only the copper Auger Cu *LMM* spectrum. The initial spectrum resembles

to some extent that of sample M2-SiC (Figure 3-12), but the oxygen peak is much weaker and those of antimony much stronger. In order to understand this we have to consider several differences between the two samples: The Sb *3d* peaks most likely emanate from the glassware, and for the sample in Main 1 there are two such sources, the beaker as well as the added glass-plate (the latter not present for M2-SiC). The leaching process of the glass has been going on for a much longer time and at other temperatures, both factors likely to yield stronger Sb peaks than found for M2-SiC. However, the latter sample contains contaminations (species containing bonds of C−O), therefore instead adding extra intensity to the oxygen peak.

The antimony peaks are much stronger than the oxygen peak but the actual amount is very low. The effect of different photoelectron emission cross-sections is very fallacious for the spontaneous estimation of amounts from intensity values (*cf.* Appendix G).

As is immediately obvious from the Cu *2p* spectrum (Figure F-3), no Cu(II) is present, since there is no tendency for satellite formation to the main peaks. The Auger spectrum (see Figure F-2) did not change its features on sputtering and only shows the characteristics of metallic copper.

An attempt was made to analyse the antimony by using XRF. It is a difficult and time-consuming task to determine small amounts with certainty since the signal approaches the background. This illustrates how much more sensitive XPS is for the detection of trace elements, especially if their peaks are inherently strong. From the XRF analysis, a fair estimation gave that the antimony content would correspond to a surface coverage below 1 Å. Considering that the atomic size (diameter) of antimony is 1.5–2 Å this means far less than a monolayer. That is in line with XPS where the peak intensities (Sb vs. O) indicate that the amount of antimony is considerably less than the oxygen that belongs to only a monolayer of water, considering the UHV conditions in the spectrometer (see discussion in Section 3.3). The sharp antimony peaks of Figure F-2 give a fallacious interpretation that there is a considerable amount, while the coverage is certainly less than a monolayer (see Appendix G for calculations). Nothing can be said as to the actual species containing antimony.

F3.2 Analyses on the water and glass

The water was analysed by ICP-MS with results given in Table F-2. The analysis was performed twice to test reproducibility and give a hint concerning the precision. Two isotopes of copper and zinc, respectively, were included as indicators of absence of systematic errors. In each case, scaling was applied in relation to isotope abundance to yield total concentrations.

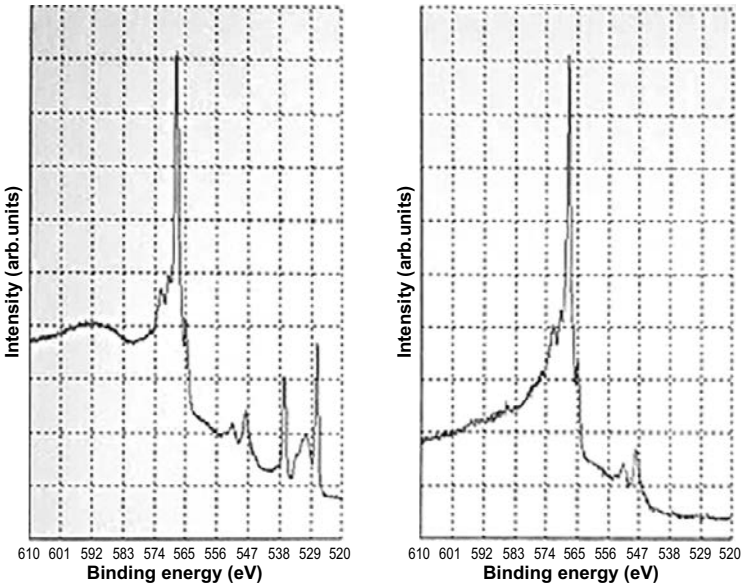

Fig F-2. *Part of overview spectrum showing spectra before and after sputtering.*

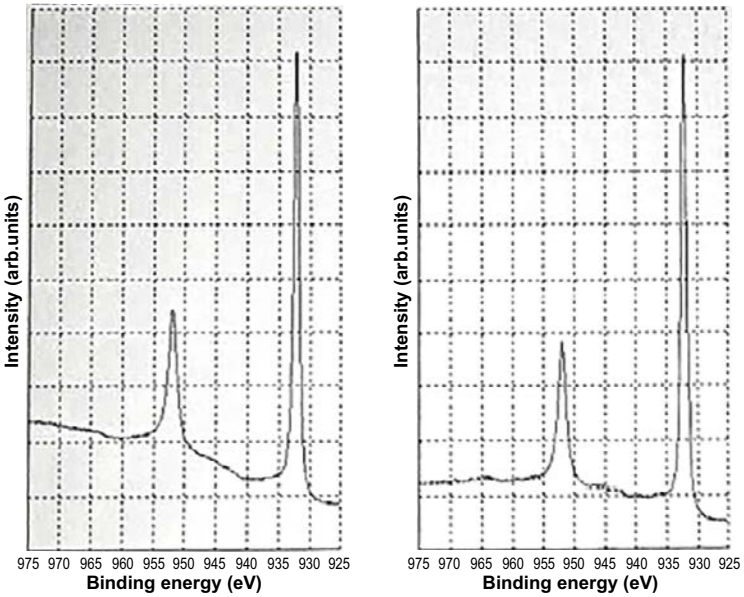

Fig F-3. *The Cu 2p spectrum before and after sputtering.*

Table F-2. Analysis results from two analyses of the water phase of Main 1. Values are given in ppb.

^{24}Mg	^{27}Al	^{63}Cu	^{65}Cu	^{66}Zn	^{67}Zn	^{121}Sb	^{57}Fe
6.1	693.2	6.8	5.9	9.0	9.6	8.6	4.8
5.2	623.5	4.7	4.7	9.5	10.2	8.6	4.8

As seen in Figure F-1, the experiment entailing Main 1 had been running for 26,500 hours when stopped, *i.e.* somewhat more than 3 years. The long immersion time in water may explain the enhanced aluminium content (coming from the glass, being a partly substituted borosilicate). On the other hand, the values found for copper, zinc and antimony are actually lower than those found for the sample from 29 months' residing in water (Table 3-4). That is an indication that there are some systematic errors attached to the 29 months' sample, and this recent finding sheds new light on the interpretation of the copper leaching by time as depicted in Figure 3-21. The erratic behaviour there put questions pointing at inaccuracy of either the 15 or the 29 months' sample. From this later analysis of Main 1 it is concluded that the data from 29 months must be erroneous which means that the copper concentration is early levelling out by time. The data from Main 1 were included in that very diagram for comparison despite a different thermal history.

The amount of antimony inherent in the glass was investigated by XRF, from analysis of a beaker as well as a glass-plate that had resided in water the whole time from the start. The analysis from the emission spectrum is condensed in Table F-3. The Sb$K\alpha$-contribution was used for estimating the amounts, with antimony (III) oxide as a standard. The accuracy is low in this regime of very low contents, but it is obvious that the added glass plate contains much more antimony than the glass beaker. However, as seen from the ICP-MS analysis of the sample from the Main 1 setup, the presence of the glass plate does not increase the antimony content compared to that found for other samples without such a plate, even if its antimony content is roughly 100 times higher than that of the beaker glass. The blank sample (without copper), as presented in Table 3-5, gave a still higher value of the antimony in water but two factors being different are influential: The immersion time was still longer, and the sample contained two glass plates. In all cases, the antimony concentration in the water is very low, a corresponding copper surface content being less than a monolayer onto copper (see Appendix G).

Table F-3. Analysis results of antimony in glass by XRF.

Sample	Estimated content by weight (as Sb_2O_3)
Beaker glass	~10 ppm
Glass plate	800–900 ppm

Appendix G

Calculation of the amount of antimony found on copper from XPS

In order to estimate amounts from XPS data, the integrated peak intensities are to be evaluated. For comparing different elements, their respective photoelectron cross-sections must then be considered, and these are also dependent on the energy of the incoming beam. Calculated data for Al*Kα* radiation were taken from Scofield (1976) for comparing the effects of oxygen in relation to antimony. In the table consulted the cross-section were scaled so that the carbon peak C *1s*, that has a cross-section of 13,600 barn, was given the relative value of 1.000. Scaled likewise, the following values are read for oxygen and antimony:

O *1s* 2.93

Sb $3d_{3/2}$ 11.35 Sb $4d_{3/2}$ 1.29

Sb $3d_{5/2}$ 16.39 Sb $4d_{5/2}$ 1.85

These values show that the antimony *3d* peak intensities *per atom* are more than 10 times stronger than that of carbon. A comparison may be made between the two Sb *3d* peaks:

Int(Sb $3d_{5/2}$) / Int(Sb $3d_{3/2}$) = 16.39 / 11.35 = 1.444

Theoretically, the intensity ratio is expected to be (5 + 1) / (3 + 1) = 3/2. It is a simple test of the validity of the computed data that the relative deviation between the two ratios is only 4%.

From this, one may dare to calculate intensity ratios also for oxygen and antimony together, in a test applied to $FeSbO_4$ (Berry et al. 1987). Using the above data one arrives at:

Sb $3d_{5/2}$ 16.39 (one atom)

O *1s* 2.93 × 4 (four atoms) = 11.72

Those emissions overlap on the energy scale, so the scaled intensity of the resulting peak is 16.39 + 11.72 = 28.11. The oxygen contribution to the intensity sum is thus 11.72 / 28.11 = 0.42.

Berry et al. (1987) compared the outcome of their *experiment* and found that the ratio between the two antimony peaks was not the expected 1.5 (theory) but 2.2, *i.e.* the Sb $3d_{5/2}$ peak had an extra contribution of (2.2–1.5) / 1.5 = 0.47, estimated well by the data given by Scofield (1976). Likewise, the oxygen contribution to the Sb $3d_{5/2}$ peak in Sb_2O_3 would be 8.79 / (8.79 + 32.78) = 0.21, *i.e.* to appear only as a broadening of (or a weak "shoulder" to) the otherwise pure antimony peak. This is indeed what is observed (Garbassi 1980).

A semi-quantitative analysis of Figure 3-10a is now possible. The ratio Int(O *1s*) / Int(Sb $3d_{5/2}$) = 2.93 / 16.39 = 0.18 is valid for *equal amounts* of respective element. The experimental ratio Int(O *1s*) / Int(Sb $3d_{5/2}$) is very large, *i.e.* there is very much more oxygen than antimony. Since the oxygen species (OH_{ads}, H_2O_{ads}) cannot cover more than a monolayer in the measuring situation, considering the UHV conditions in the spectrometer, the total amount of antimony is only a tiny percentage of a monolayer at the copper surface.

The result demonstrates how extremely surface sensitive electron spectroscopic methods are.

Arkitektkopia AB, Bromma, 2016

SKB is tasked with managing Swedish nuclear and radioactive waste in a safe way.

skb.se